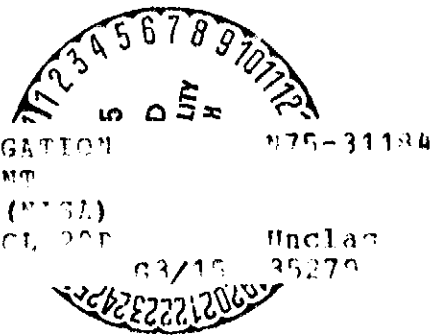


NASA TM X-71759

**NASA TECHNICAL
MEMORANDUM**

NASA TM X-71759

(NASA-TM-X-71759) WIND TUNNEL INVESTIGATION
OF A CENTAUR STANDARD SHROUD COMPARTMENT
VENT FROM MACH NUMBER OF 0.70 TO 1.96 (NASA)
CSCL 20F
01 D UC \$4.75



**WIND TUNNEL INVESTIGATION OF A CENTAUR
STANDARD SHROUD COMPARTMENT VENT FROM
MACH NUMBER OF 0.70 TO 1.96**

by Albert L. Johns and Merle L. Jones
Lewis Research Center
Cleveland, Ohio
August 1975

1. Report No. NASA TM X-71759	2. Government Accession No.	3. Recipient's Catalog No.	
4. Title and Subtitle WIND TUNNEL INVESTIGATION OF A CENTAUR STANDARD SHROUD COMPARTMENT VENT FROM MACH NUMBER OF 0.70 TO 1.96		5. Report Date	
7. Author(s) Albert L. Johns and Merle L. Jones		6. Performing Organization Code	
9. Performing Organization Name and Address Lewis Research Center National Aeronautics and Space Administration Cleveland, Ohio 44135		8. Performing Organization Report No. E-8461	
12. Sponsoring Agency Name and Address National Aeronautics and Space Administration Washington, D.C. 20546		10. Work Unit No.	
		11. Contract or Grant No.	
		13. Type of Report and Period Covered Technical Memorandum	
		14. Sponsoring Agency Code	
15. Supplementary Notes			
16. Abstract <p>An experimental investigation was conducted in the Lewis Research Center 8- by 6-Foot Supersonic Wind Tunnel to determine the vent discharge coefficient for the Centaur Standard Shroud/Liquid Hydrogen tank compartment vent. The test was conducted from Mach 0.70 to 1.96 with the vent mounted in a flat plate. Full scale simulated flight hardware, such as the vent, corrugations, aft field joint ring and ice bag clip was used. Air was discharged from a plenum chamber, located on the tunnel sidewall behind the plate, through five 6.35 cm (2.50 in.) diameter vent orifices into the free stream. Boundary layer thickeners were used to vary the boundary layer height and profile. As a result of using thickeners, analytically predicted displacement thickness for the vehicle nominal flight trajectory could be simulated over the Mach number range. The highest vent discharge coefficient for any given Mach number and vent pressure ratio generally occurred at the maximum displacement thickness.</p>			
17. Key Words (Suggested by Author(s))		18. Distribution Statement Unclassified - unlimited	
19. Security Classif. (of this report) Unclassified	20. Security Classif. (of this page) Unclassified	21. No. of Pages	22. Price ⁴

¹ For sale by the National Technical Information Service, Springfield, Virginia 22151

WIND TUNNEL INVESTIGATION OF A CENTAUR STANDARD SHROUD

COMPARTMENT VENT FROM MACH NUMBER OF 0.70 TO 1.96

by Albert L. Johns and Merle L. Jones

SUMMARY

An experimental program was conducted in the Lewis Research Center 8- by 6-foot Supersonic Wind Tunnel to determine the vent discharge coefficient for the Centaur Standard Shroud (CSS)/liquid hydrogen (LH_2) tank compartment vent. The test was conducted over a free-stream Mach number range of 0.70 to 1.96 with the vent mounted in a flat plate. The plate was flush mounted to the tunnel sidewall with coinciding center-lines. Air was discharged from a plenum chamber, located on the tunnel sidewall behind the plate, through five 6.55 cm (2.50 in.) diameter vent orifices into the free-stream. The test was conducted to provide data for the analysis of the CSS/ LH_2 compartment venting during ascent through the atmosphere. Full scale simulated flight hardware, such as the vent, corrugations, aft field joint ring and ice bag clip was used. Boundary layer thickeners were used to vary the boundary layer height and profile. The thickeners consisted of several rods fastened to a plate mounted at the leading edge of the test section. The boundary layer height varied from a maximum of 30.5 cm (12 in.) at $M_o = 0.70$ to a minimum of 15.8 cm (6.25 in.) at $M_o = 1.40$ using thickeners. Without thickeners, the boundary layer height varied from a maximum of 29.8 cm (8.20 in.) at $M_o = 0.70$ to a minimum of 15.25 cm (6 in.) at $M_o = 1.40$.

The highest vent discharge coefficient for any given Mach number and vent pressure ratio generally occurred at the maximum displacement thickness.

The peak pressure coefficients caused by the ice bag clip and aft field joint ring were greatly influenced by the boundary layer characteristics. For example, without boundary layer thickeners, the peak pressures caused by the ice bag clip and the aft field joint ring were about the same. But with thickeners, the peak pressure caused by the ice bag clip was less than that for the aft field joint ring up to Mach 1.20.

Vent flow increased the static pressure ahead of the vent and decreased the static pressure aft of the vent.

INTRODUCTION

During ascent through the atmosphere, several compartments in the Titan/Centaur launch vehicle are vented overboard into the free stream. The venting during this portion of the flight must be controlled in such a way that the compartment walls will not be exposed to excessive crush or

F-1
E-1
F-1
E-1
F-1
E-1

burst pressures. In designing a vent system which will meet this requirement, it is necessary to know the discharge characteristics of the vent openings as they are affected by both the geometry of the openings and the external environmental elements such as local velocity, pressure, and boundary layer thickness, references 1 through 9.

One of the compartments to be vented during atmospheric ascent is an annulus bounded by the hydrogen tank, the Centaur Standard Shroud, and the bulkhead/seals at each end of the hydrogen tank. This compartment is vented through the door on the hydrogen fill and draw valve chute. The vent configuration consists of a cluster of five orifices 6.35 cm (2.50 in.) in diameter.

The present test was conducted primarily to determine the discharge characteristics of this particular vent configuration at various external environmental conditions. A secondary objective was the determination of aerodynamic pressure in the vicinity of the vents. The test was conducted in the Lewis Research Center 8- by 6-foot Supersonic Wind Tunnel over a range of free stream Mach numbers from 0.70 to 1.96. The test configuration consisted of a full-scale simulation of the door with vent holes mounted on a flat plate attached to the wind tunnel wall. Also included were full scale sections of shroud corrugations and other protuberances which are located in the vicinity of the vent orifices. Air was discharged through the vent orifices into the wind tunnel stream from a plenum mounted on the backside of the wind tunnel wall.

SYMBOLS

CP	pressure coefficient, $(p_v - p_0)/q_0$
d_i	diameter of each vent orifice=6.35 cm (2.50 in.)
K	vent discharge coefficient based on one-dimensional flow rate that assumes a static pressure representative to the vent region when there is no vent flow
M_l, M_L	local Mach number at the vent, based on local static pressure with no vent flow and free stream total pressure
M_0, M_0	free stream Mach number
N	power of power-law profile
p_0	local static pressure
p_o	free stream static pressure
PE/PI	plenum pressure ratio, ratio of external static pressure at vent without jet-free stream interaction-to-plenum pressure

q_0	free-stream dynamic pressure
VL/VLMAX	boundary layer velocity ratio measured at tunnel stations 619.77 cm and 624.85 cm
X/LREF	ratio of axial distance from aft field joint ring leading edge (tunn 1 station 679.00 cm (267.40 in.)) to-reference length. Where reference length, LREF = 2.54 cm (1.00 in.)
Y	normal distance from trough of corrugated surface
z	distance above (+) and below (-) plate centerline
δ	boundary-layer thickness, height of the boundary-layer where local velocity becomes 99 percent of maximum local velocity
δ^*	displacement thickness, a measure of deficiency in mass flow through the boundary-layer as a result of the stream having been slowed by friction
H	shape factor, ratio of displacement thickness-to-momentum thickness, where momentum thickness is the thickness of the free-stream flow necessary to make up the deficiency in momentum flux within the boundary layer

APPARATUS

The test installation in the 8- by 6-foot Supersonic Wind Tunnel is shown in figure 1. The plate was flush mounted to the tunnel sidewall, the centerline of the plate and tunnel wall coinciding. The plate leading edge was located 92.7 centimeters (36.50 in.) downstream of the boundary layer thickener plate, (fig. 1(a)). Sections of full-scale simulated flight hardware such as the vent, the shroud corrugations, tee bag clip, and aft field joint ring were attached to the plate, (fig. 1(b)).

A schematic of the vent flow system is shown in figure 1(c). The plenum chamber was attached to the backside of the tunnel sidewall. Air was obtained from the atmosphere. The flow rate was measured with a flow metering orifice and regulated by a butterfly valve located upstream of the orifice. Figure 1(d) shows the installation of the boundary layer rakes.

Details of the test hardware are shown in figure 2. The plate was 243.84 cm (96.00 in.) long and 121.92 cm (48.00 in.) wide with a 15° ramp leading edge, (fig. 2(a)). It was partially covered with a 165.10 cm (65.00 in.) corrugated section, (fig. 2(b)). This corrugated section, the tee bag clip, and the aft field joint ring were full scale simulated flight hardware, details are shown in figure 2(e) through 2(i). Details of the boundary layer thickeners are shown in figure 3.

INSTRUMENTATION

The boundary-layer survey hardware consisted of two rakes (fig. 4(a)). The larger boundary-layer rake contained 19 probes. The lower five probes were concealed by the corrugation crest. The small rake contained 6 probes and was located in the corrugation trough, (fig. 1(d)). The large boundary layer rake covered a distance of 33.02 centimeters (13.00 in.) from the corrugation trough. Normal distance from the corrugation trough to each probe is given in the table of figure 4(a).

The boundary-layer rakes were used to survey the local flow field and to measure the boundary-layer height. Rakes were located at tunnel stations 619.77 cm (244.00 in.) and 624.85 cm (246.00 in.), at distances of 51.56 cm (20.30 in.) and 44.45 cm (17.30 in.) respectively above the centerline of the vent. The static pressure instrumentation is shown in figure 4(b) and table I.

Static pressure orifices ahead of the vent were located in the corrugation trough corner. Static pressure orifices aft of the vent region were located along both the corrugation trough and crest. The field joint ring was also instrumented, (fig. 4(c)). The vent and flow system instrumentation is shown in figure 4(d).

CONFIGURATIONS

A configuration summary is given in table II. Five configurations were tested: three were the flight configuration with variation in the boundary layer thickeners; and two with the aft field joint ring removed and no boundary-layer thickeners. One of the latter two configurations had the vents orifices plugged and was made to obtain the effect of open vent orifices on the localized pressures.

RESULTS AND DISCUSSION

Plenum pressure ratio, P_E/P_1 , is defined as the ratio of a local static (reference, p_{203} , see table I and figure 4(b)) pressure to plenum pressure. The reference pressure used to set the plenum pressure ratio and to compute the local Mach number was obtained from a no-vent-flow condition. A comparison of the reference-to-free-stream static pressure ratio for open vent (no vent flow) and plugged vent is shown in figure 5. With the exception of Mach numbers of 1.05, 1.20 and 1.96, the open vent had little or no effect on the reference pressure.

The local Mach number M_L , based on reference static pressure is shown in figure 6 as a function of the free stream Mach number for the five configurations tested with no vent flow. The local Mach number had an insignificant deviation from the free stream Mach number at the subsonic

conditions. But, at supersonic Mach numbers, particularly between Mach 1.05 and 1.40, the deviations were significant.

The boundary layer velocity profiles, figure 7, were obtained for each configuration. The velocity profiles in the lower region (first six probes) were measured by the small rake in the corrugation trough, which was located at tunnel station 619.77 cm (244.00 in.) and 51.56 cm (20.30 in.) above the plate centerline. A large boundary layer rake located at tunnel station 624.85 cm (246.00 in.) and 44.45 cm (17.30 in.) above the plate centerline was used to obtain the velocity profiles above the corrugation crest to a height of 33.02 cm (13.00 in.). The first six probes of the larger rake were masked by the corrugation crest. At the upper subsonic, transonic and supersonic Mach numbers a slight distortion occurred at the transition from the smaller rake to the larger rake. The distortion was caused by the seventh probe on the large rake being near the corrugation crest surface, resulting in a slightly lower velocity than that which existed at the preceding probe on the small rake.

The differences in the velocity ratio profiles, figure 7, for the various configurations reflect the thickening of the boundary layer through the use of tie thickener rods, (fig. 8(a)). A comparison of the measured boundary layer displacement thickness (with and without thickener rods) with analytical predictions for the flight vehicle is shown in figure 8(b). The boundary-layer velocity shape factors for the various configurations are shown in figure 8(c) over the Mach number range tested. Also shown in the figure is the boundary-layer velocity power profiles, N , of 5 and 11 taken from reference 9. Boundary-layer velocity power profile from $N = 5$ to 11 is the approximate range of fully-developed turbulent boundary-layers. In general, the shape factors for the various configurations were within the range of the fully-developed turbulent boundary-layers velocity power profiles.

Variation of vent discharge coefficients with the plenum pressure ratio, PE/PI , is shown in figure 9 for the free-stream Mach number range investigated. Also presented for each configuration is the local Mach number at the vent region. As discussed earlier both PE and local Mach number were determined from the zero flow condition.

At the no-vent-flow condition the internal pressure, PI , should theoretically equal the local external pressure, PE . However, internal and external pressures were affected differently by the corrugations, tee bag clip-boundary-layer interaction and aft field joint ring. For example, at supersonic Mach numbers, $M_\infty = 1.18$, the aft field joint ring had no effect on the internal pressure, whereas a noticeable effect occurred on the external pressure, PE . In addition, pressure gradients in both the span and axial direction, in the immediate vent area, could cause recirculation which would effect the internal pressure and not the external pressure PE . Consequently, the no-flow vent pressure ratio PE/PI varied from 0.94 to 1.035.

The effect of the aft field joint ring on the vent discharge coefficients can be ascertained from a comparison of configurations 1 and 3 (with and without aft field joint ring, respectively). The vent discharge coefficient was higher with the aft field joint ring for a given vent pressure ratio. The foregoing was caused by the aft field joint ring, as expected, increasing the pressures in the vent region. This effect is shown in a later figure (fig. 10).

The differences in vent discharge coefficients in the other configurations (1, 2 and 5) are due to variations in the boundary-layer displacement thickness. The maximum vent discharge coefficient, for a given plenum pressure ratio, was obtained with the maximum displacement thickness, configuration 2.

The effect of boundary layer displacement thickness on the pressure distribution is shown in figure 10 for no-vent-flow condition. Increasing the boundary layer displacement thickness caused a reduction in static pressure both upstream and downstream of the vent at subsonic speeds. However, at some supersonic Mach numbers the thicker boundary layer conditions resulted in a large pressure rise in the vent region (for example $M_0 = 1.2$ and 1.6 (fig. 10(i) and 10(k))). The pressure coefficients, aft of the vent, for the two configurations, 3 and 4, without the field joint ring are substantially lower than the pressure coefficients with the field joint ring.

The effect of the ice bag clip and aft field joint ring on the static pressure field was greatly influenced by the boundary layer characteristics. For example, at both subsonic and supersonic conditions for configuration 1, (without boundary layer thickeners) the peak pressure caused by the section of the ice bag clip ahead of the vent was as large as that caused by the aft field joint ring. Whereas for the configurations 2 and 5, with boundary layer thickeners the ice bag clip effect varied from approximately one-half of the field joint ring peak pressure coefficient ($M_0 = 0.90$, fig. 10(e), configuration 2) to about 0.08 higher ($M_0 = 1.40$, fig. 10(j), configuration 5).

The effect of vent flow on the pressure distribution is shown in figures 11 through 14. Generally, the effect of vent flow was to increase the pressure upstream of the vent and decrease the pressure downstream of the vent.

SUMMARY OF RESULTS

An experimental investigation was conducted in the Lewis Research Center 8- by 6-foot Supersonic Wind Tunnel to determine the discharge coefficients of the Centaur Standard Shroud/Liquid Hydrogen tank compartment vent. The test was conducted with full scale simulated flight hardware over a free-stream Mach number range of 0.70 to 1.96 with the vent and shroud configurations mounted to a flat plate. The flat plate was

flush mounted to the tunnel sidewall such that the centerlines coincided. Air was discharged through five 6.35 cm (2.50 in.) diameter vent orifices into the free-stream. Vent pressure ratio varied from 1.035 to 0.45.

The following observations were made:

1. Generally, the vent discharge coefficient is directly influenced by the boundary layer displacement thickness. The highest discharge coefficient, for a given Mach number and vent pressure ratio, usually occurred at the maximum boundary layer displacement thickness.
2. The analytically predicted displacement thickness for the vehicle nominal flight trajectory could be simulated over the Mach number range by using a boundary layer thickener.
3. The effect of the ice bag clip and aft field joint ring on the static pressure field was greatly influenced by the boundary layer characteristics. For example, without boundary layer thickeners, the peak pressures caused by the ice bag clip and the aft field joint ring were about the same. But with thickener rods, the peak pressure for the ice bag clip was less than that for the aft field joint ring up to Mach 1.20.
4. The effect of vent flow on the static pressure distribution was to increase the static pressure upstream of the vent region and lower the static pressure aft of the vent.

REFERENCES

1. Vick, Allen R.: An Investigation to Determine the Discharge and Thrust Characteristics of Auxiliary-Air Outlets for a Stream Mach Number of 3.25. NASA TN D-1478, 1962.
2. Kallioretene, C. A.; Leonor, A. P.; and Frandson, N. P.: Weight Flow Rates Through Circular Holes in a Flat Plate Immersed in a Subsonic or Supersonic Airstream. NOL-TR-61-125, U.S. Naval Ordnance Lab., 1963.
3. Callaghan, E. E.; and Bowden, D. T.: Investigation of Flow Coefficients of Circular, Square, and Elliptical Orifices at High Pressure Ratios. NACA TN 1947, 1949.
4. Struck, H. G.; and Barkins, J. A.: Compartment Venting and Pipe Flow with Heat Addition. NASA TM X-53734, 1968.
5. Walters, W. P.; Glasgow, R. M.; and Baker, J. M.: Generalized Gaseous Discharge Characteristics of Flat-Plate Orifices. (TR-794 S-435, Nortronics) NASA CR 20200, 1968.

6. Ramsey, P. E.: Flow Characteristics of Orifices for Venting Launch Vehicle Compartments. Research Achievements Review. Vol. 3: Aerophysics Research at Marshall Space Flight Center, NASA TM X-53799, 1968, pp. 25-34.
7. Compartment Venting: Space Vehicle Design Criteria. NASA SP-8060, 1970.
8. Johns, Albert L.; and Jones, Merle L.: Venting Characteristics of Gaseous Helium and Nitrogen Discharging into a Free Stream at Mach Numbers from 0.60 to 1.57. NASA TM X-2995, 1974.
9. Tucker, Maurice: Approximate Calculation of Turbulent Boundary-Layer Development in Compressible Flow. NACA TN 2337, 1951.

TABLE I. - MODEL STATIC PRESSURE INSTRUMENTATION

Region	Static pressure orifice number	%/REF
Plate	1	-84.67
	2	82.67
	3	80.67
	4	72.67
	5	70.67
	6	68.57
	7	65.67
Upstream trough	100	64.67
	101	58.67
	102	52.67
	103	46.67
	104	42.67
	105	39.67
	106	37.67
	107	36.67
Upstream vent	108	31.23
	109	28.42
Below vent	203	23.42

Region	Static pressure orifice number	X/LAST
Downstream of vent	110	-23.79
	111	21.29
	112	18.39
	113	14.09
Vent region off center-line $z=9.11\text{cm}(3.6\text{in})$ $r=1.97\text{cm}(5.50\text{in})$ $z=13.07\text{cm}(5.50\text{in})$	115	26.77
	119	26.77
	120	19.09
Downstream trough	111	6.36
	115	3.30
	116	1.50
	117	.57
Downstream crest $z=6.60\text{cm}(2.50\text{in})$	200	6.36
	201	4.36
	202	2.30
Aft field joint ring	300	0
	301	.4
	302	.5

PRECEDING PAGE BLANK NOT FILMED

TABLE II. - CONFIGURATION SUMMARY

Configuration		Boundary-layer thickener	Aft field joint ring
Symbol	Number		
0	1	None	Installed
◊	2	4 rows- 12.70cm(5.00in) height rods (18 rods per row)	Installed
△	3	None	Removed
□	4*	None	Removed
△	5	1 row- 12.70cm (5.00in) height rods. 1 row- 7.62cm (3.00in) height rods. 18 rods per row.	Installed

*Pressure data, vent plugged.

Tunnel station: 344.68 (135.20) 437.39 (172.20) 681.23 (268.20) 715.01 (281.51)



38.1 (15.0)

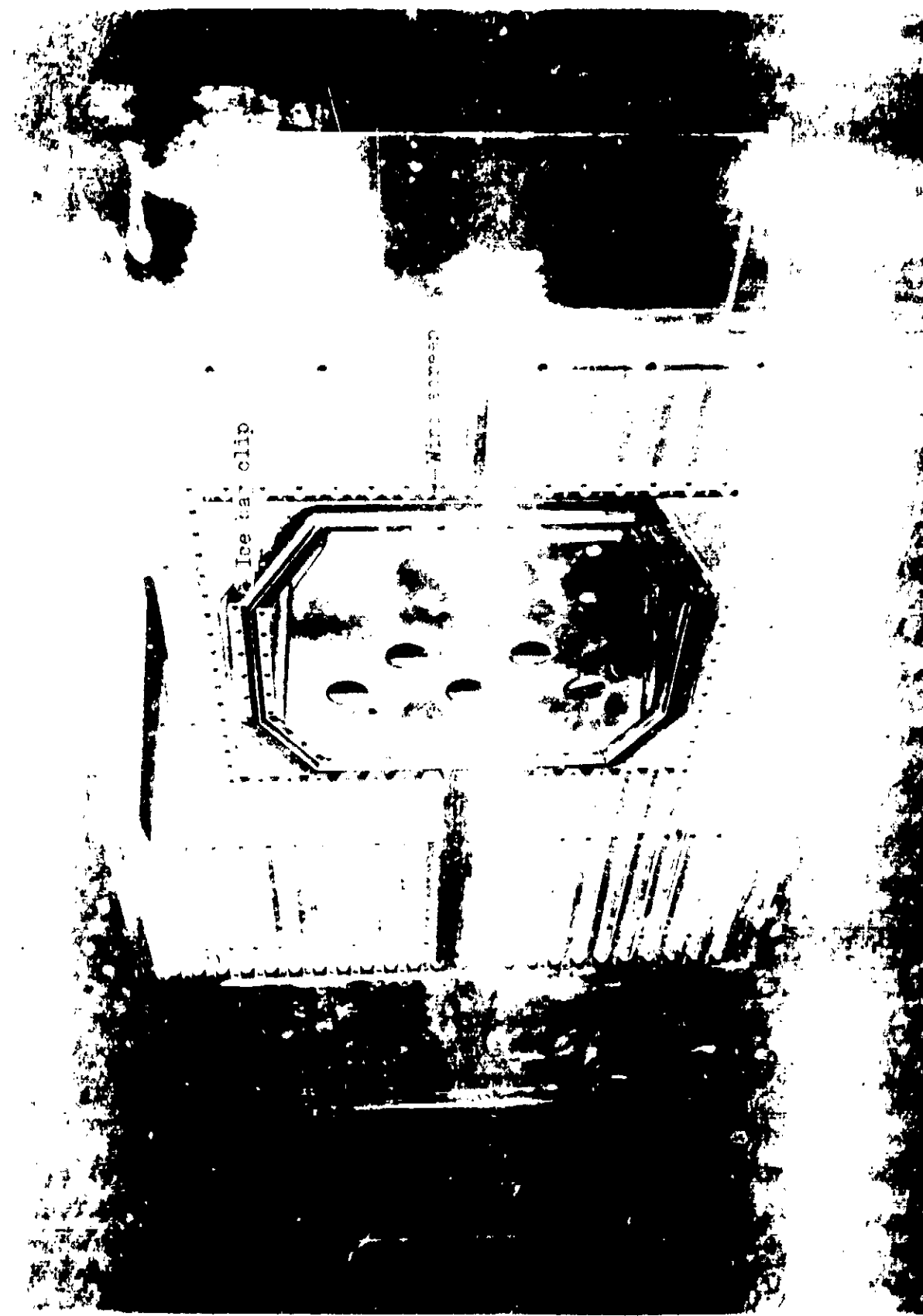
Boundary-layer
thickener plate

1.27(0.50) Thk. alum. plate
mounted on the south sidewall

REVERSING PAGE BLANK NOT FILMED

(a) Schematic of test installation

Figure 1. - Test installation in 8- by 6-
Foot Supersonic Wind Tunnel.
(Dimensions are in centimeters
(in).)



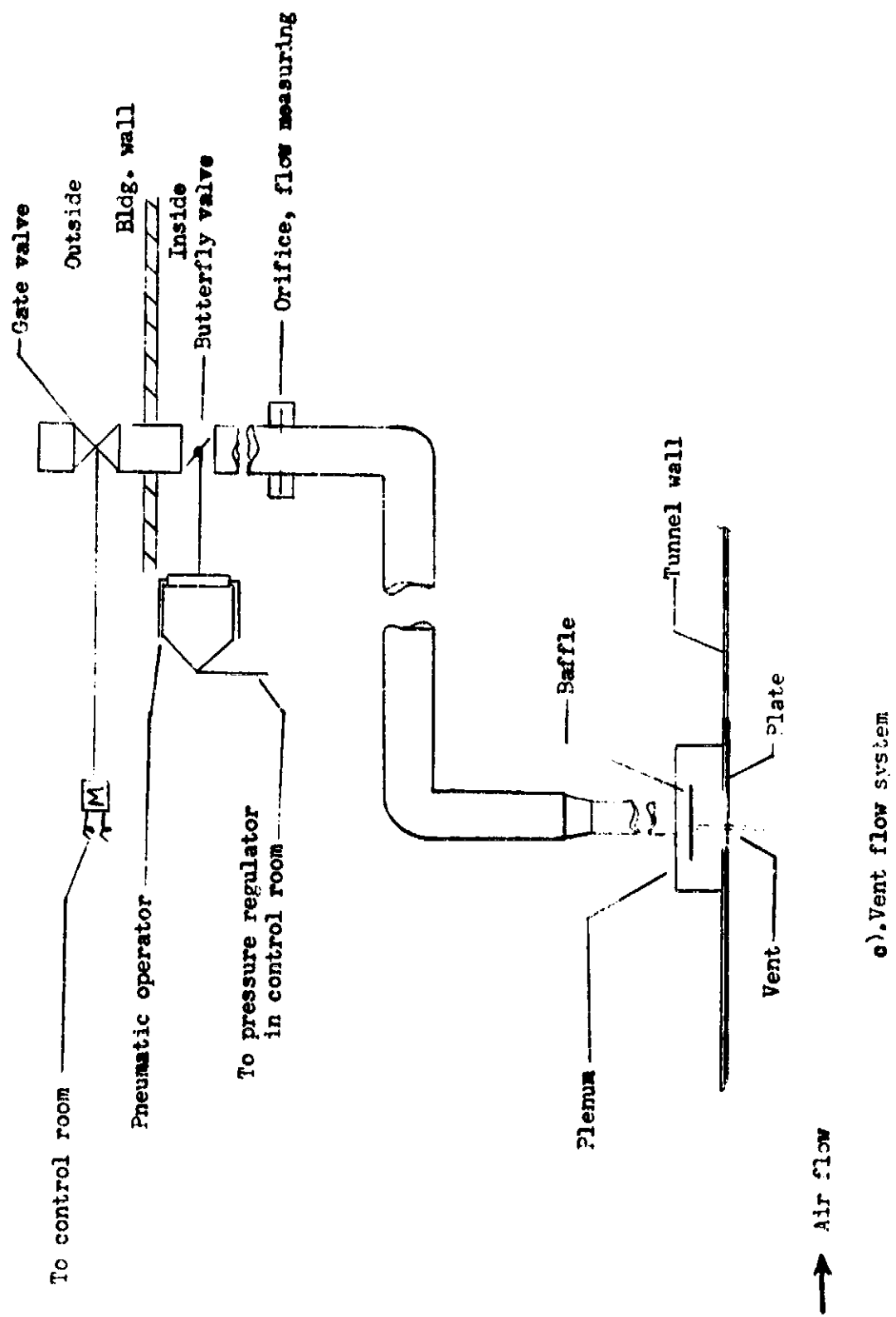
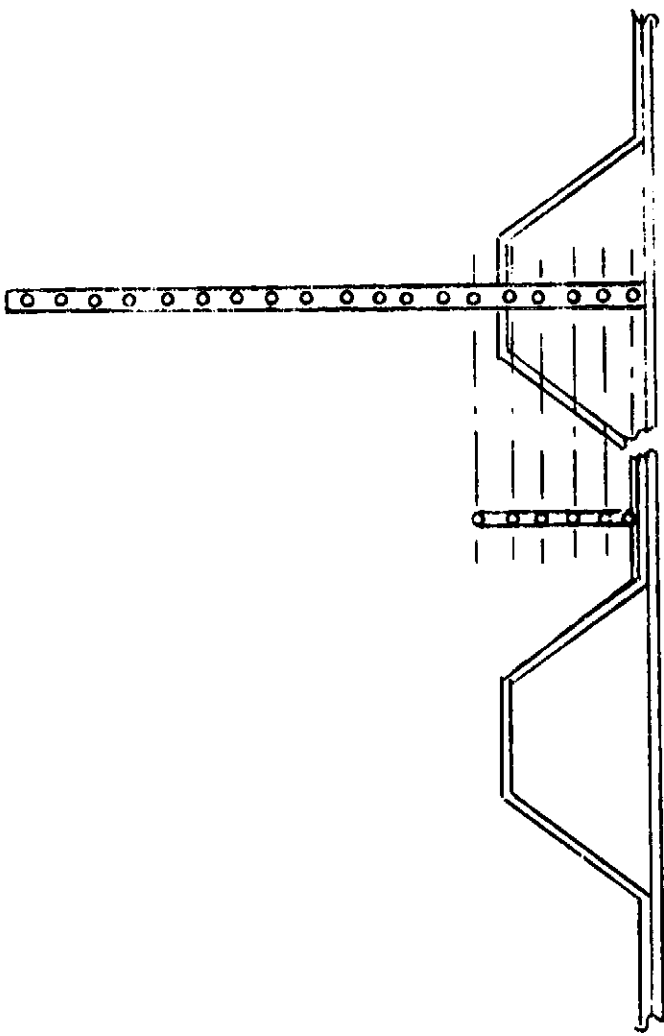


Figure 1.-Continued.

a). Vent flow system

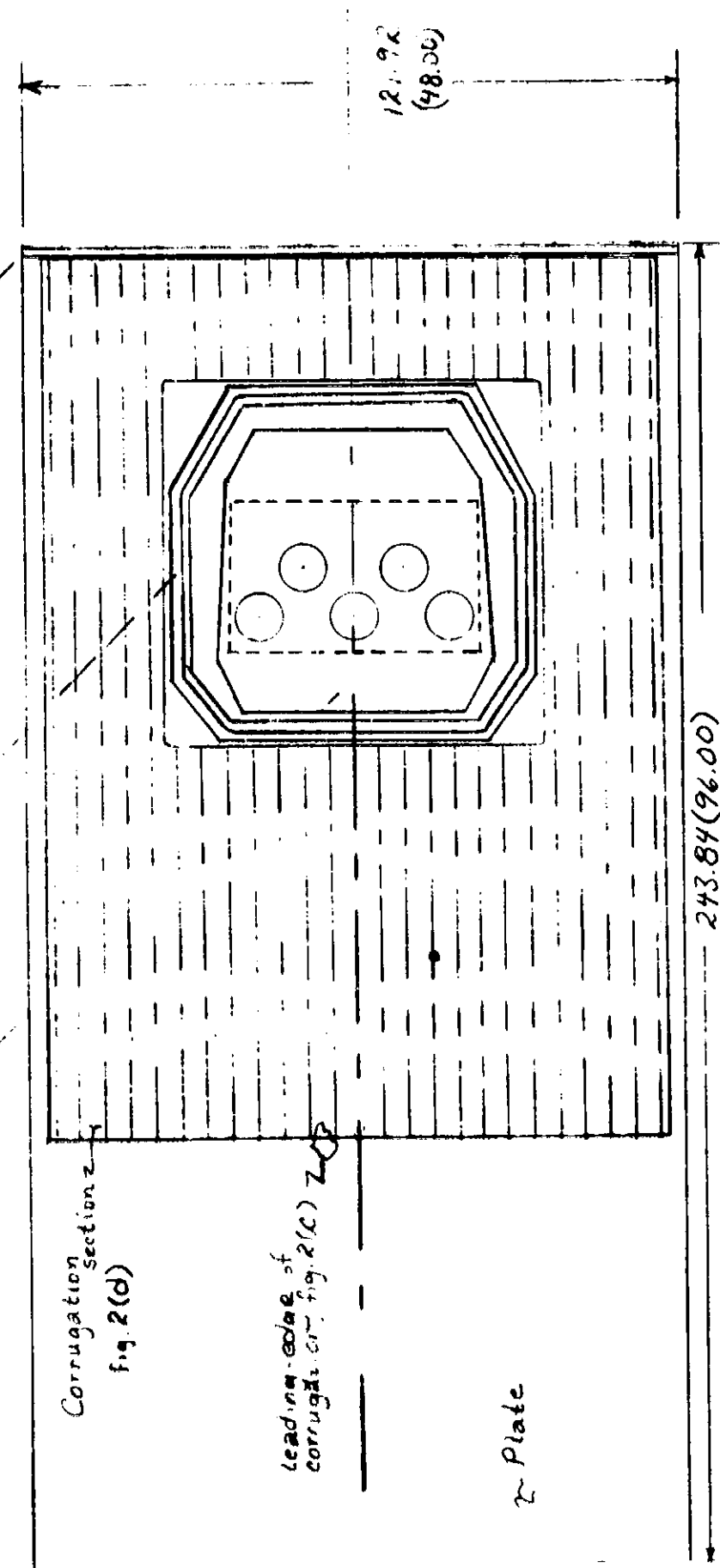


(d) Schematic of boundary-layer survey
rake installation

Figure 1. - Concluded

Vert details, figures 2 (g & h)

- field joint ring, fig. 2(i)
- ice bag clip, fig. 2(f)



(a) Assembly of test hardware

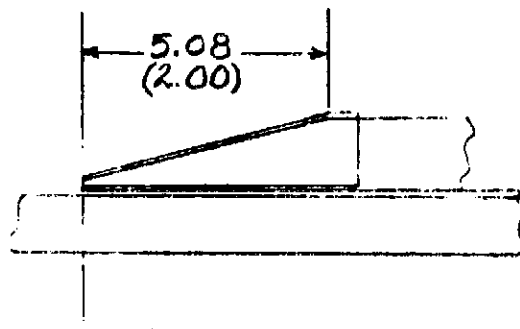
Figure 2. - Details of test geometry.
(Dimensions are in centimeters
(in).)

ORIGINAL PAGE IS
POOR QUALITY



(A) Three-quarter view (A)

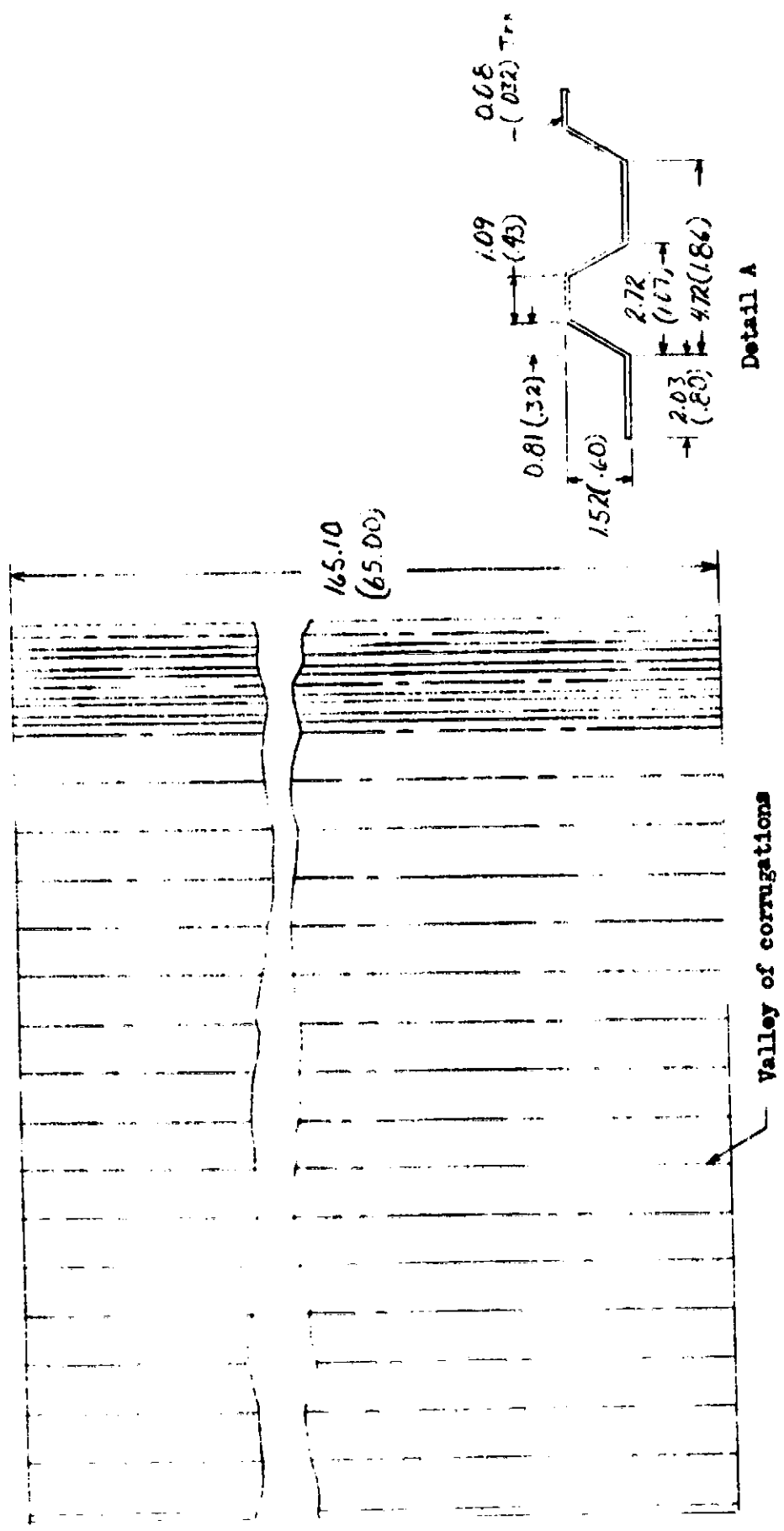
100% - 100% - 100%



Tunnel station: 513.77 (202.27)

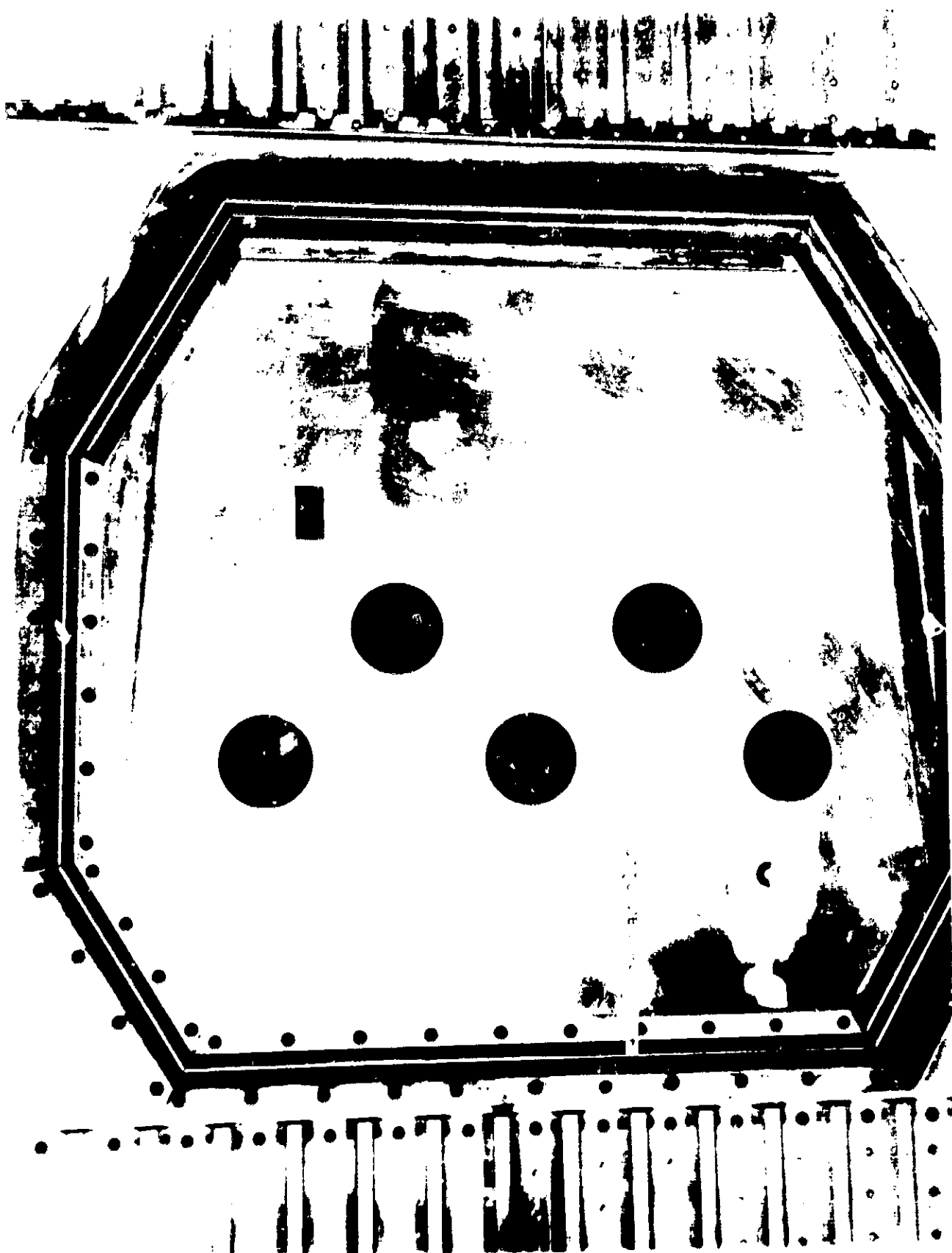
(c) Leading-edge of corrugation details

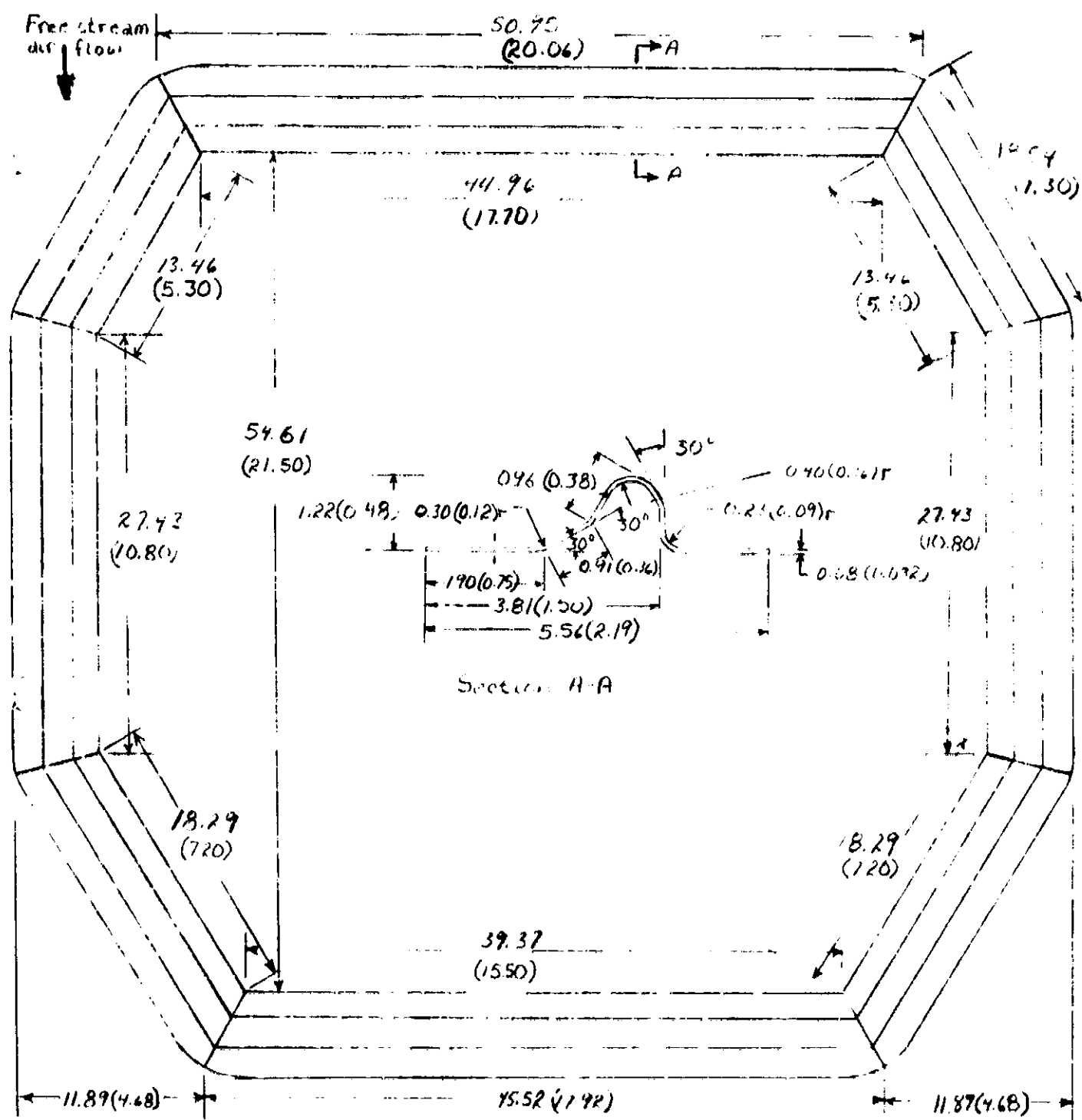
Figure 2. - Continued



(d) Corrugated panel and cross section details

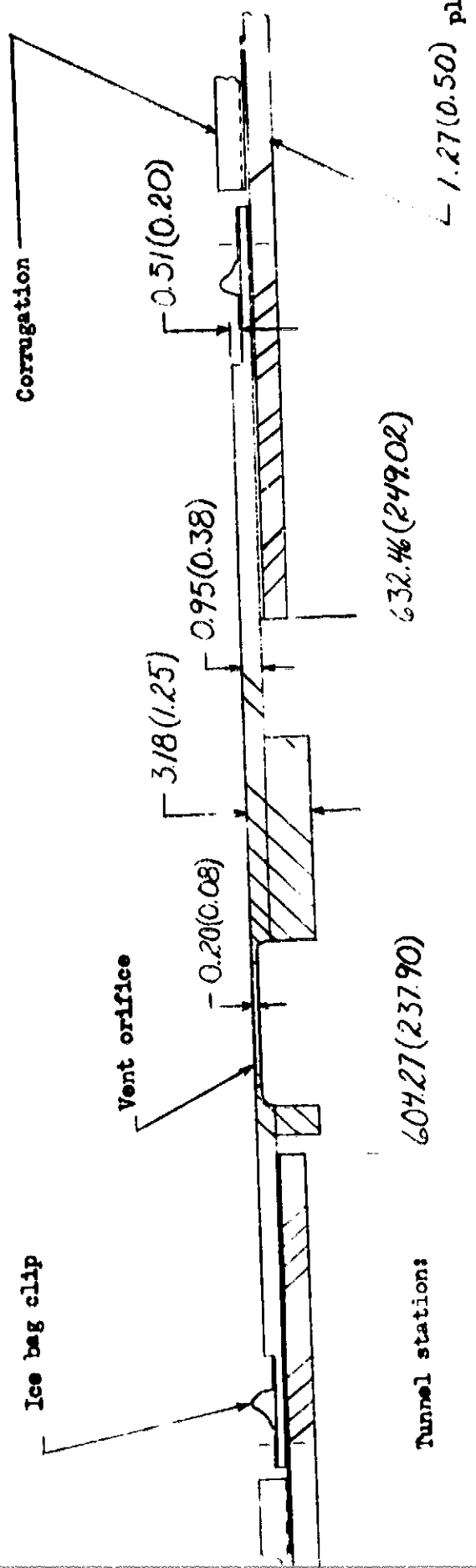
Figure 2. - Continued





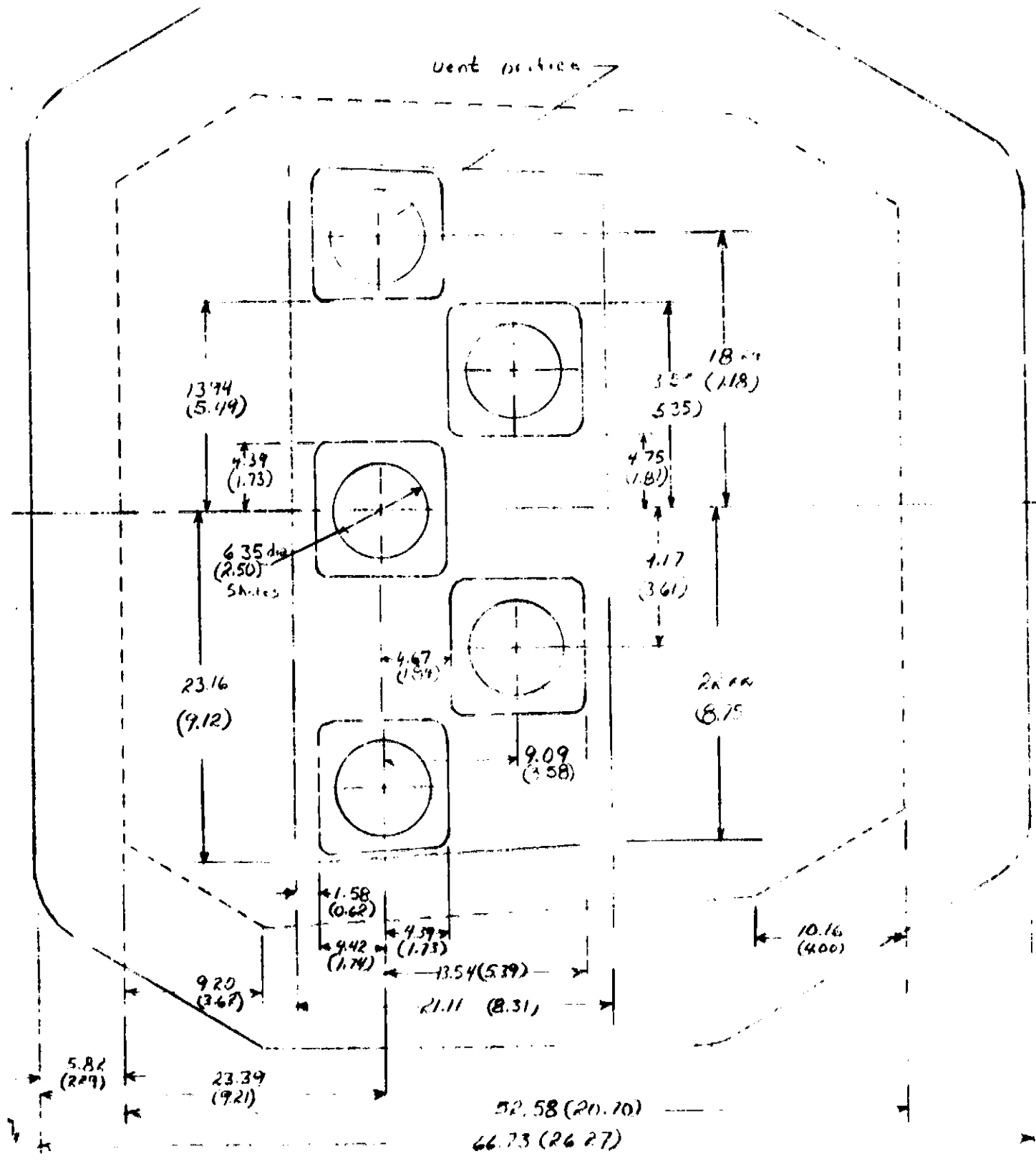
(f) Tee bag chip details

Figure 2. - Continued



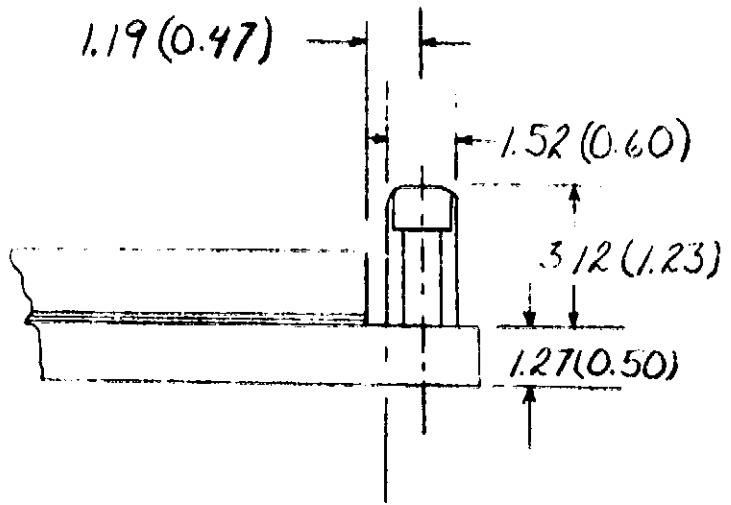
(g) Cross section of vent

Figure 2. - Continued



(b) Internal vent details

Figure 2. - Continued



Tunnel station: 679.0(267.4)

(i) Details of field joint ring

Figure 2. - Concluded

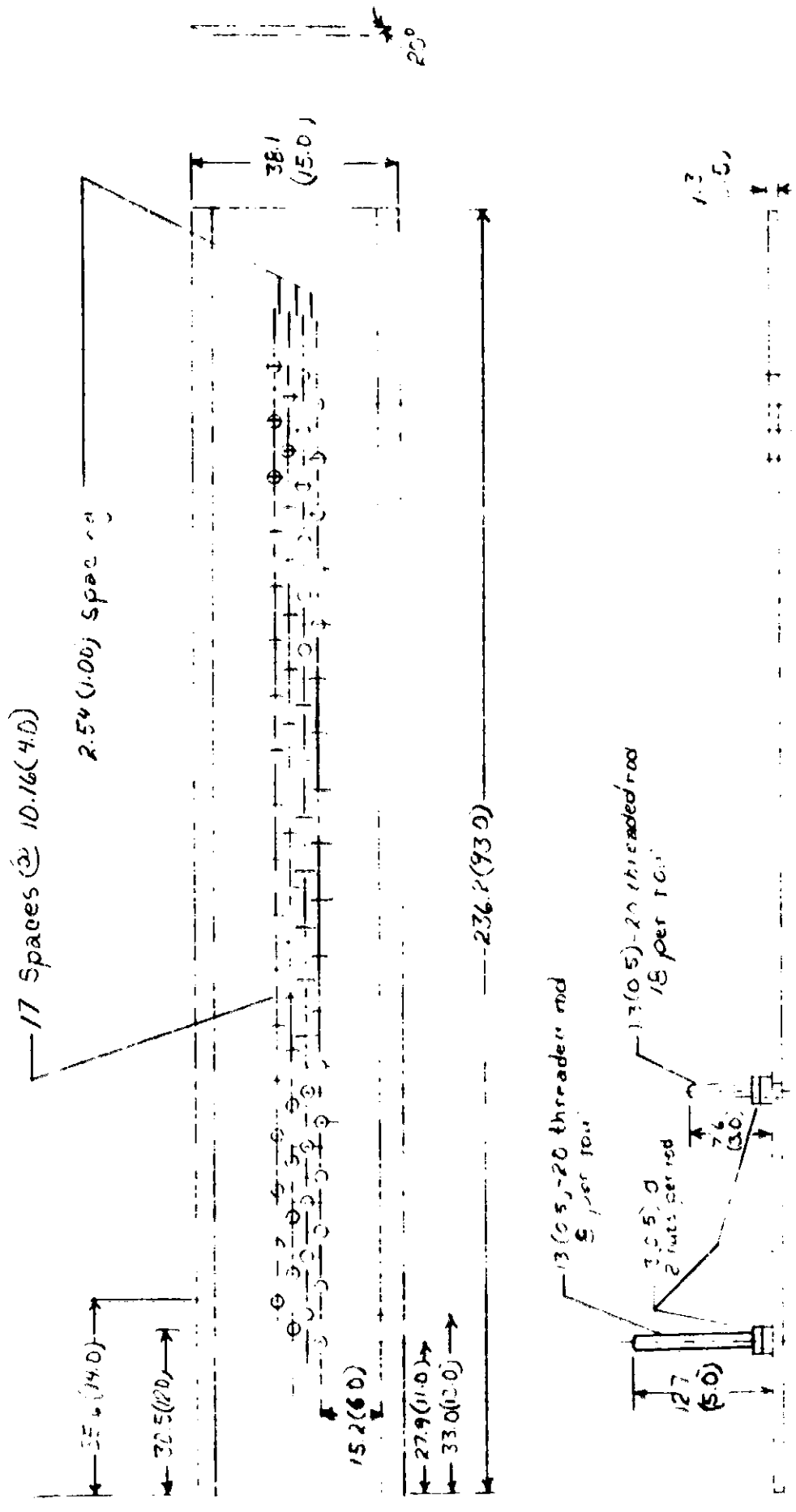
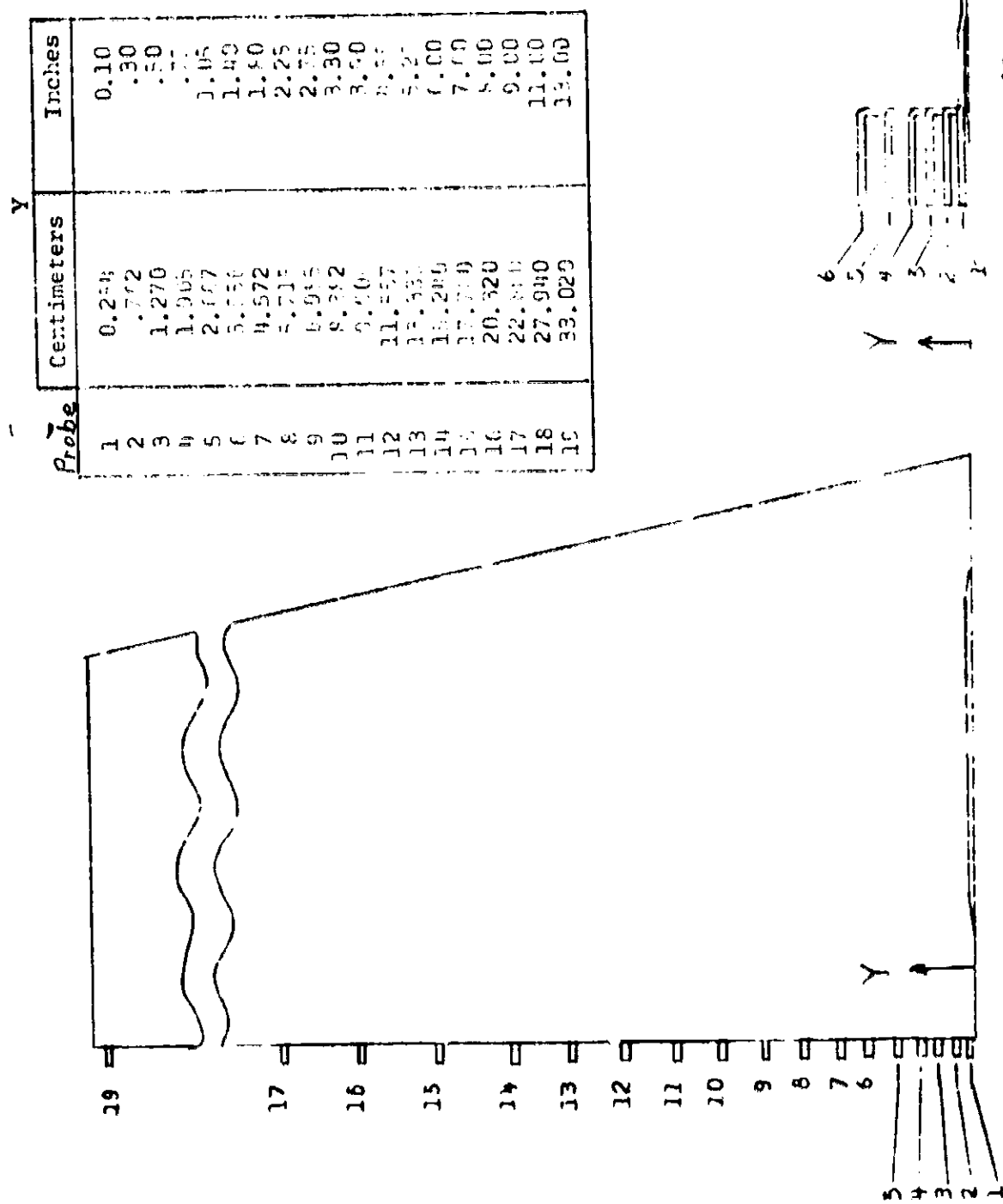


Figure 3. - Details of boundary-layer
thickeners. (Dimensions are
in centimeters (in).)

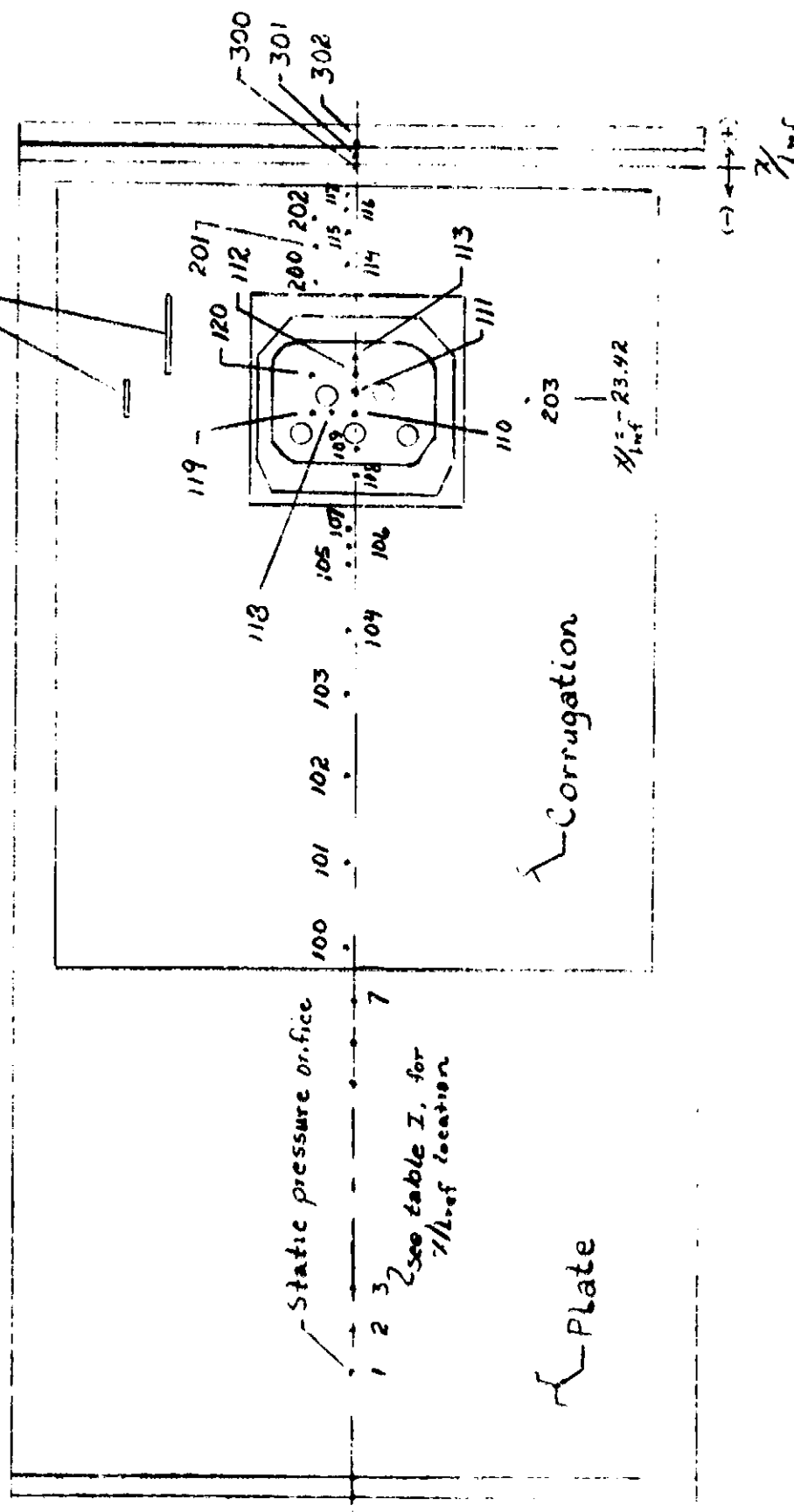


619.77cm (244.02m)
51.56cm (20.30in)
-23.40

(a) Boundary-layer survey rakes

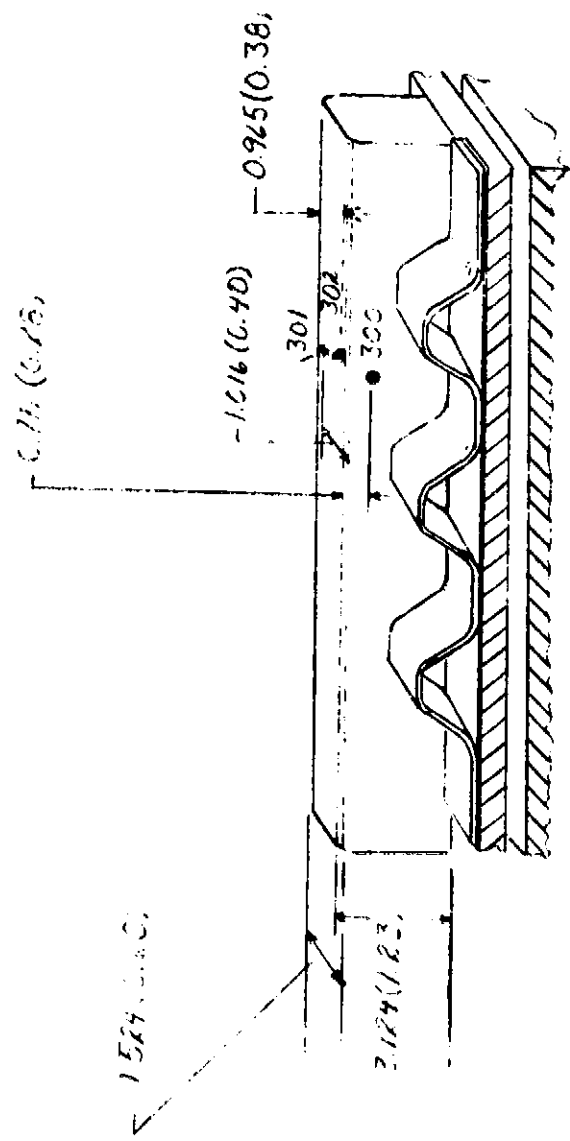
Figure 4. - Instrumentation

Boundary-layer survey rakes



(b) Model instrumentation

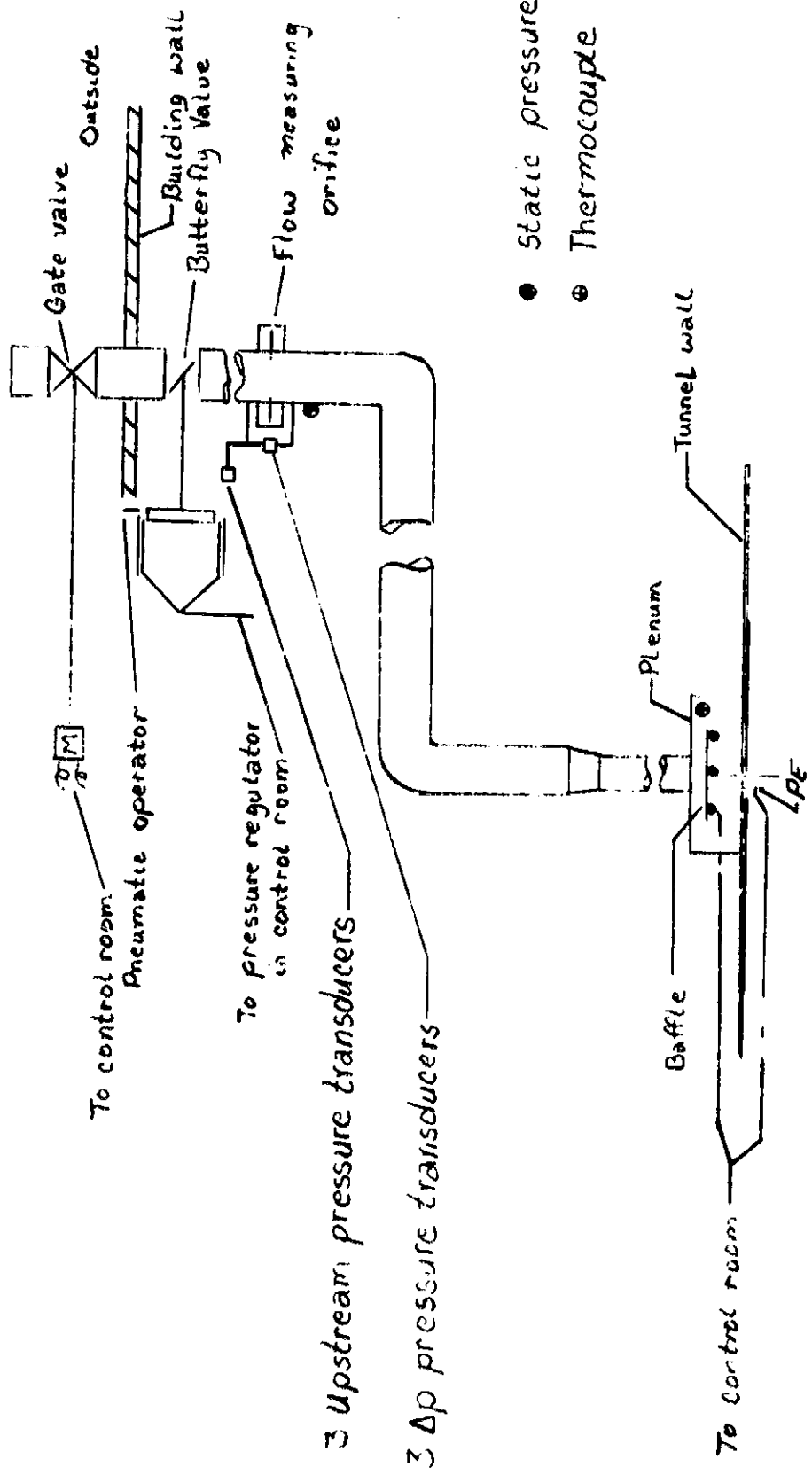
Figure 4. - Continued



• Static pressure orifice

(c) Field joint ring instrumentation

Figure 4. - Continued



(d) Plenum and flow system instrumentation

Figure 4. - Concluded

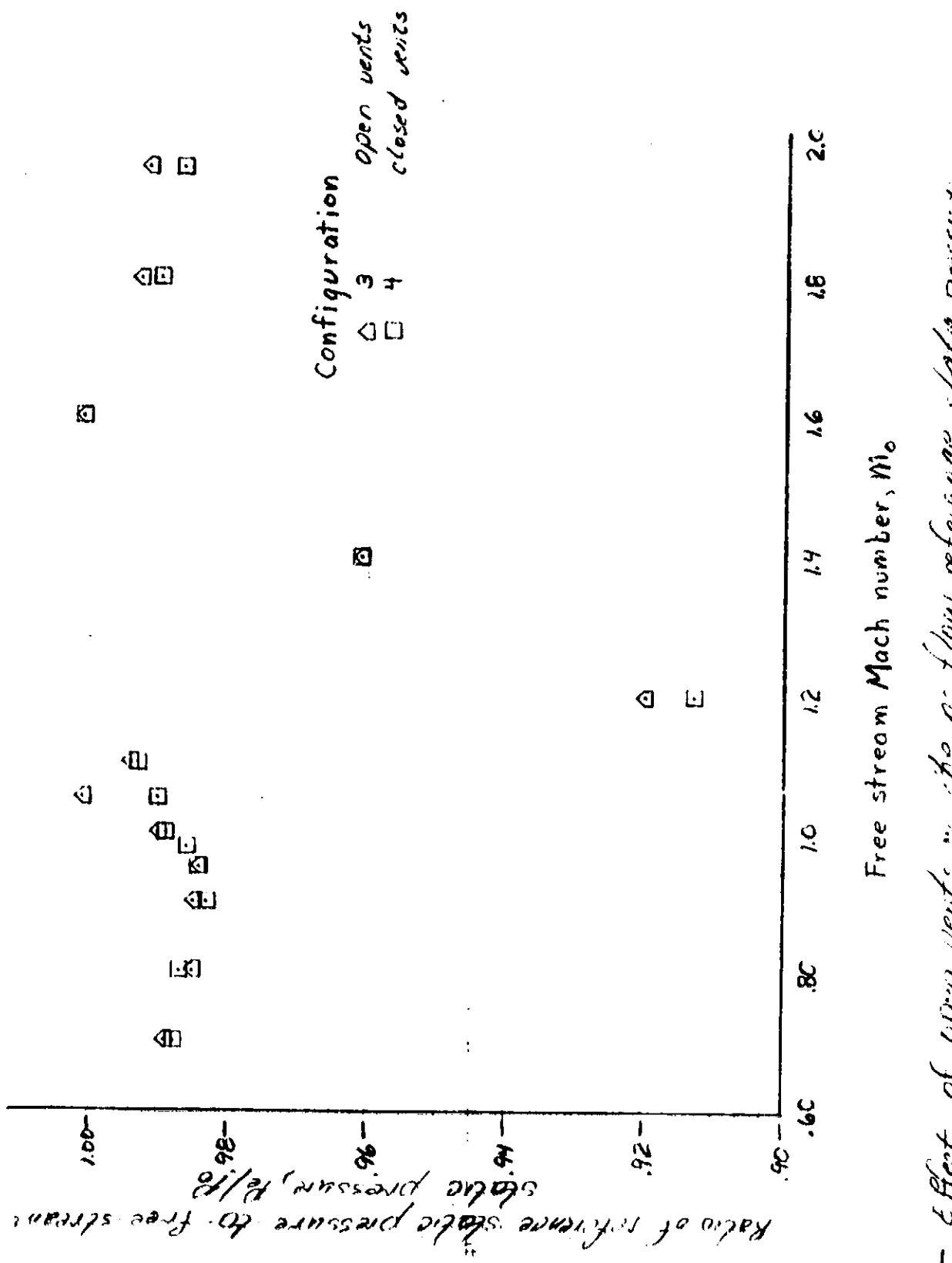


Figure 5—Effect of open vents on the flow reference static pressure.

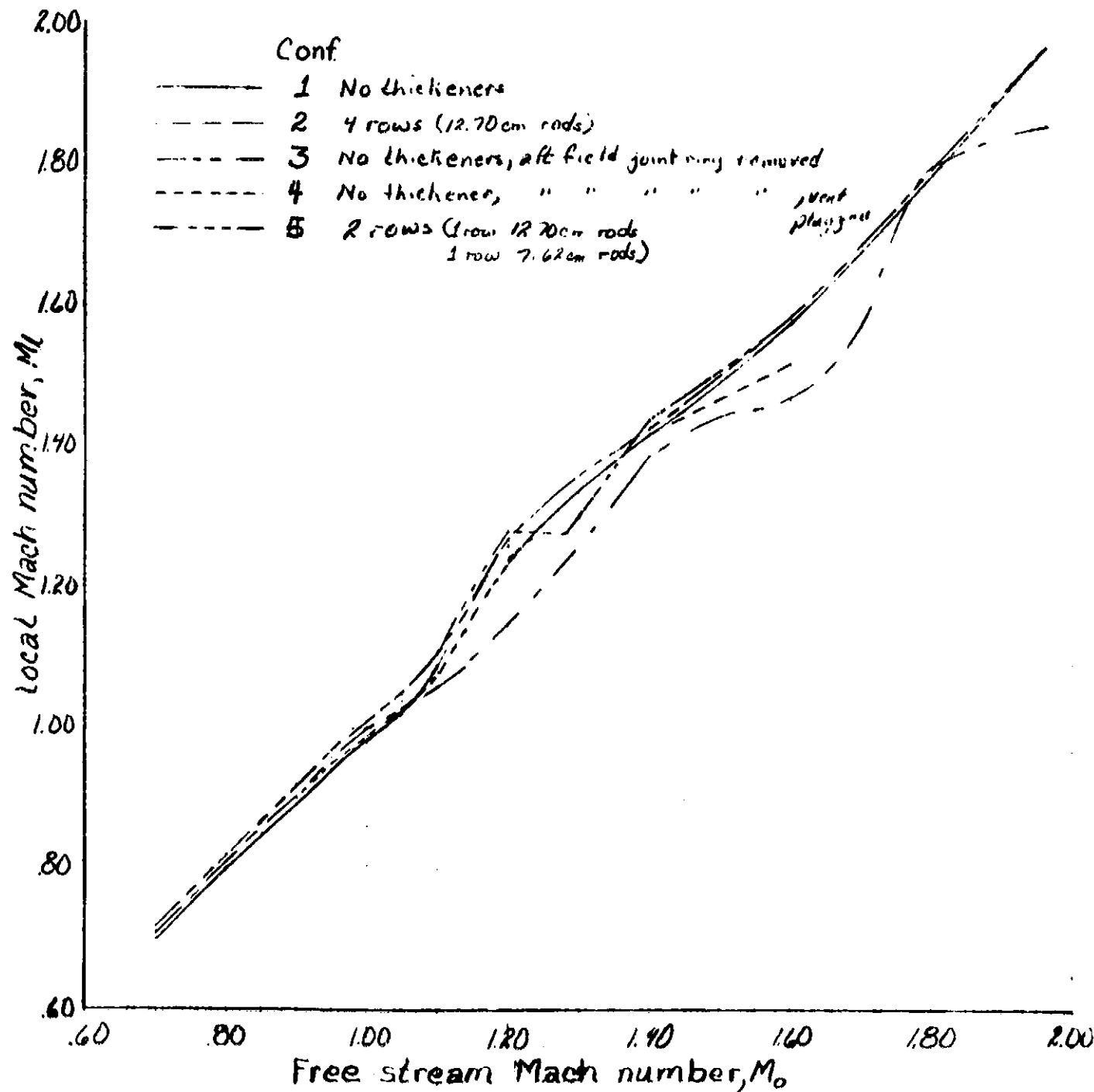


Figure 6.— Local Mach number, M_l , for no vent flow as a function of the free stream Mach number.

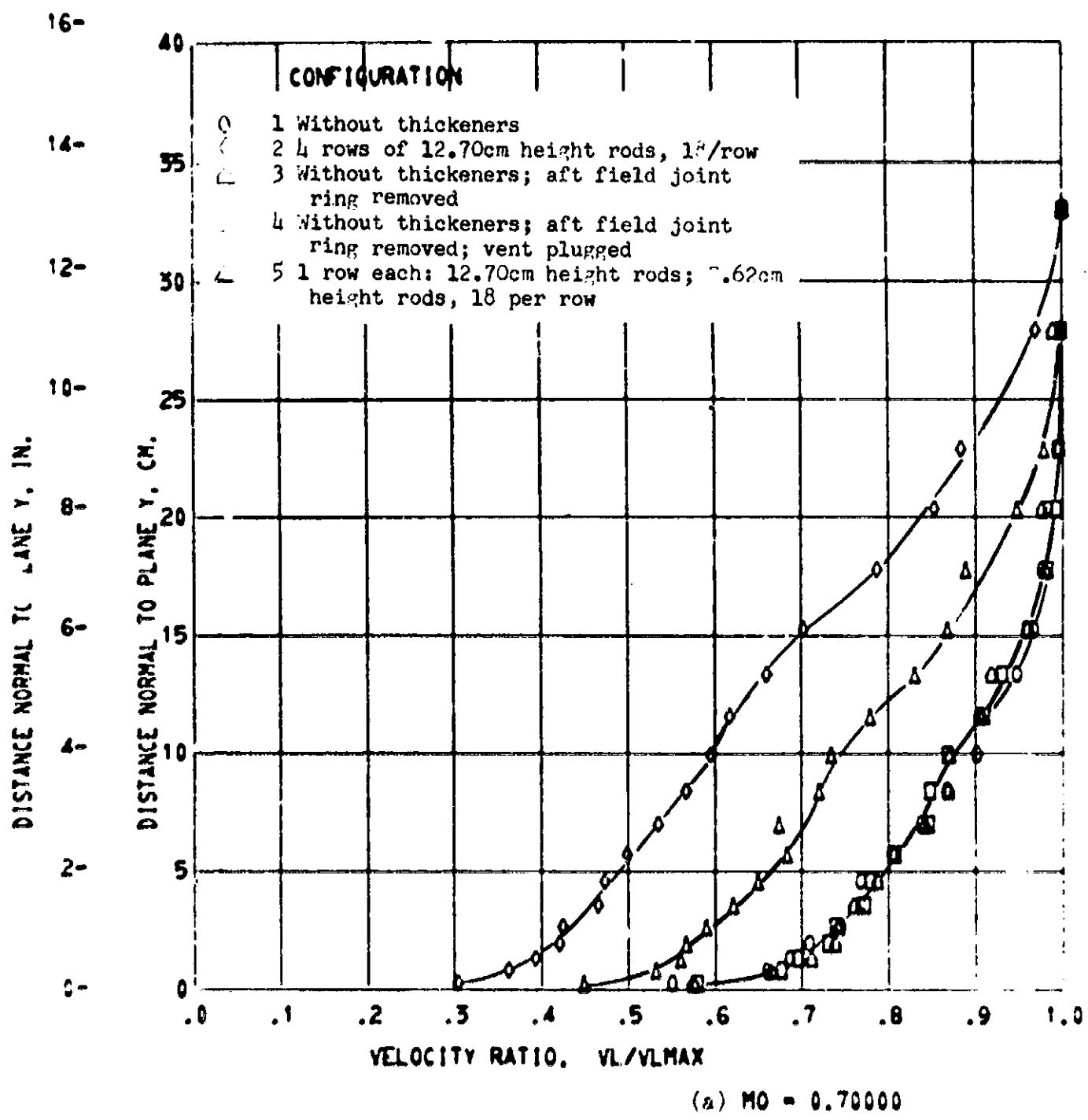


Figure 7. - Boundary-layer velocity profiles.

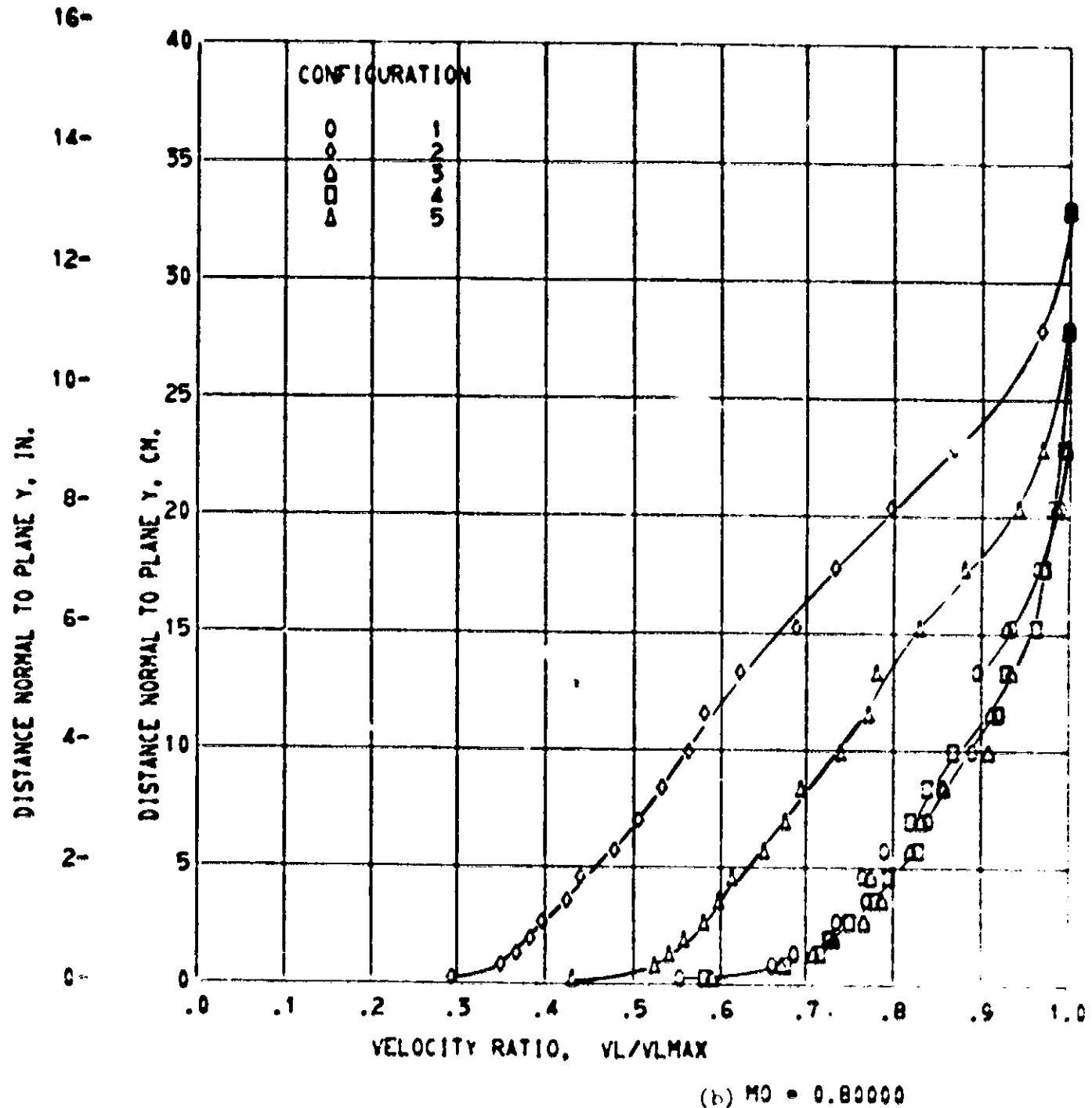
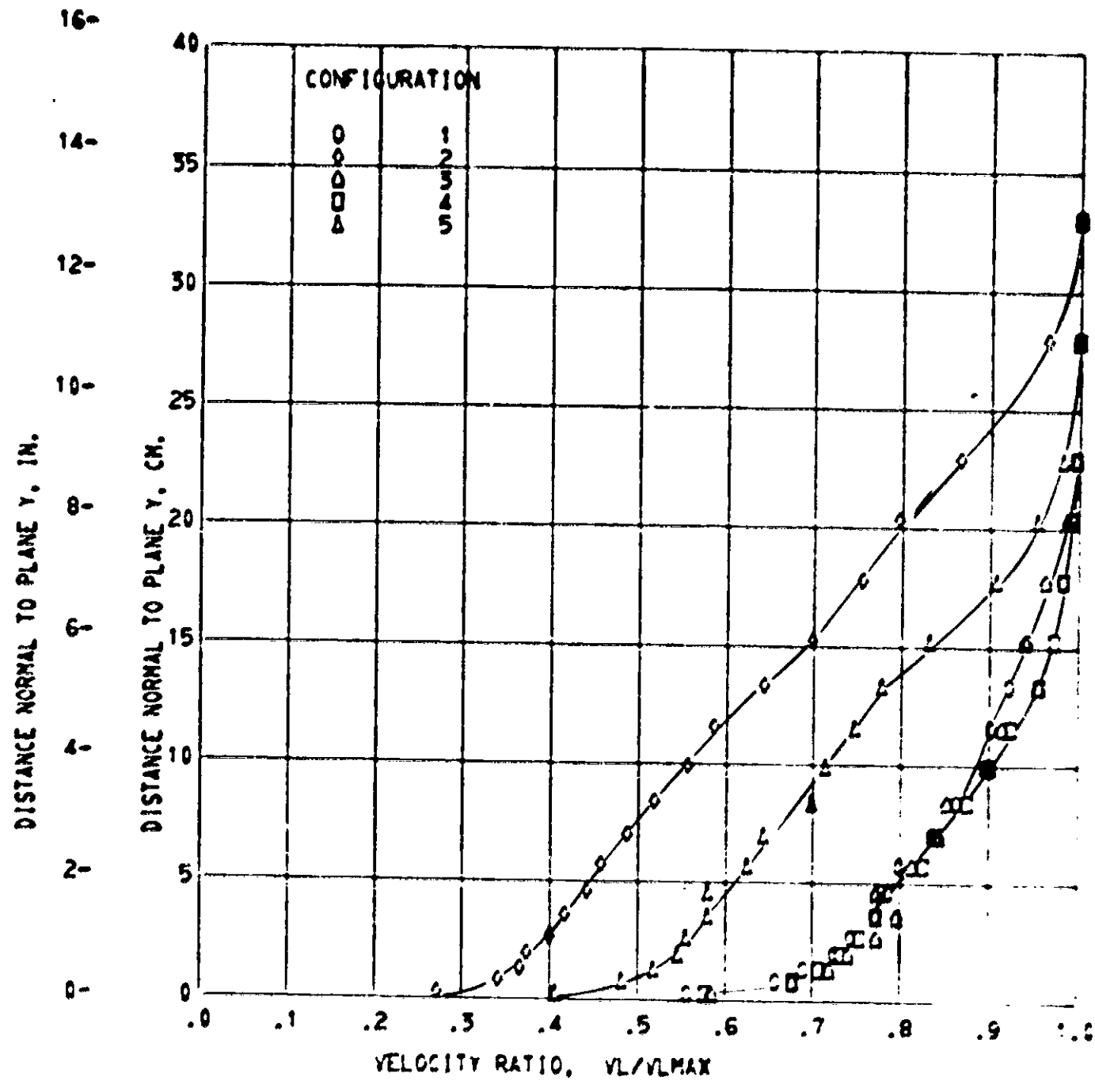


Figure 7. - Continued.



$$(a) M_0 = 0.9666$$

Figure 7. - Continued.

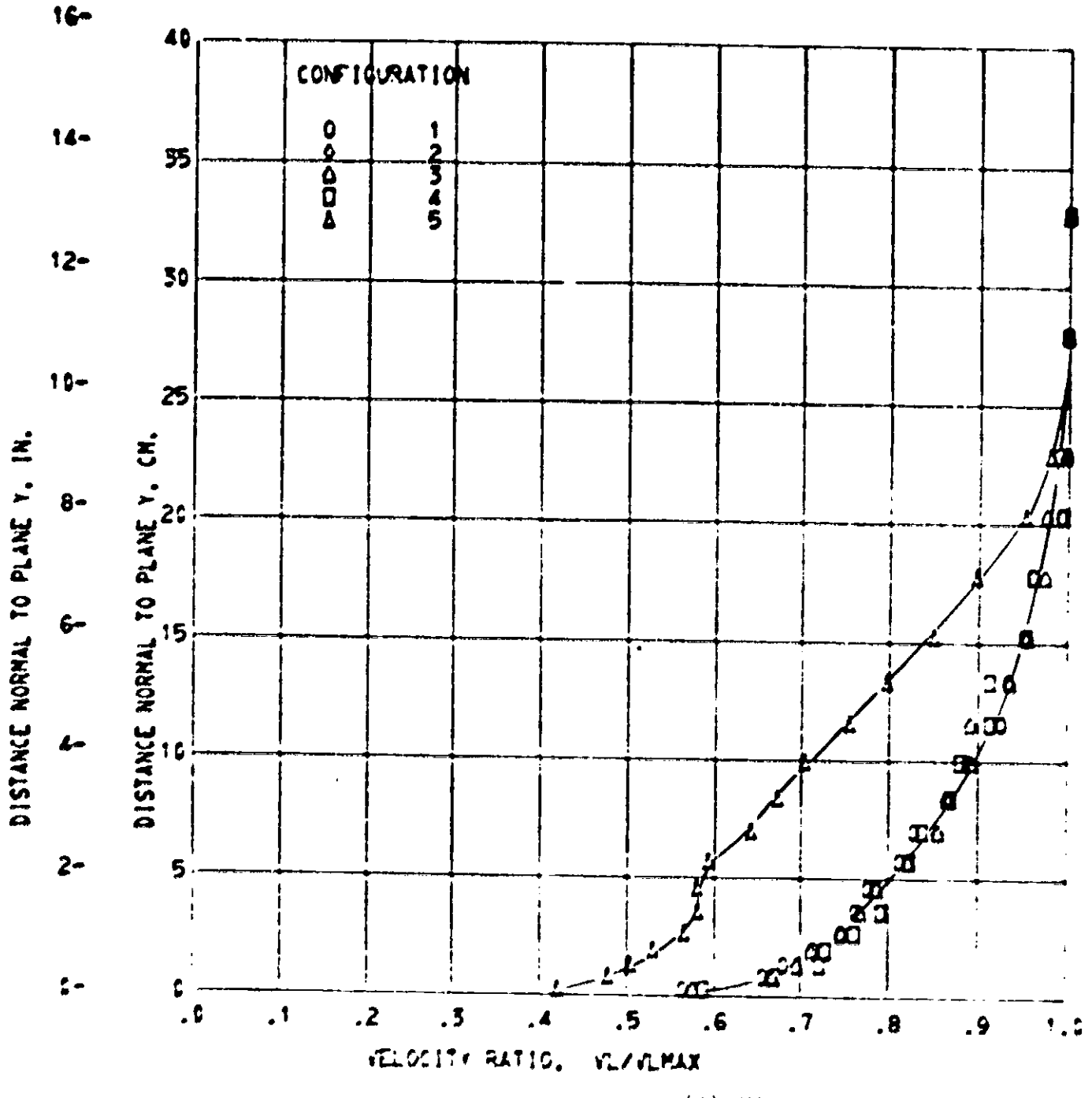


Figure 1. - (continued).

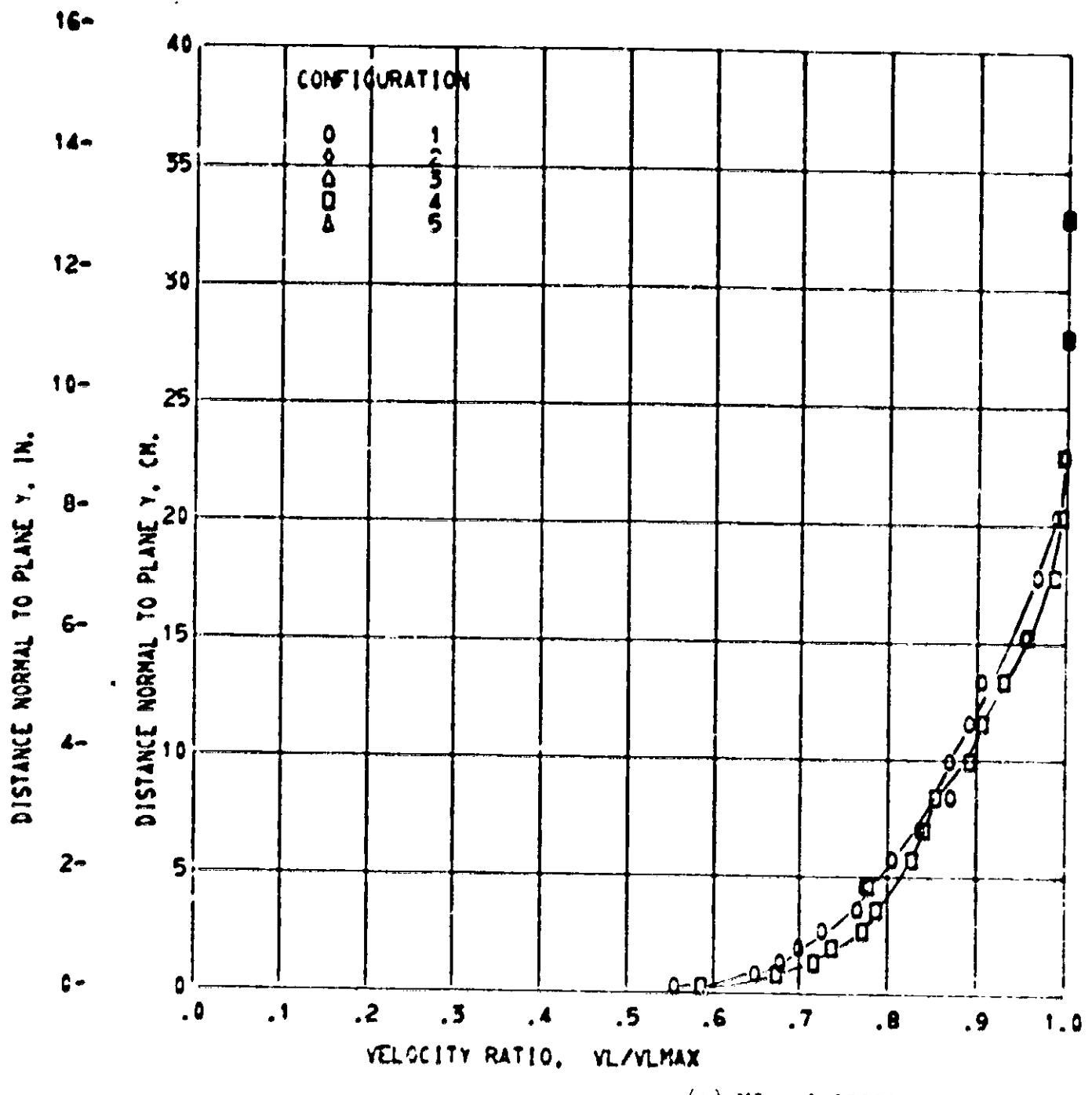


Figure 7. - Continued.

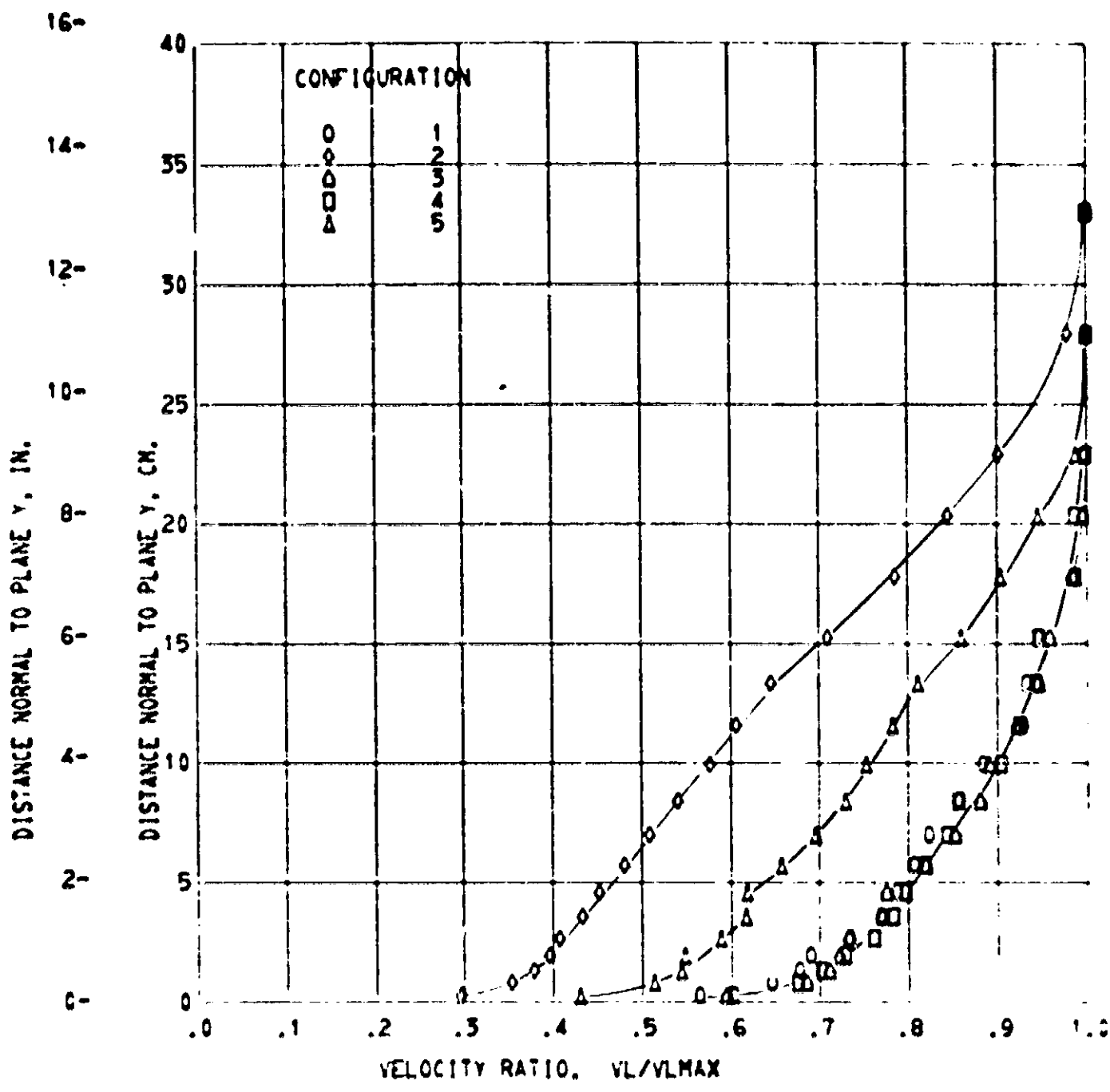
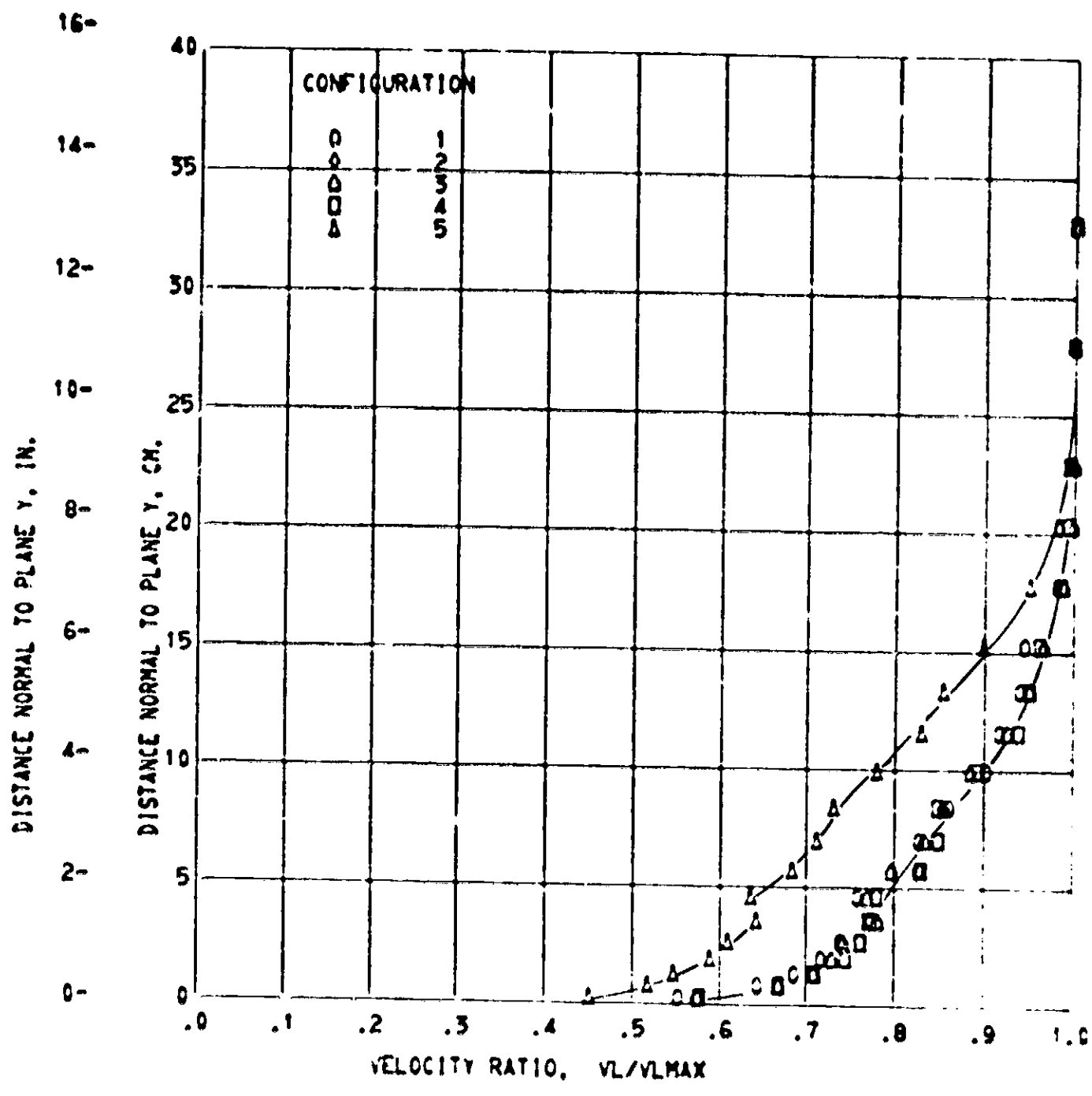
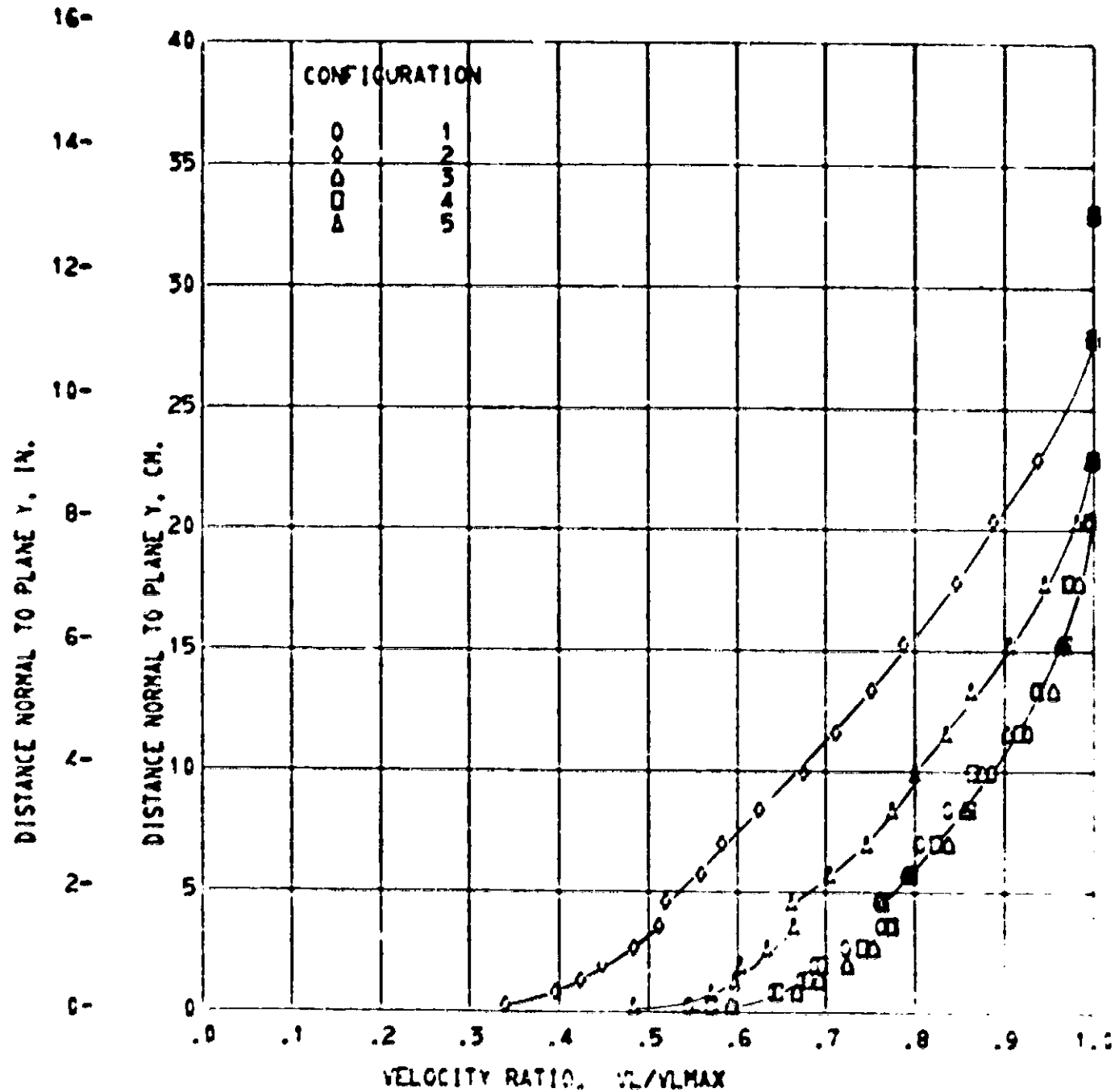


Figure 7. - Continued.



$(\rho) M_0 = 1.0500$

Figure 7. - Continued.



(h) $M_0 = 1.1000$

Figure 7. - Continued.

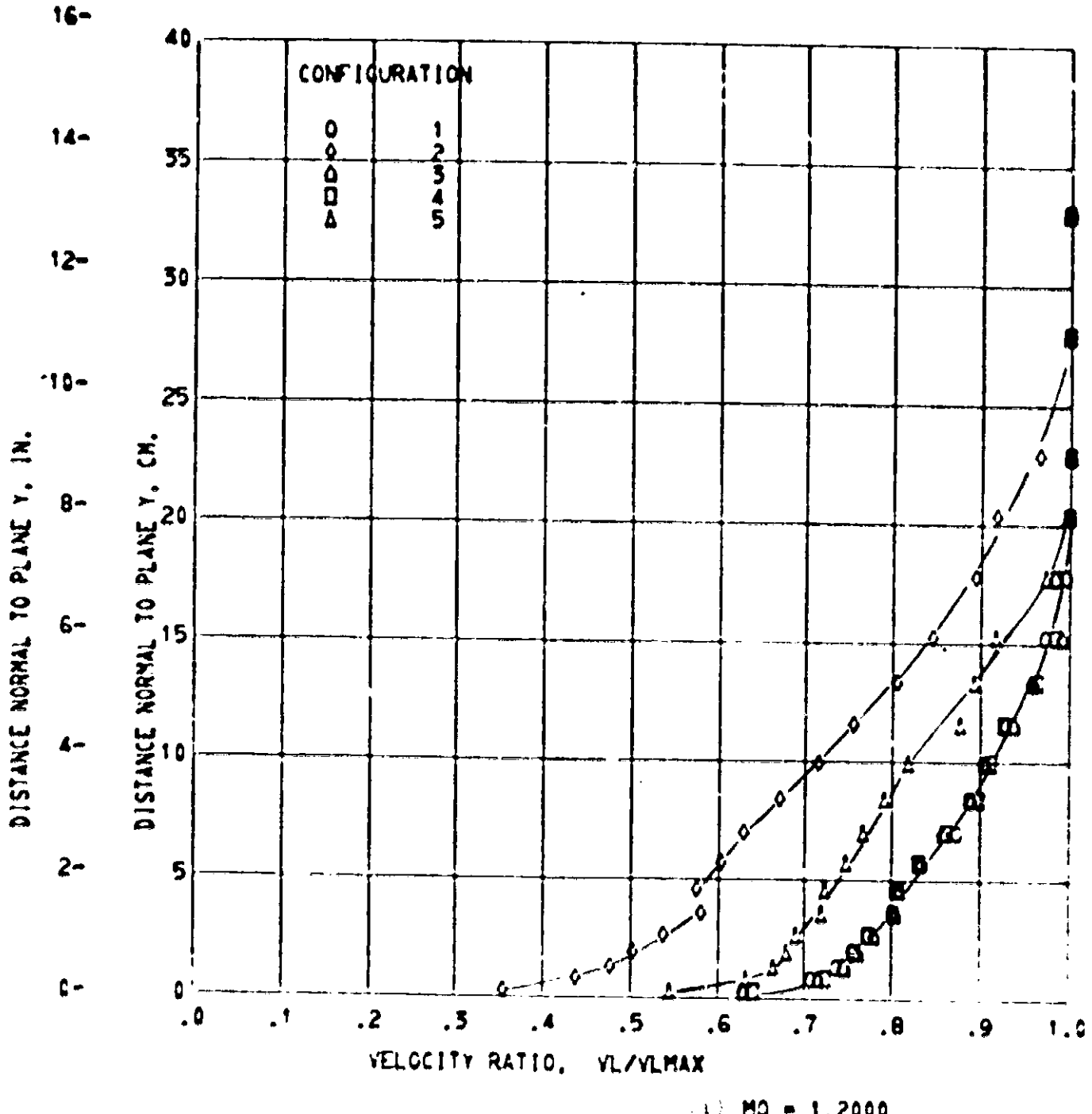
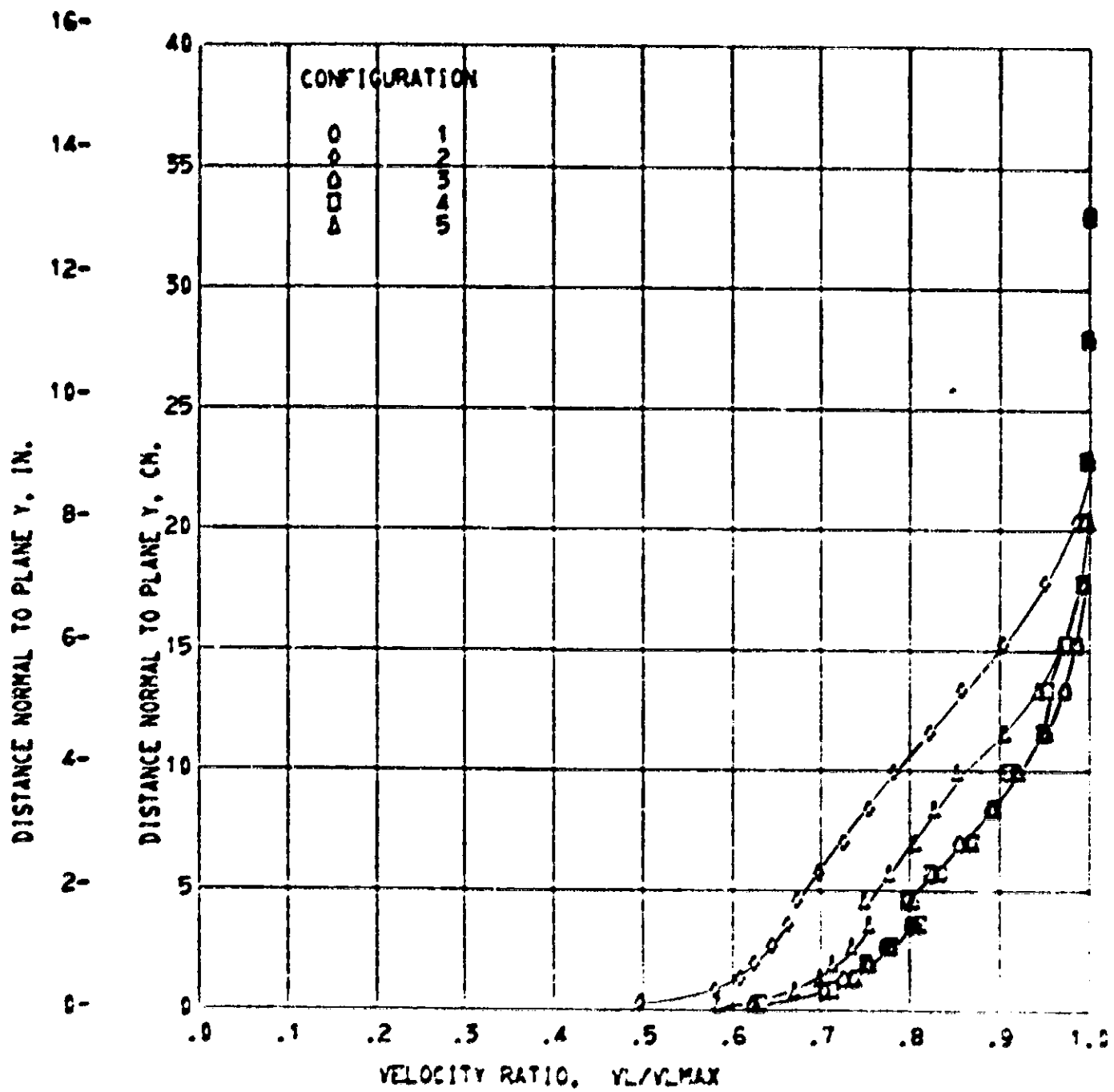


Figure 7. - (continued).



(j) $M_0 = 1.4669$

Figure 7. - Continued.

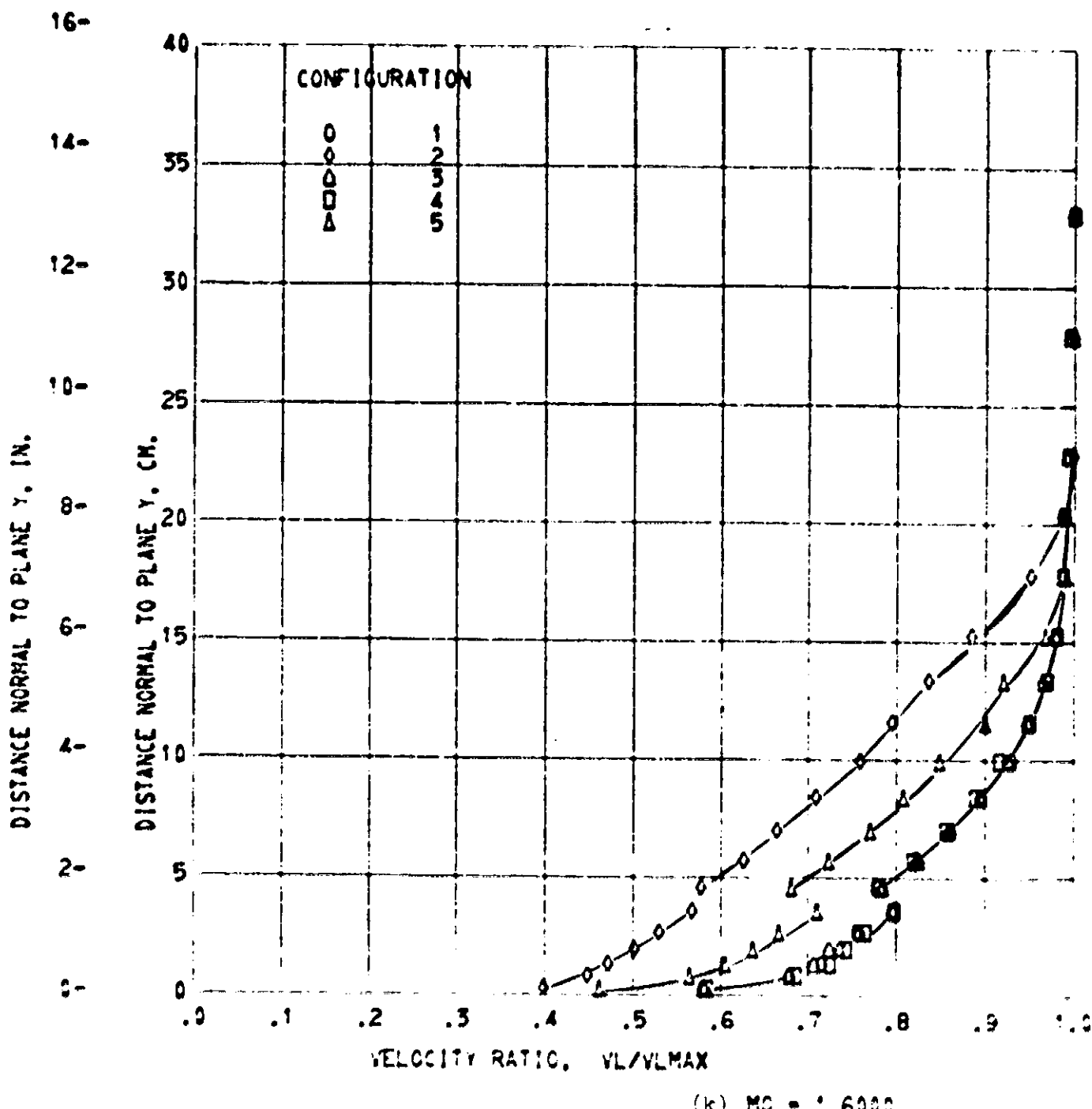


Figure 7. - Continued.

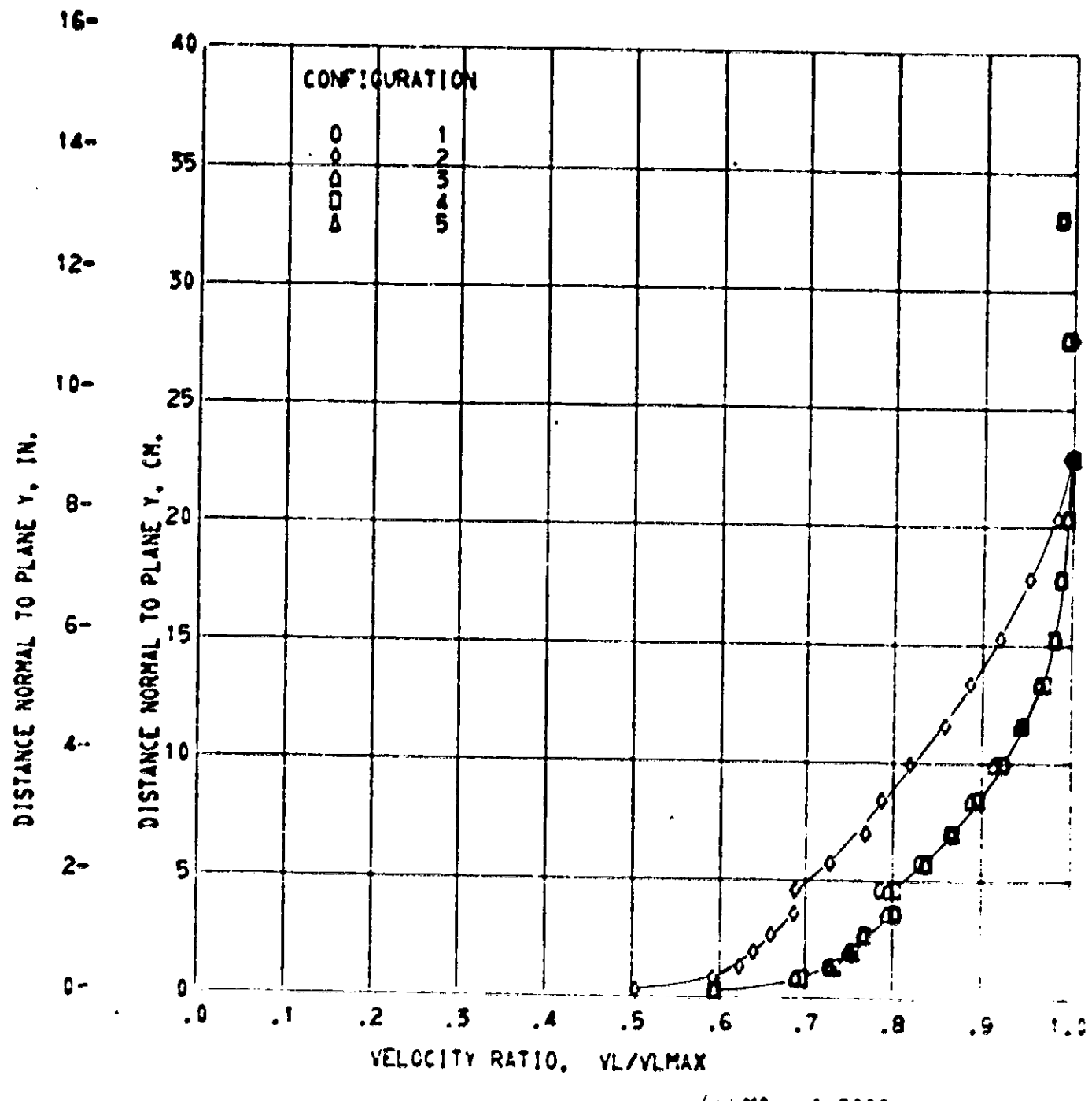
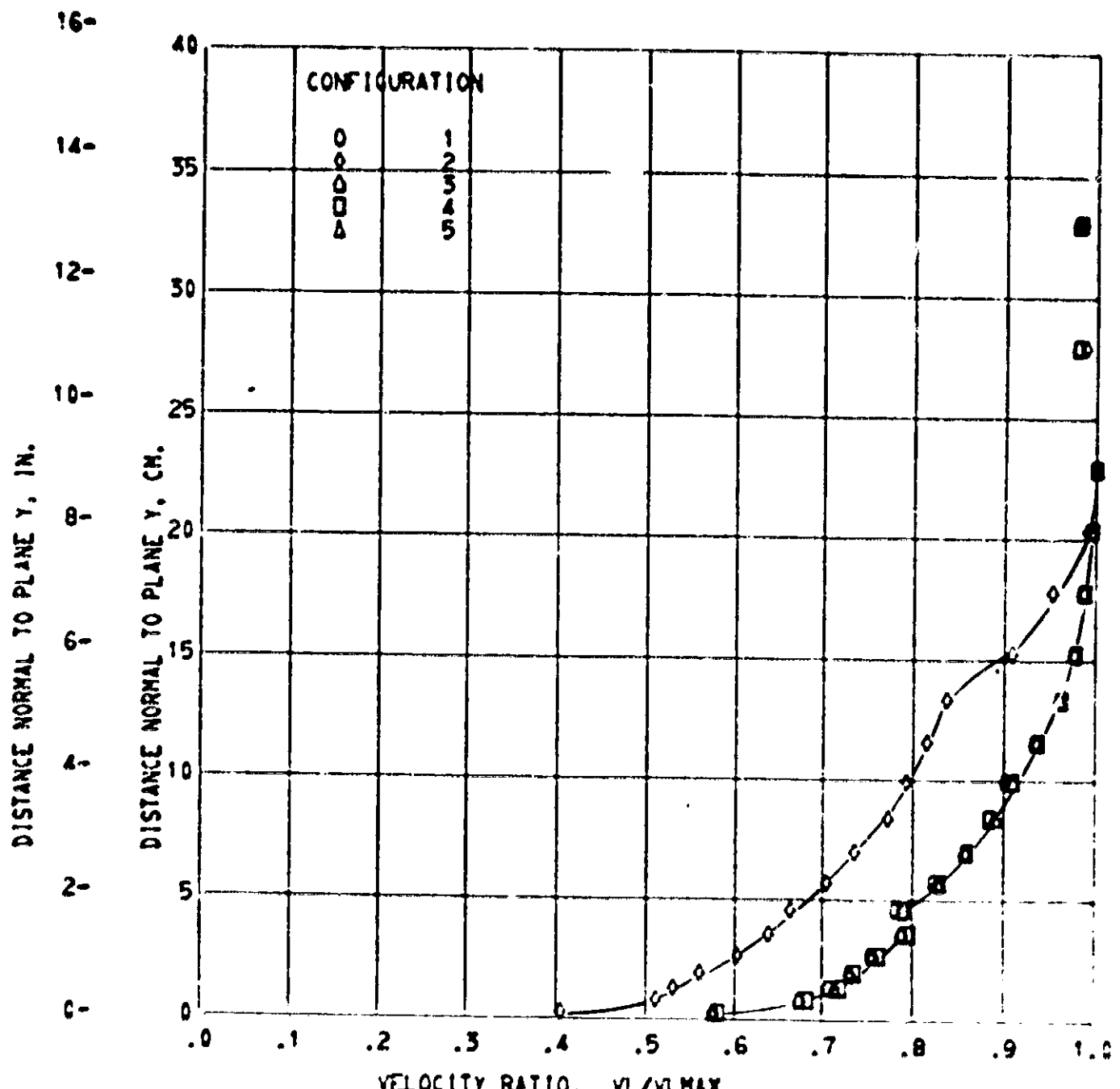


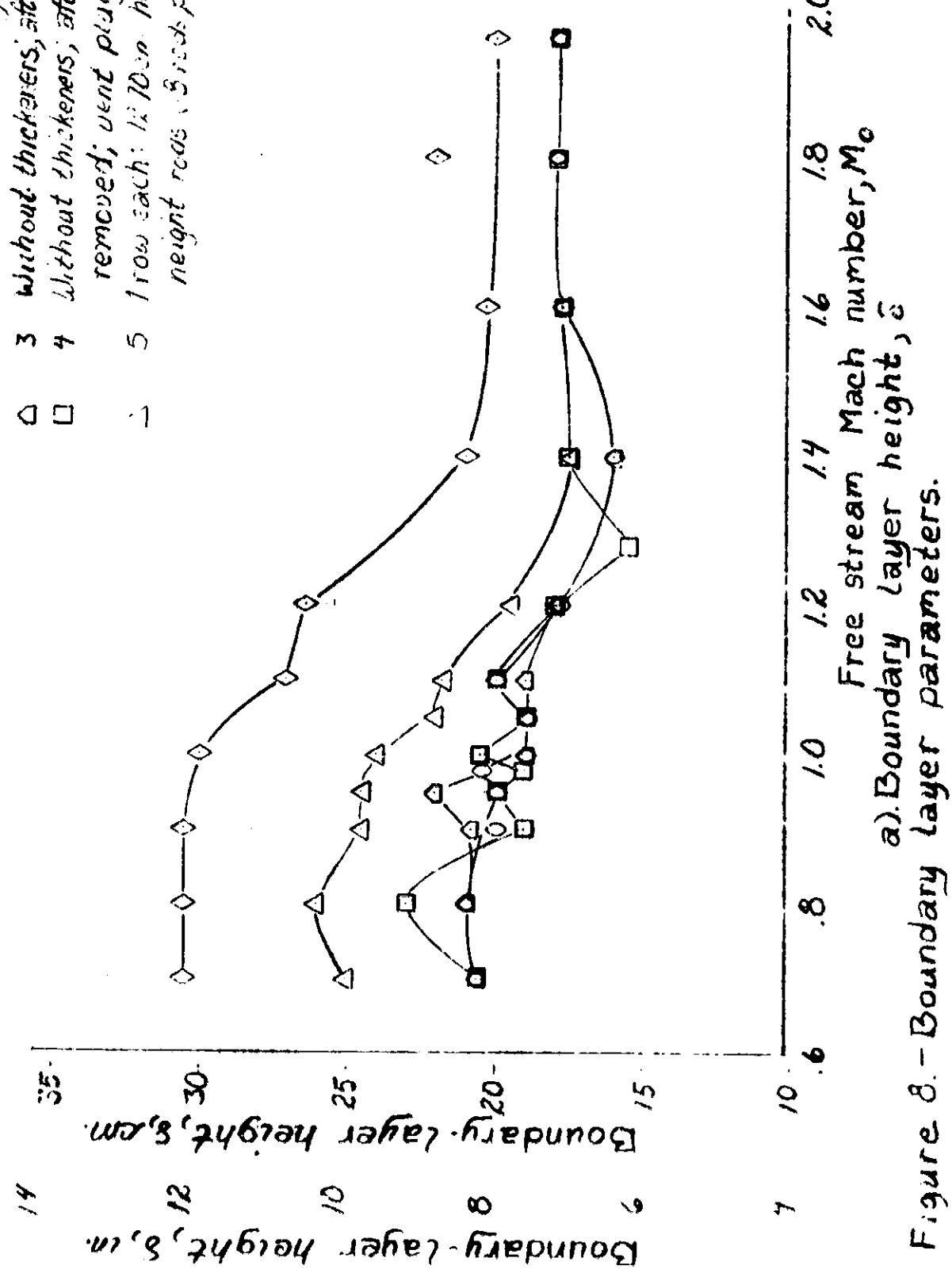
Figure 7. - Continued.



(n) $M_0 = 1.9600$

Figure 7. - Concluded.

- Configuration
- 1 Without thickeners
 - 2 4 rows of 12.10cm height rods (18 per row)
 - 3 Without thickeners; stiff field joint removed
 - 4 Without thickeners; stiff field joint ring removed; vent plugged.
 - 5 1 row each: 12.10cm height rods (18 per row) height rods (18 per row)



a) Boundary layer height, ϵ
Boundary layer parameters.

Figure 8.- Boundary layer parameters.

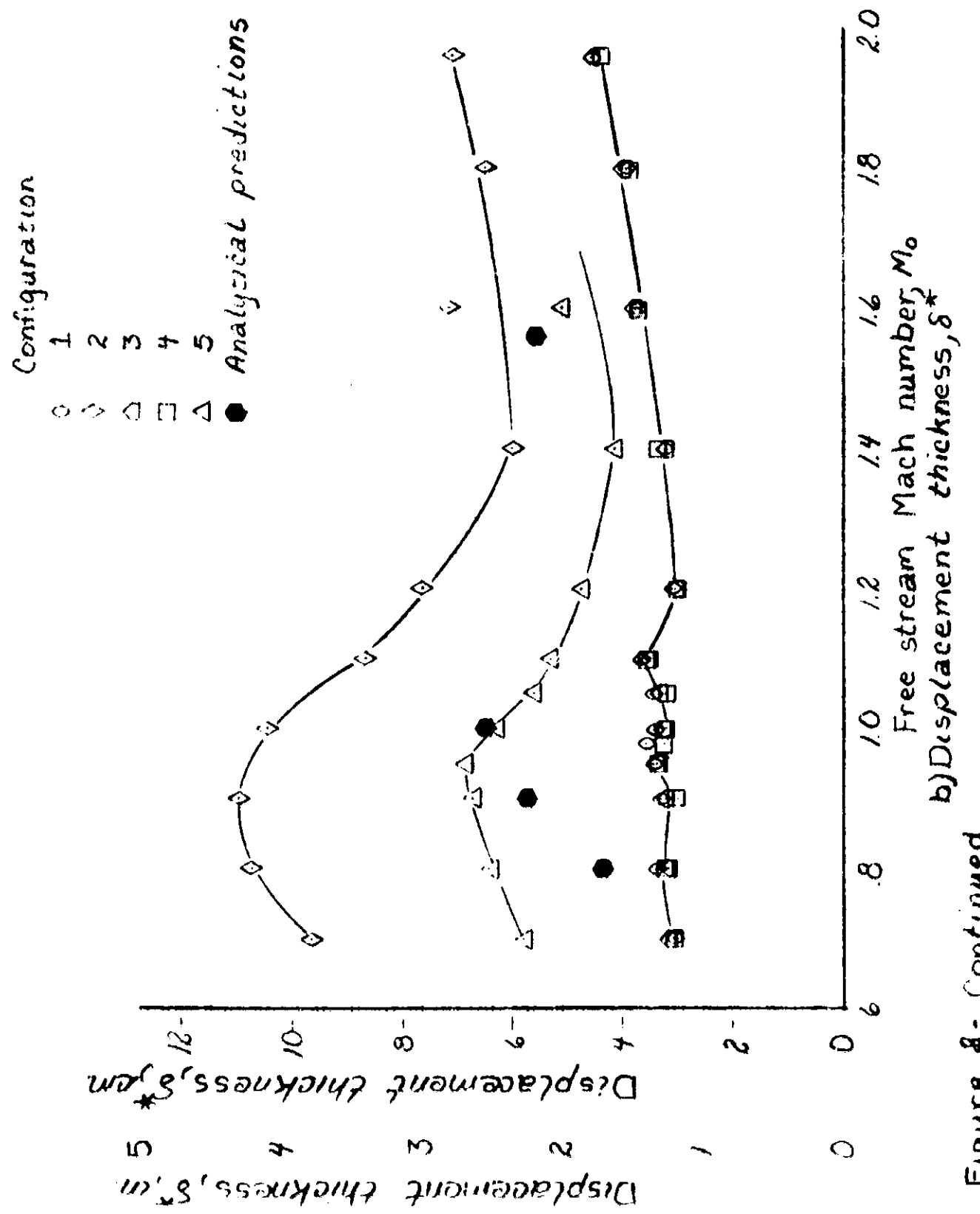


Figure 8 - Continued.

Configuration:

- 1
- 2
- 3
- 4
- 5

— Ref. 9

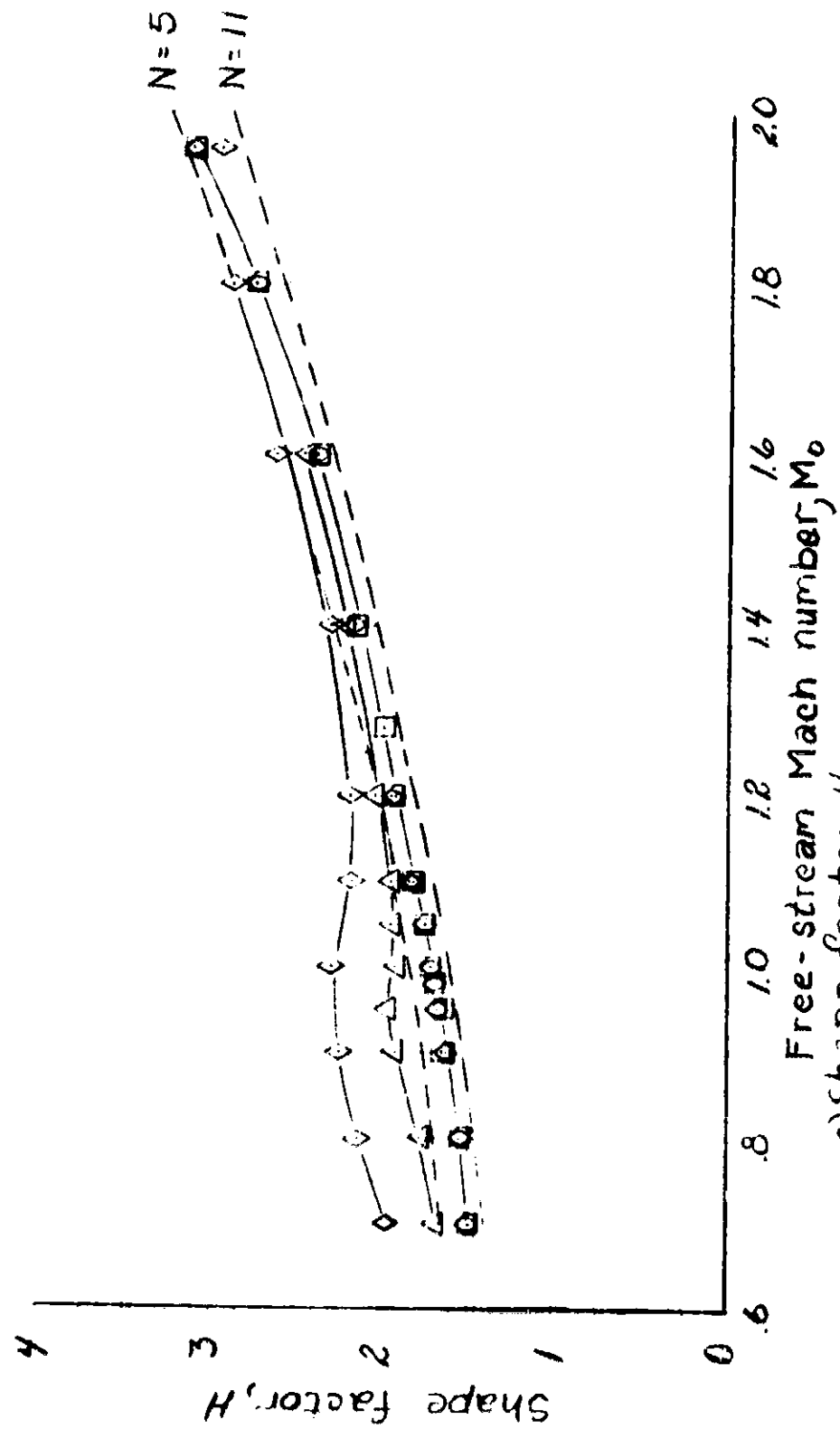


Fig. 8 - Conclusion.

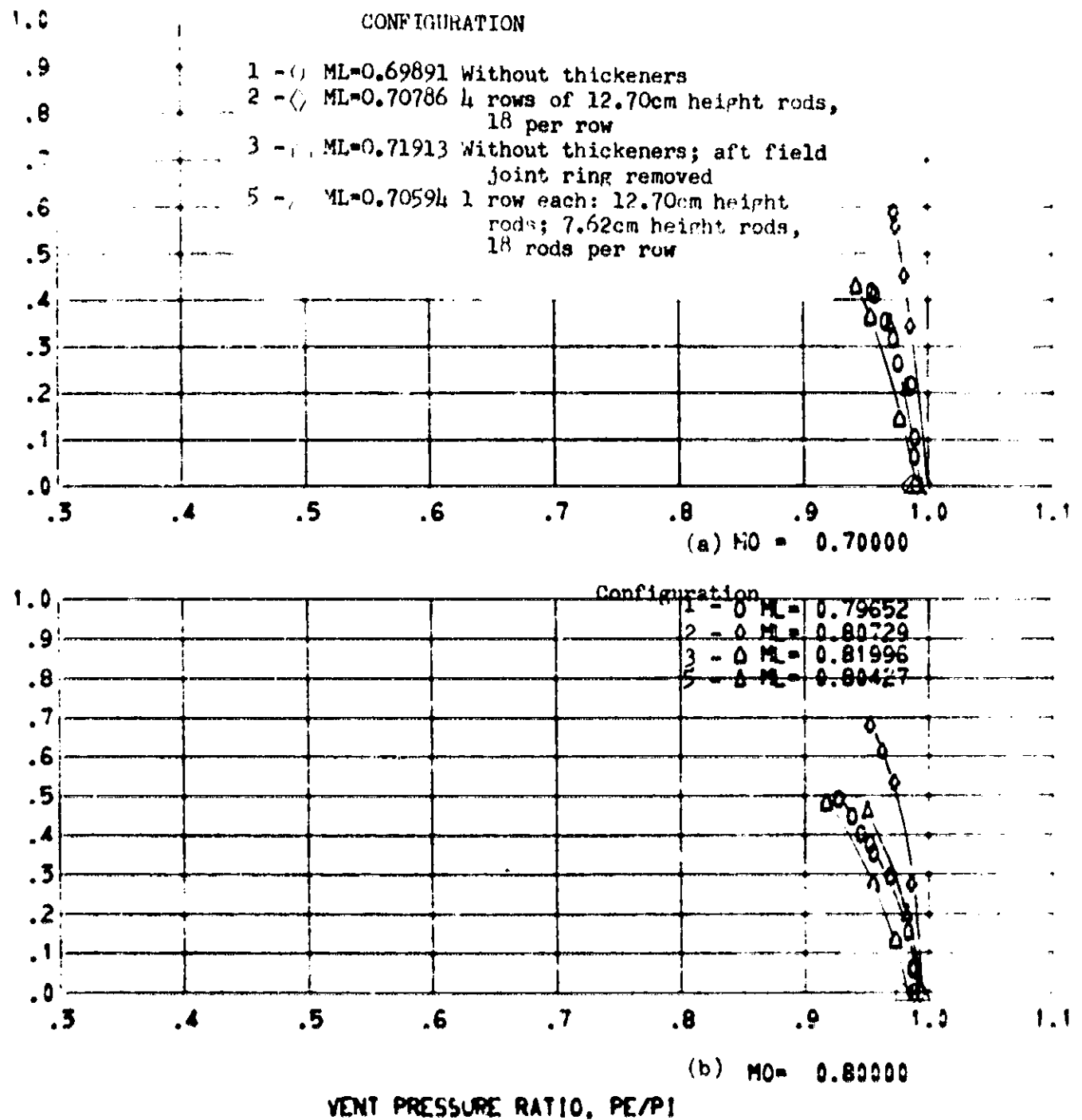


Figure 9. - Variation of vent discharge coefficient with vent pressure ratio

VENT DISCHARGE COEFFICIENT, K

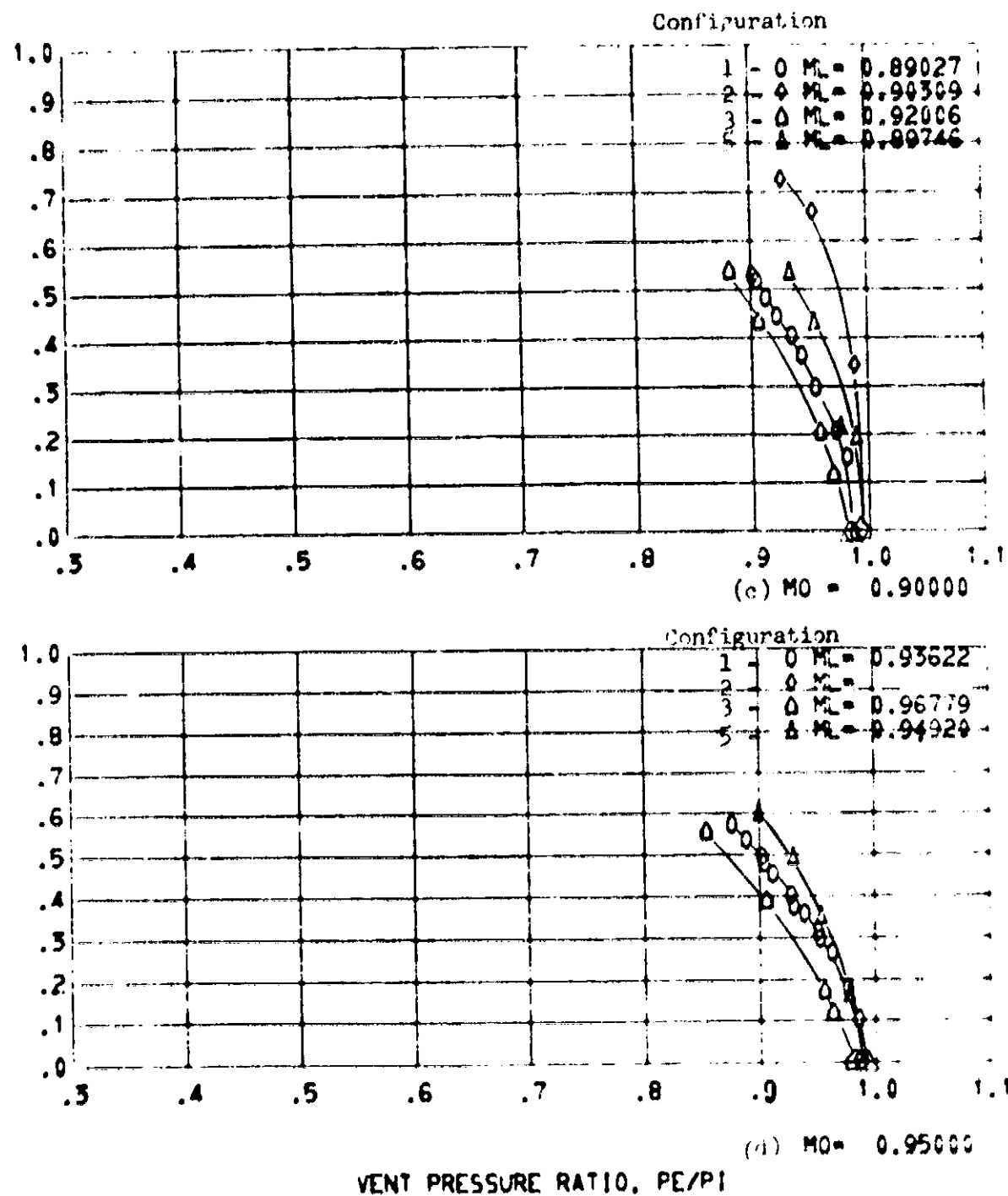


Figure 9. - Continued.

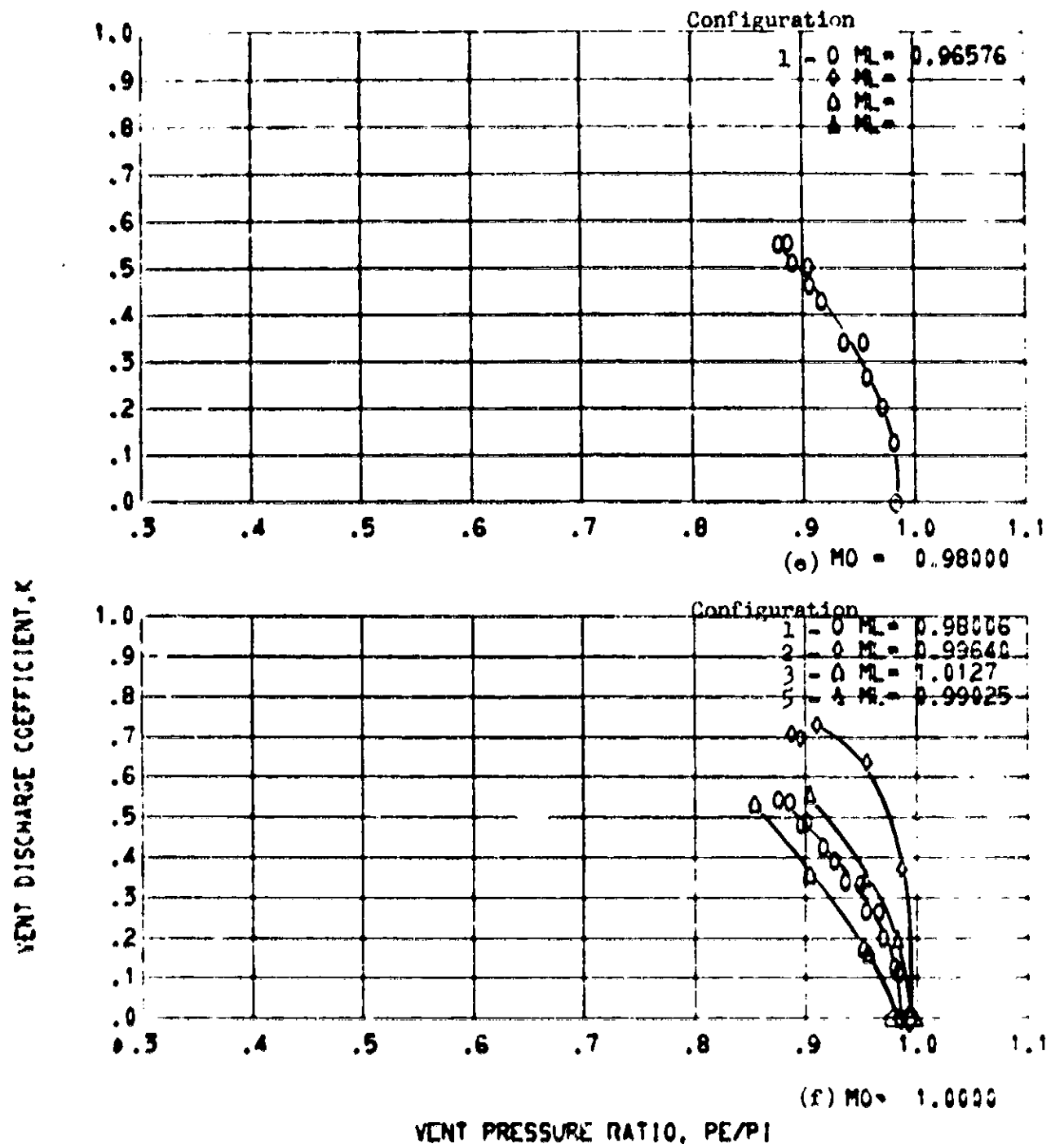


Figure 9. - Continued.

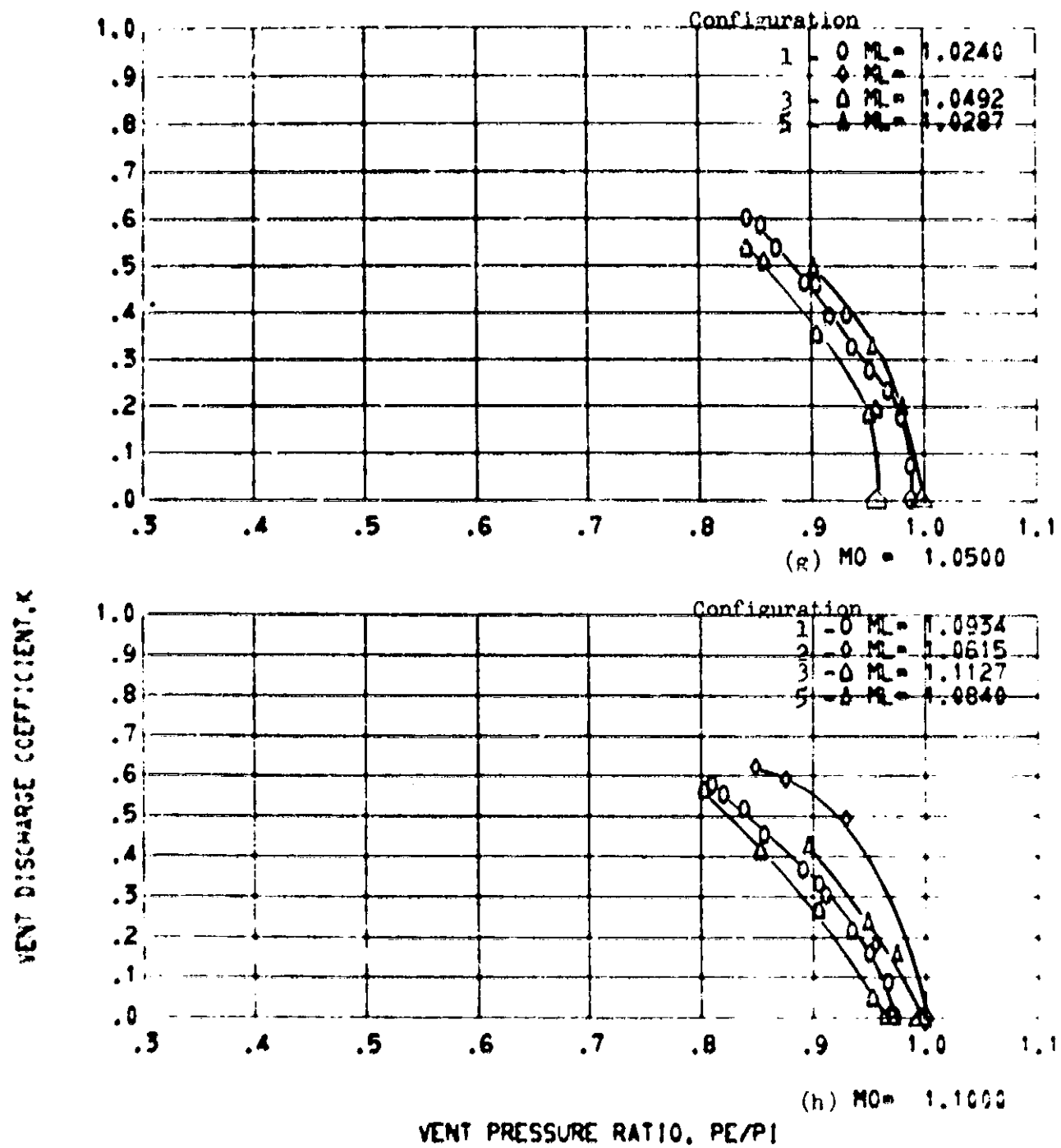


Figure 9. - Continued.

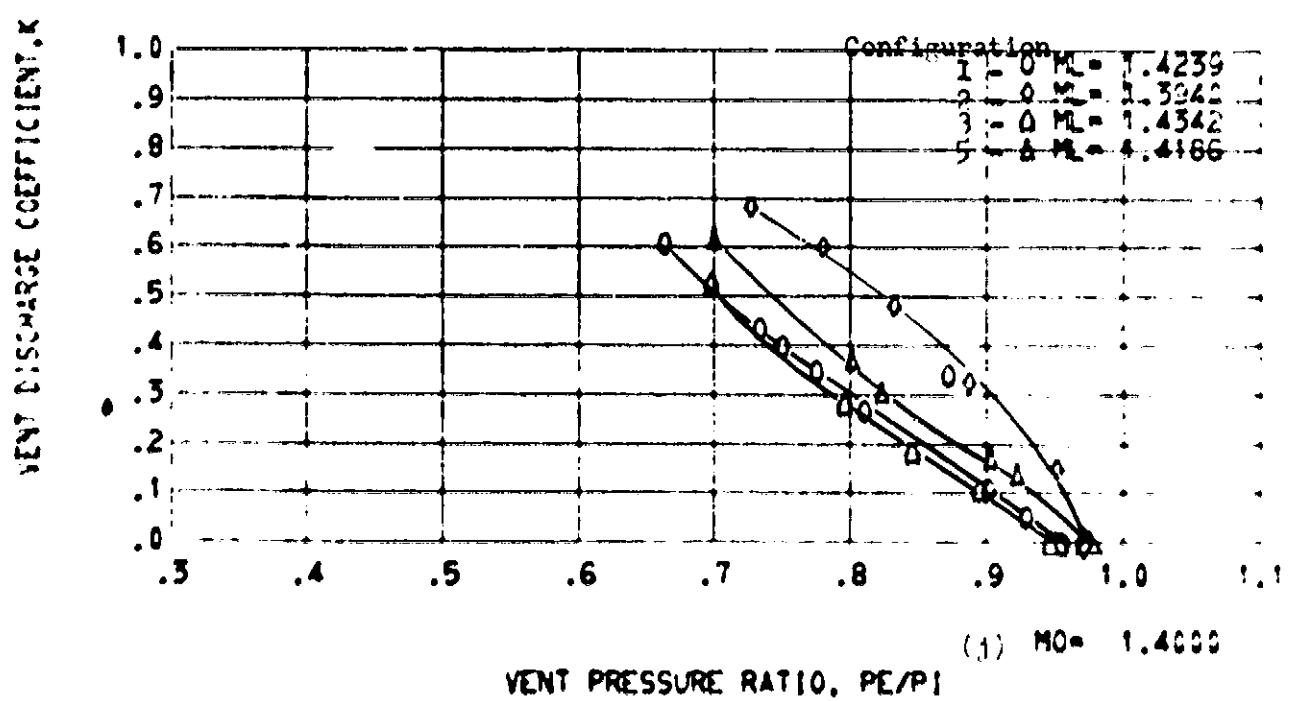
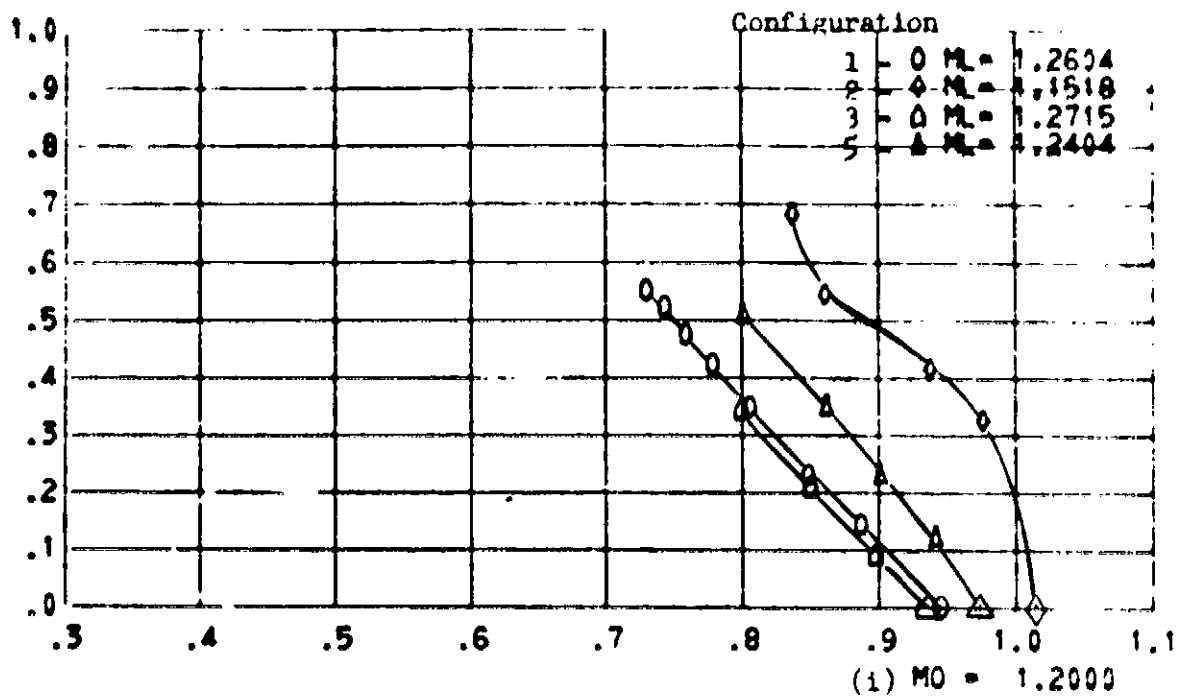


Figure 9. - Continued.

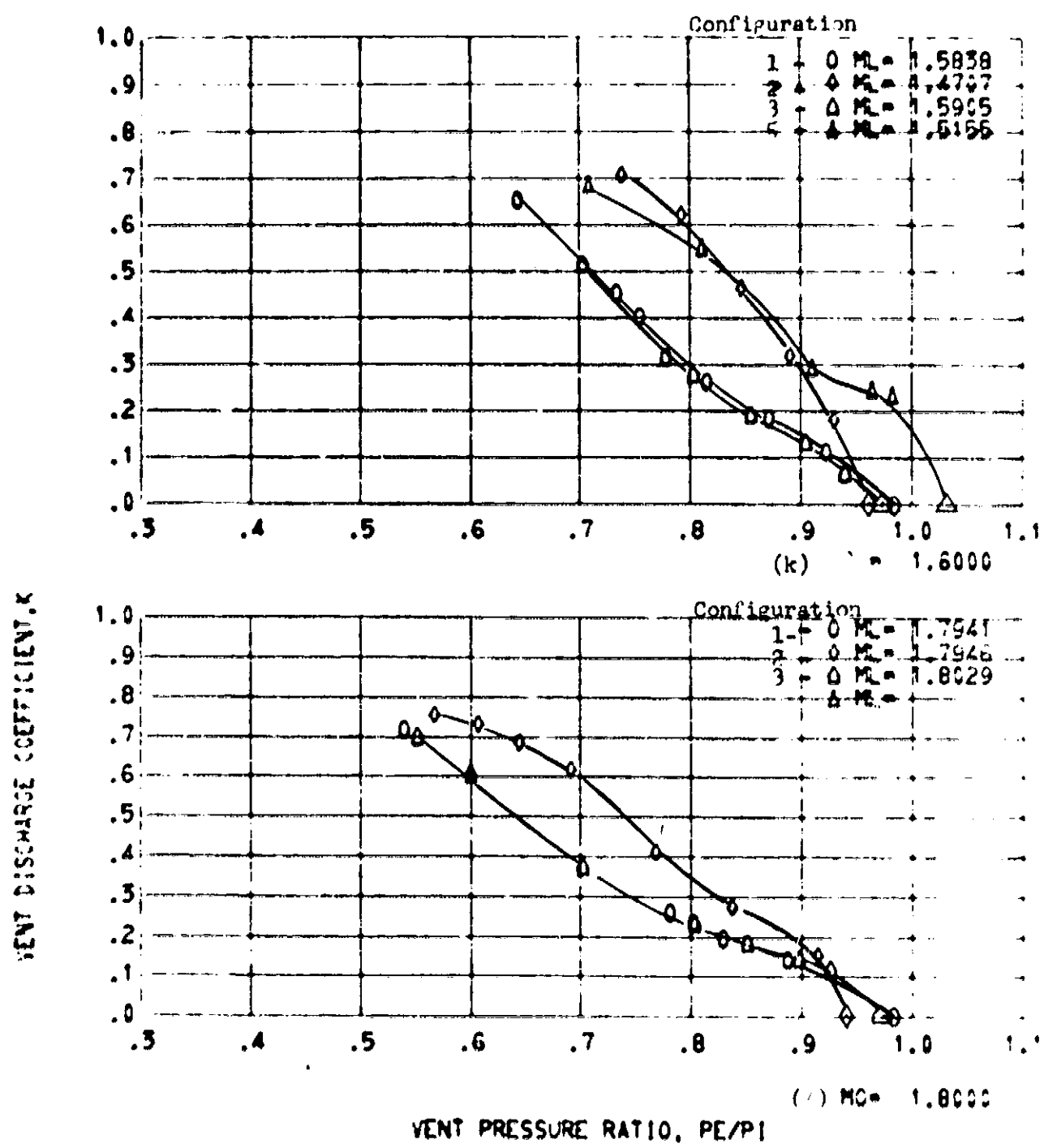


Figure 9. - Continued.

VENT DISCHARGE COEFFICIENT, K

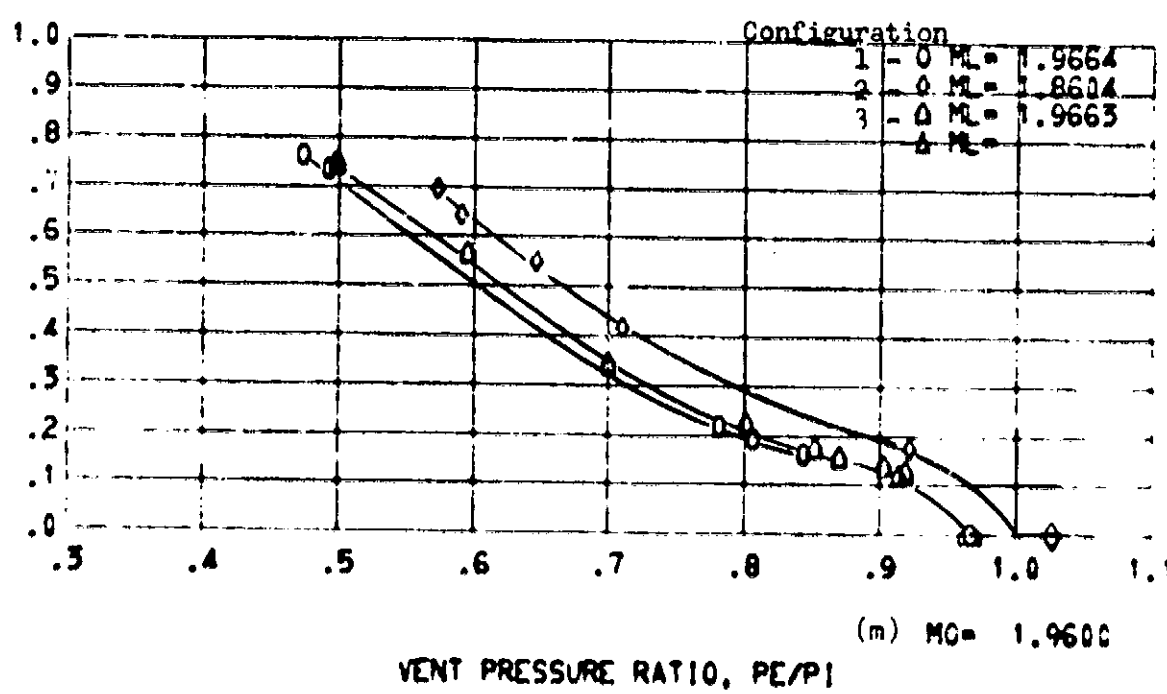


Figure 9. - Concluded.

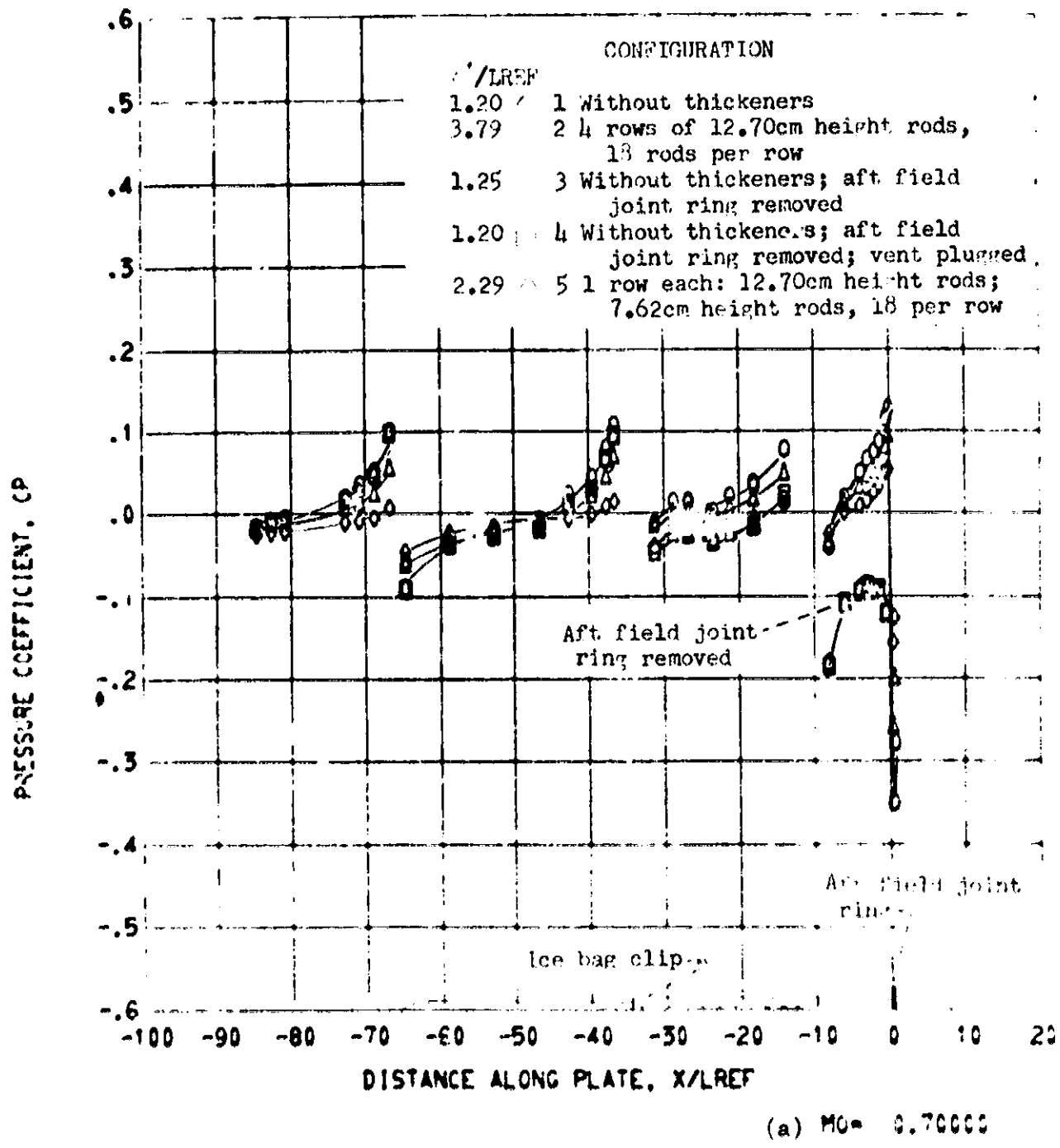
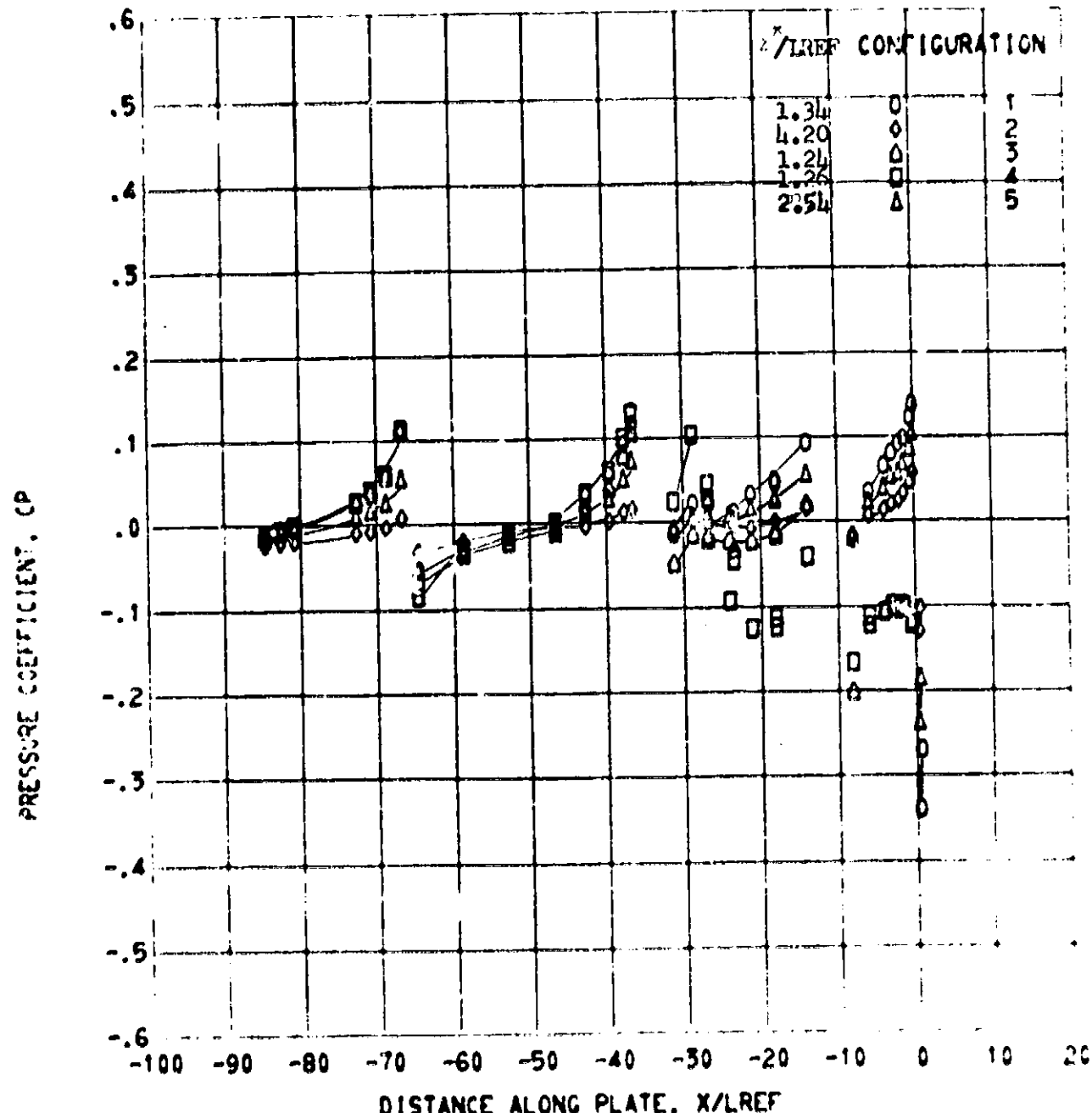


Figure 10. - Effect of displacement thickness on incremental pressure coefficient distributions with no vent flow.



(b) $M_0 = 0.80029$

Figure 10. - Continued.

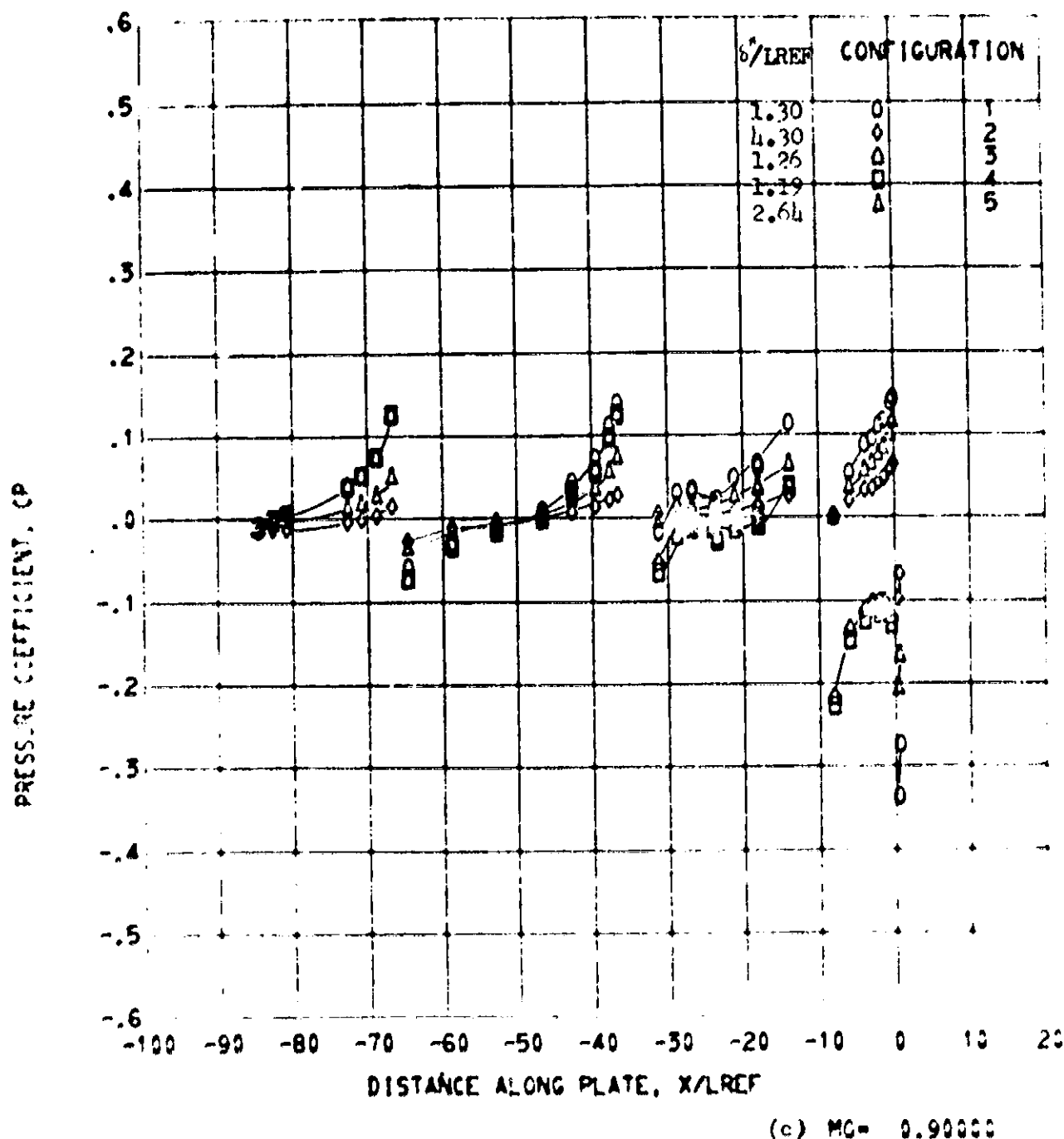


Figure 10. - Continued.

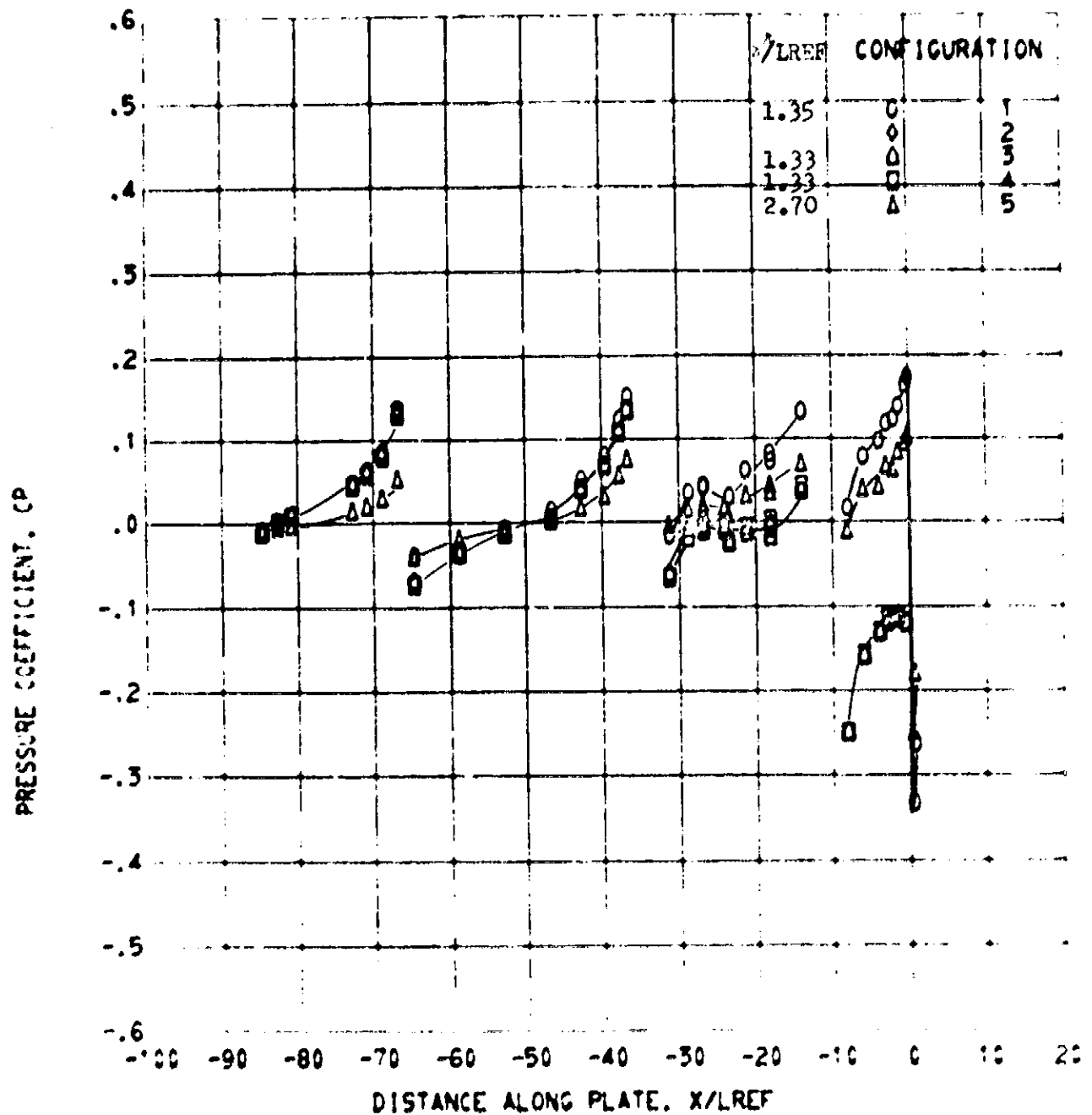


Figure 10. - Continued.

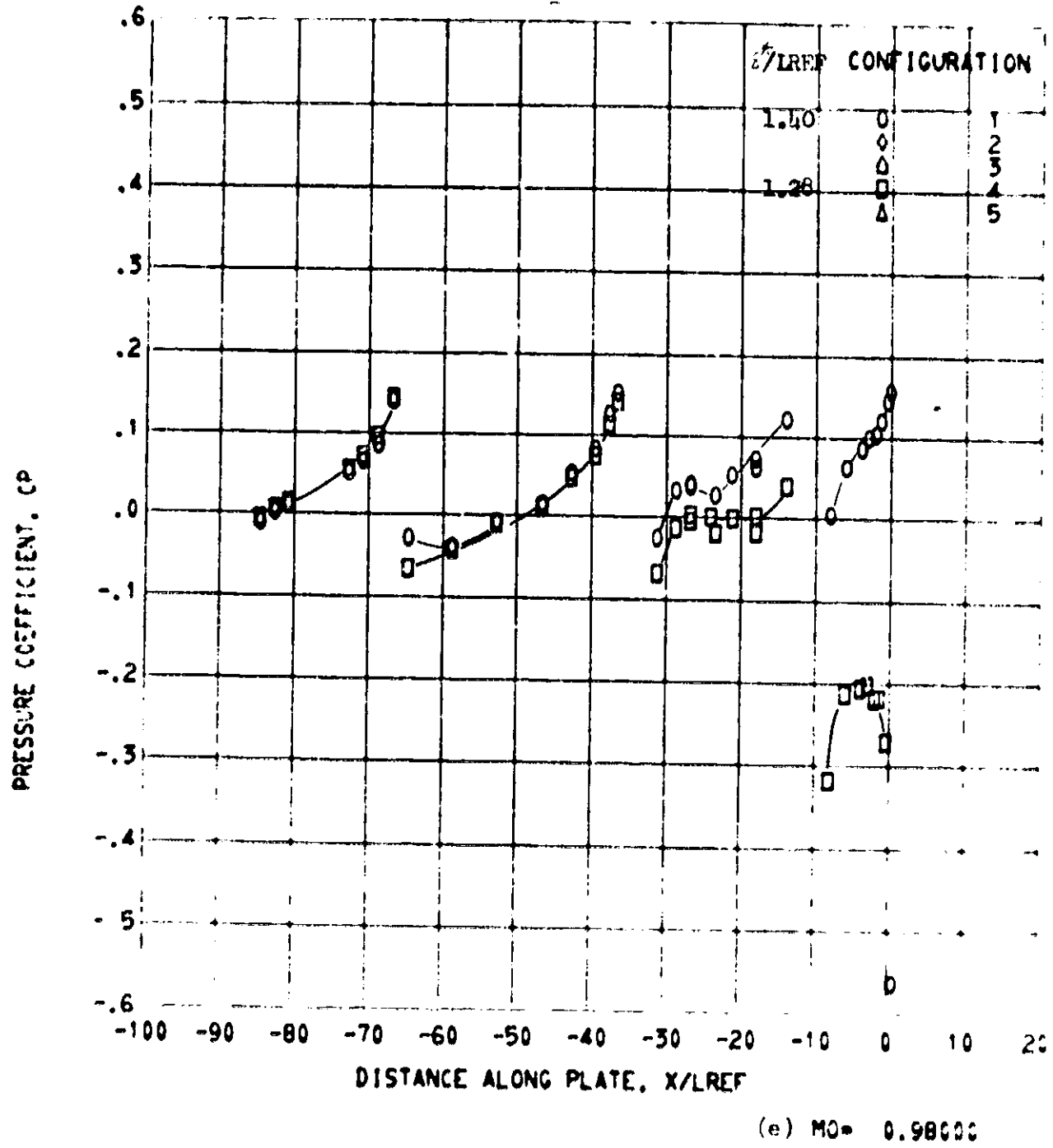


Figure 10. - Continued.

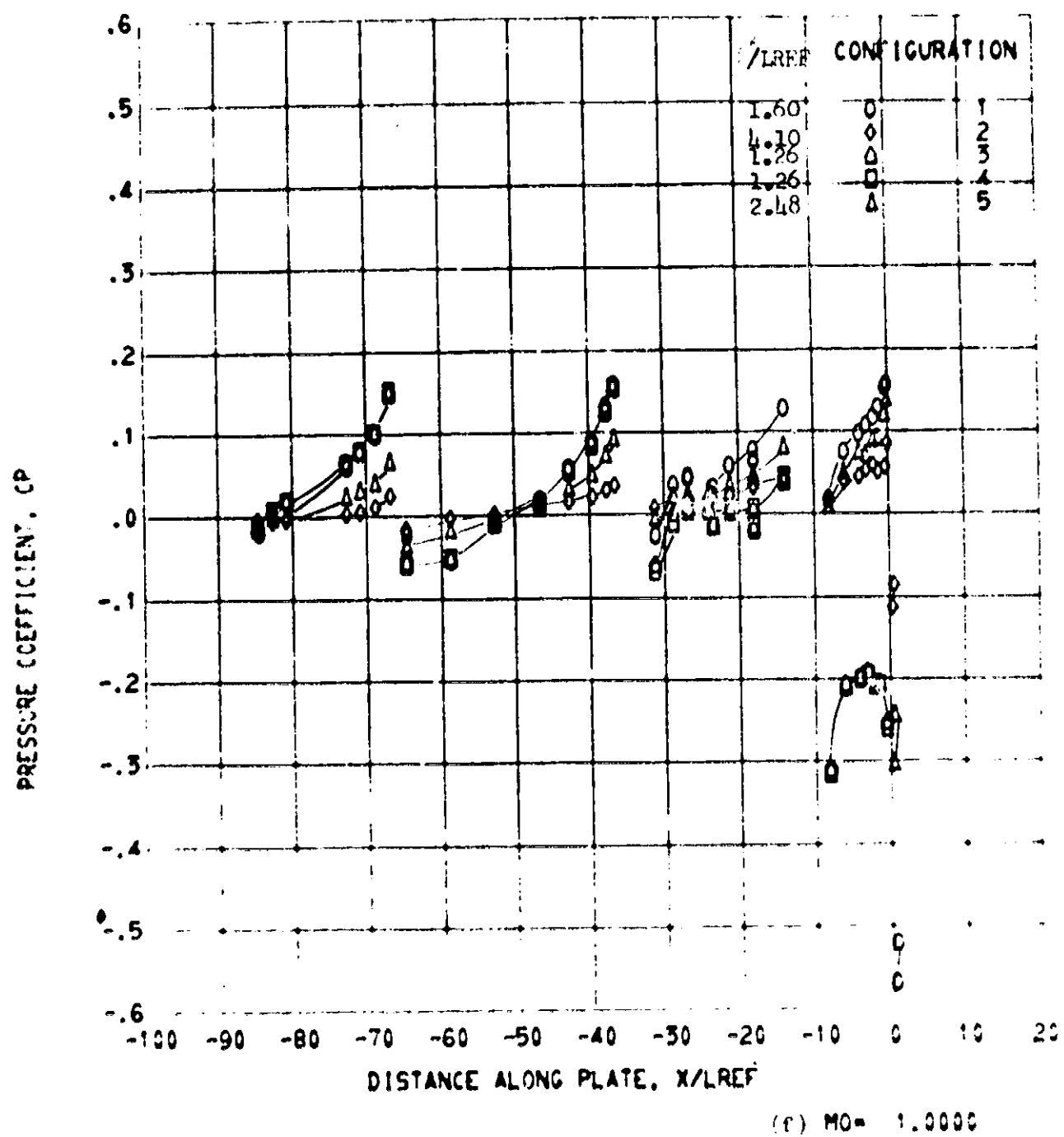
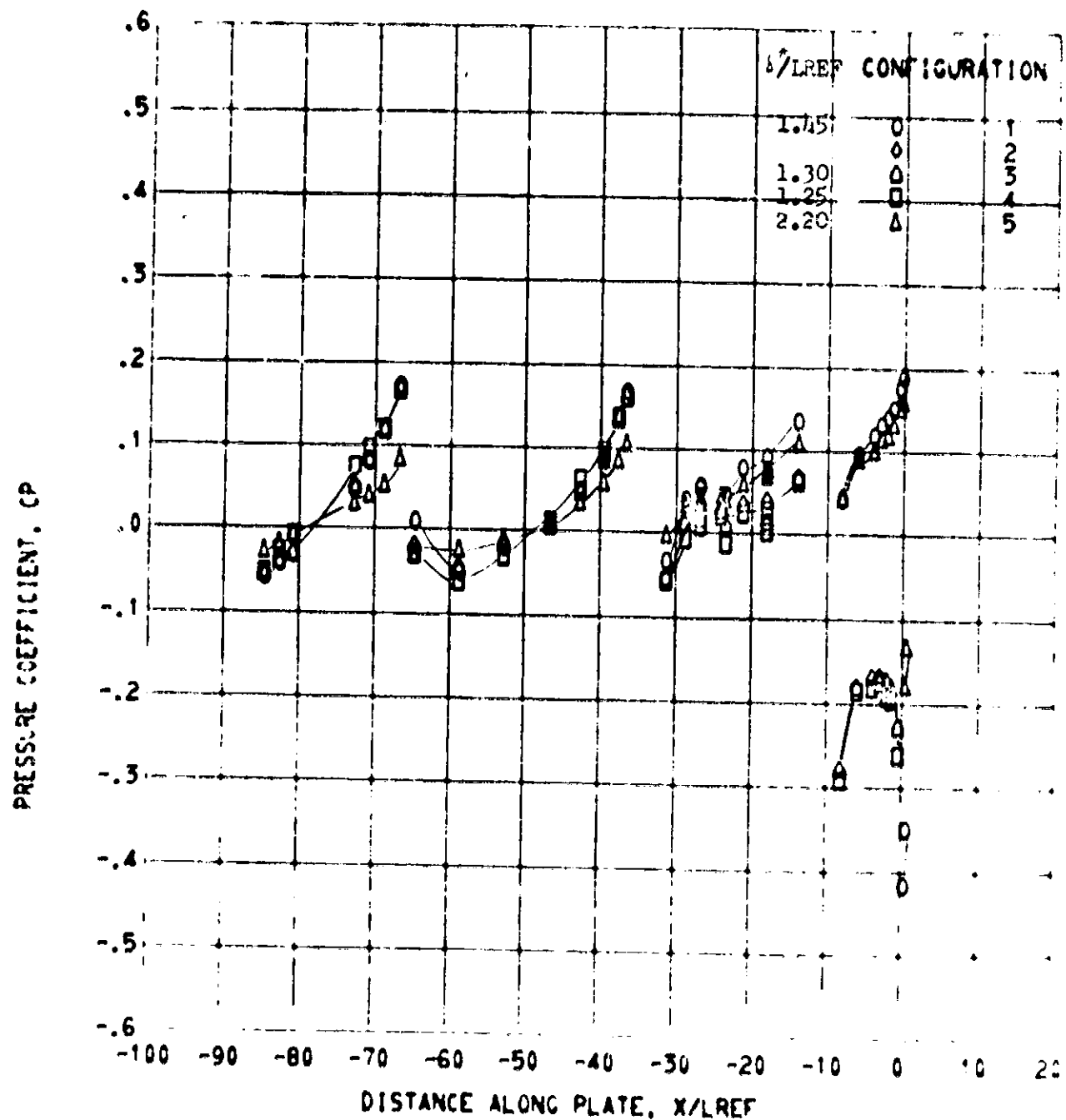


Figure 10. - Continued.



(P) M0= 1.0500

Figure 10. - Continued.

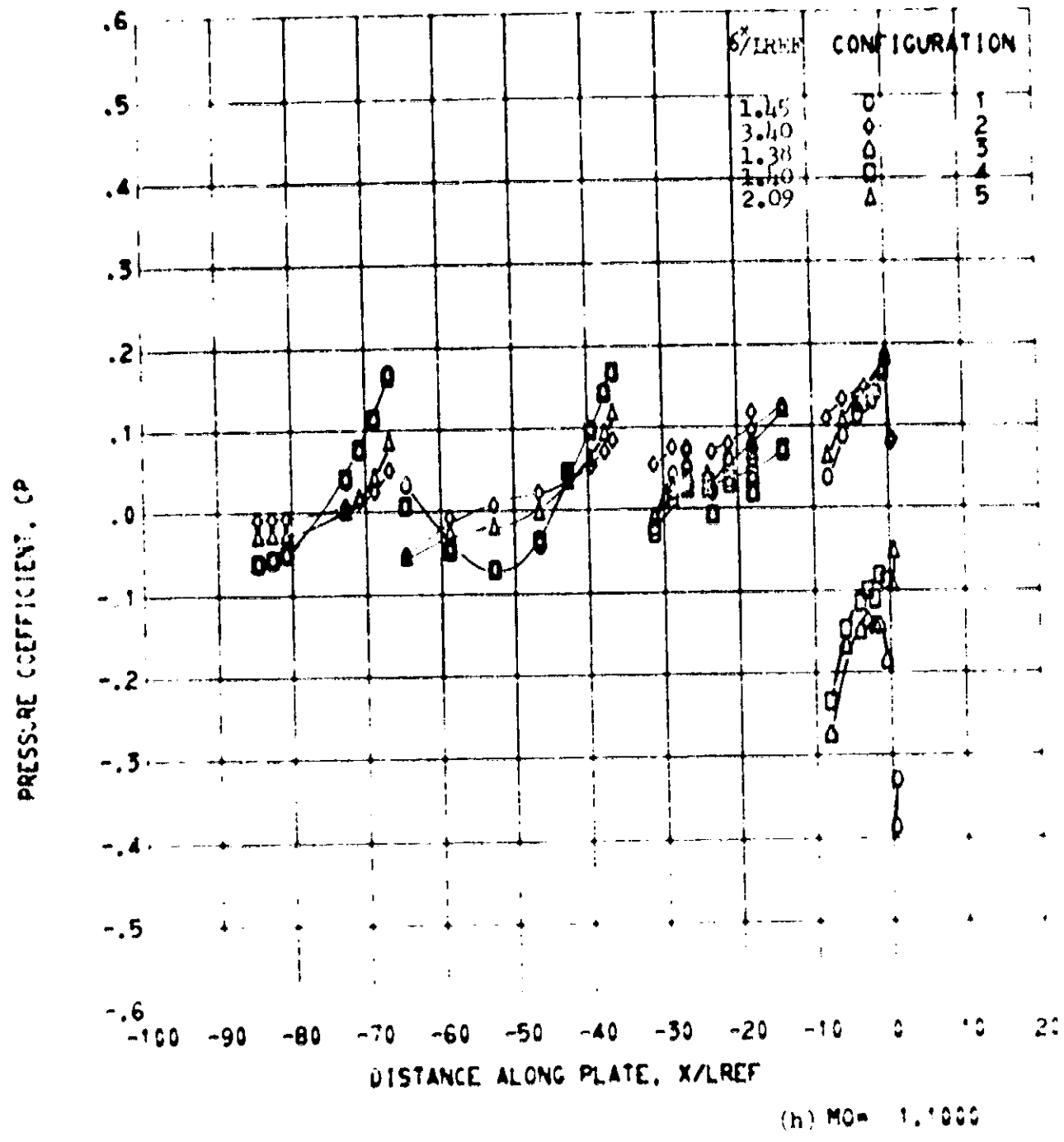


Figure 10. - Continued.

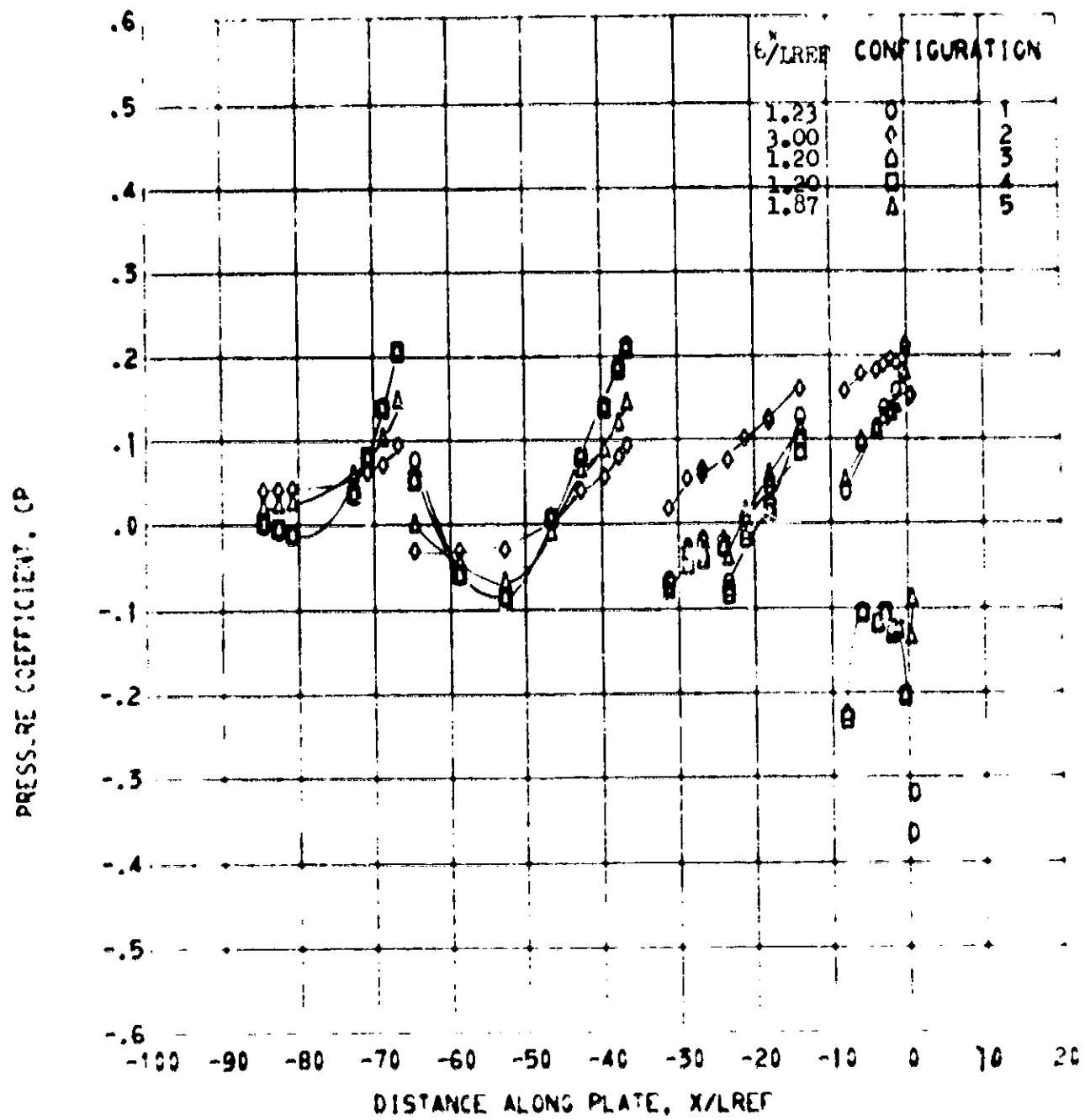


Figure 1b. - Continued.

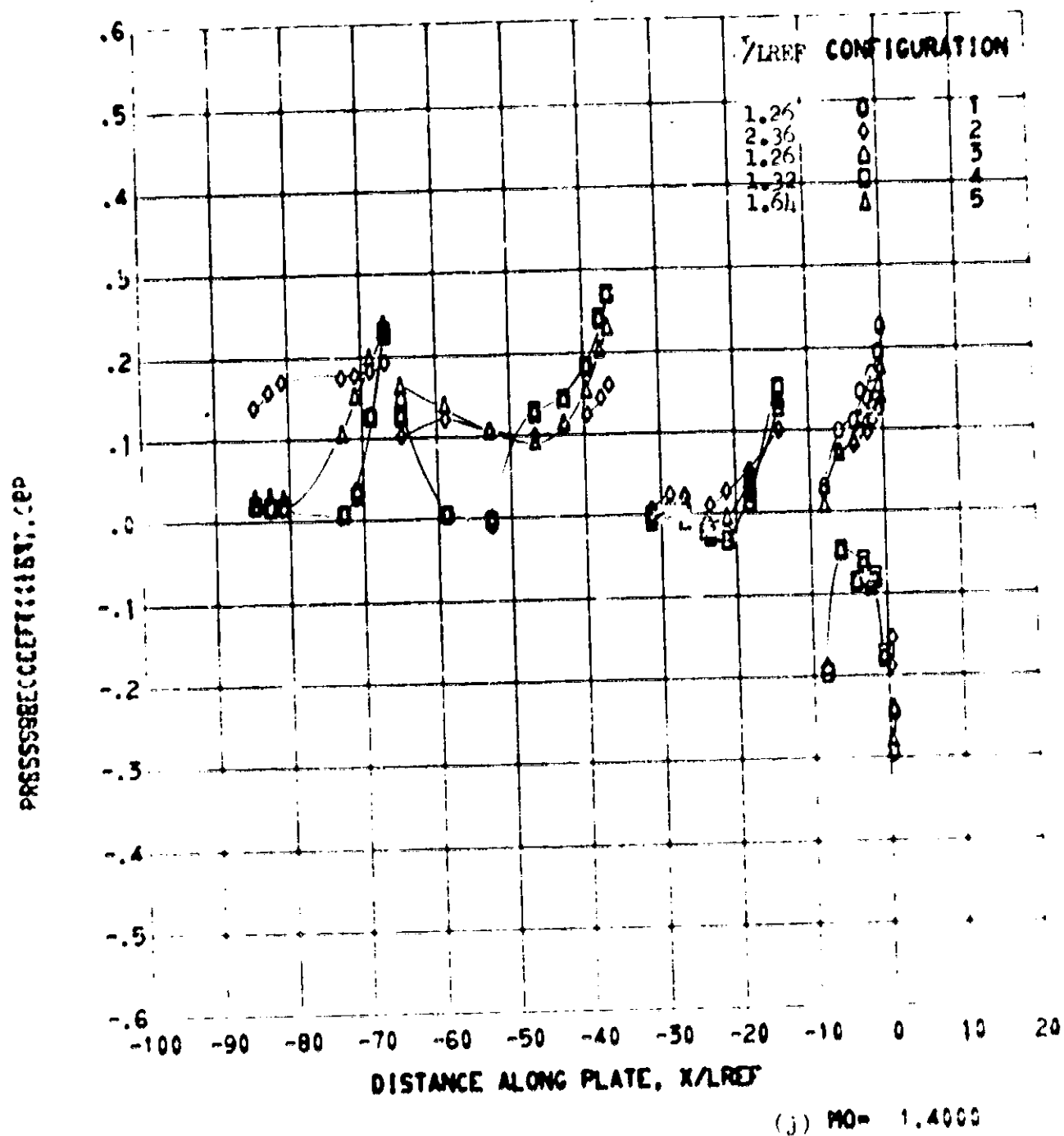
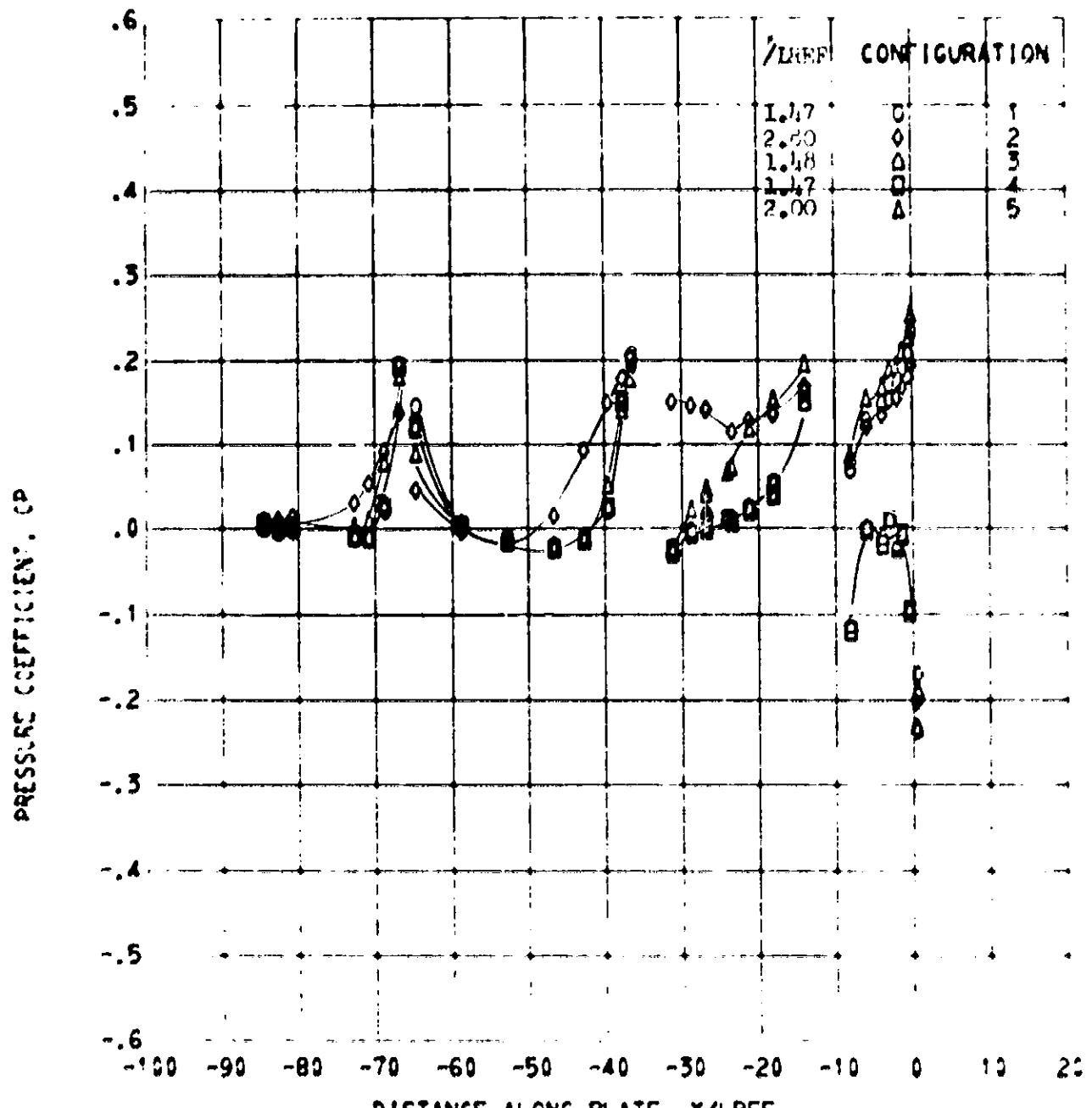


Figure 10. - Contuned.



(k) $M_0 = 1.600$

Figure 10. - Continued.

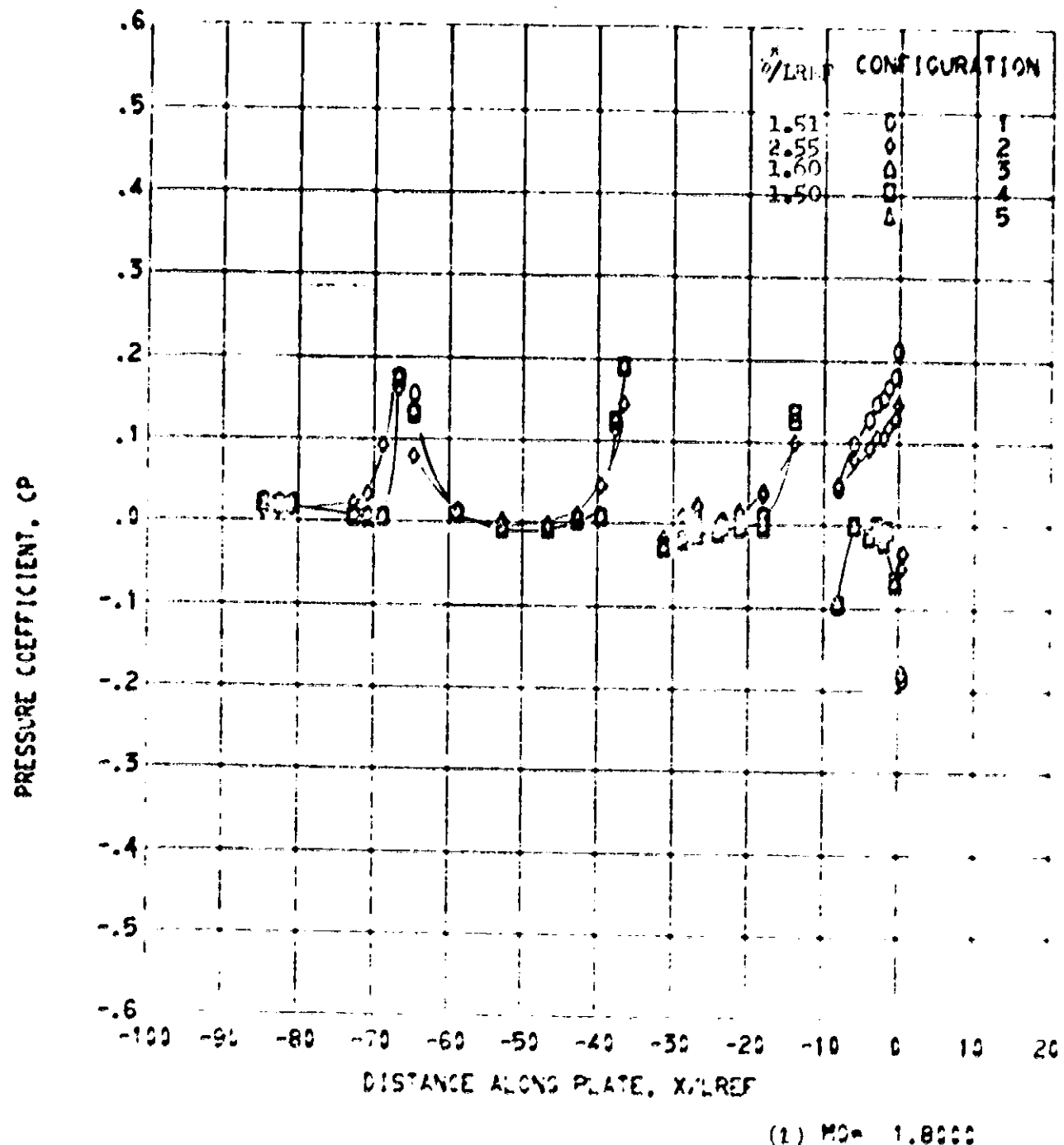


Figure 10. - Continued.

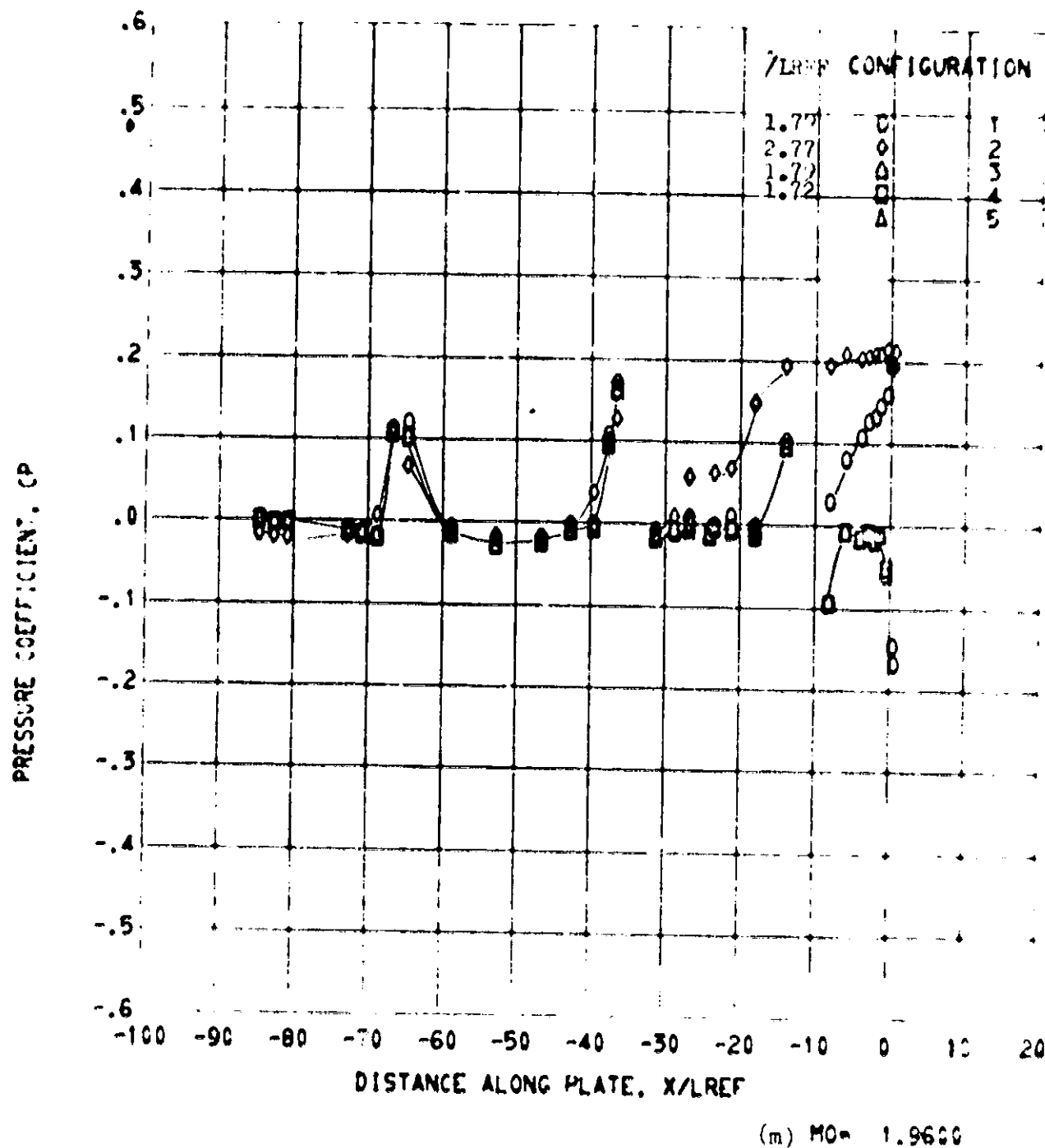


Figure 10e - Concluded.

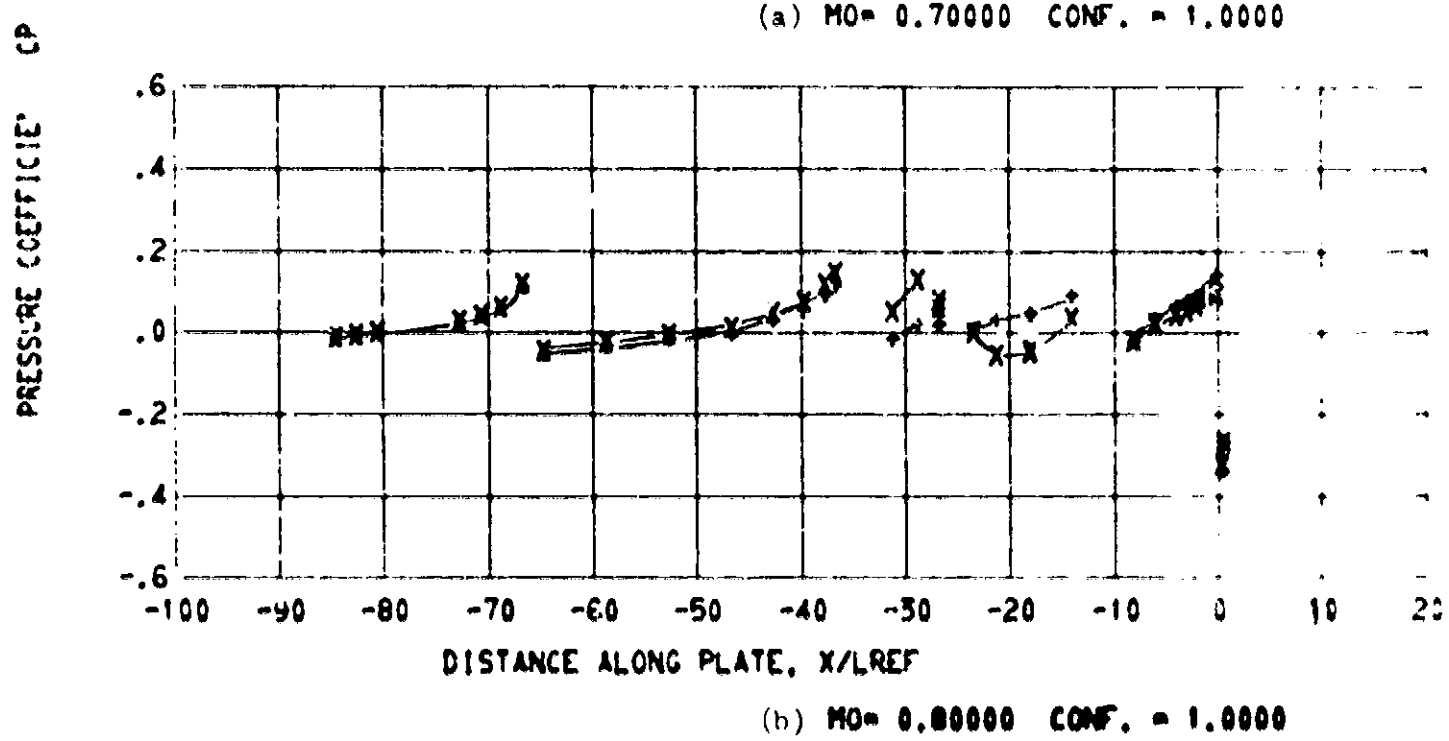
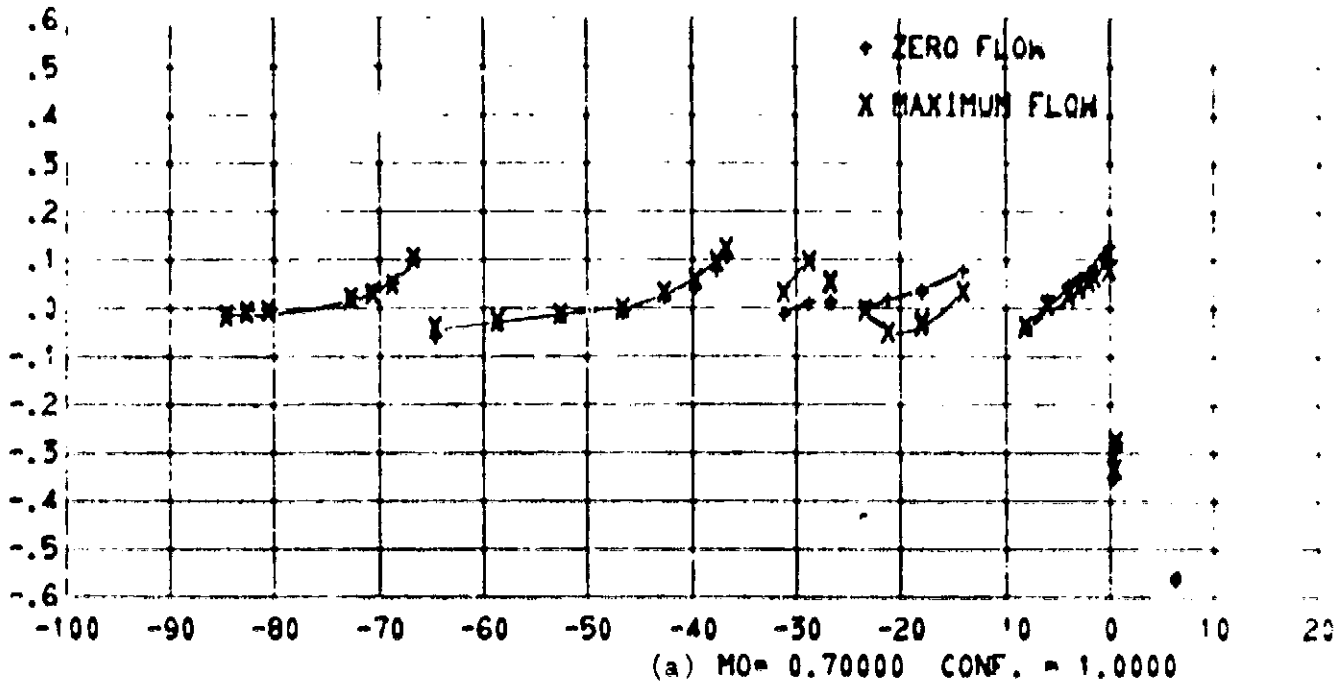


Figure 11. - Effect of vent flow on the pressure distribution, Configuration 1.

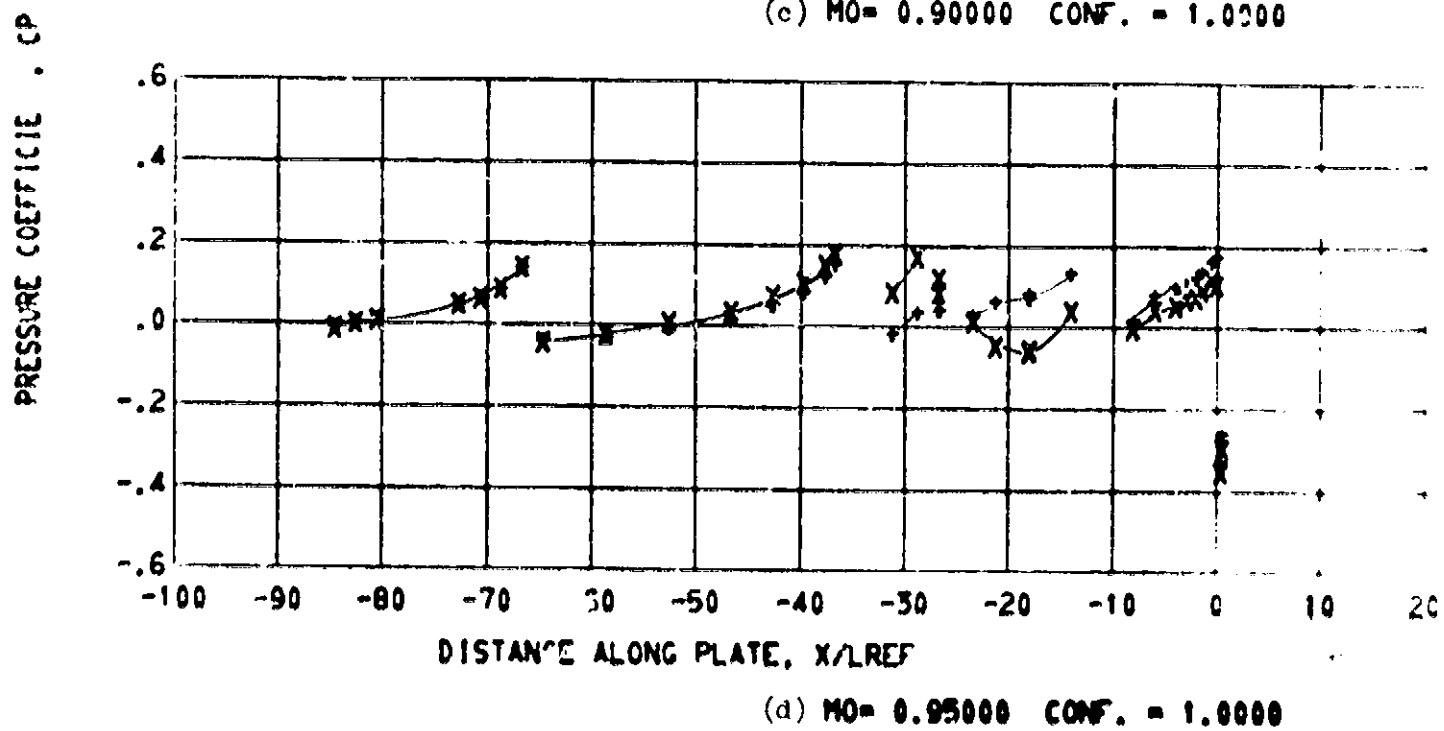
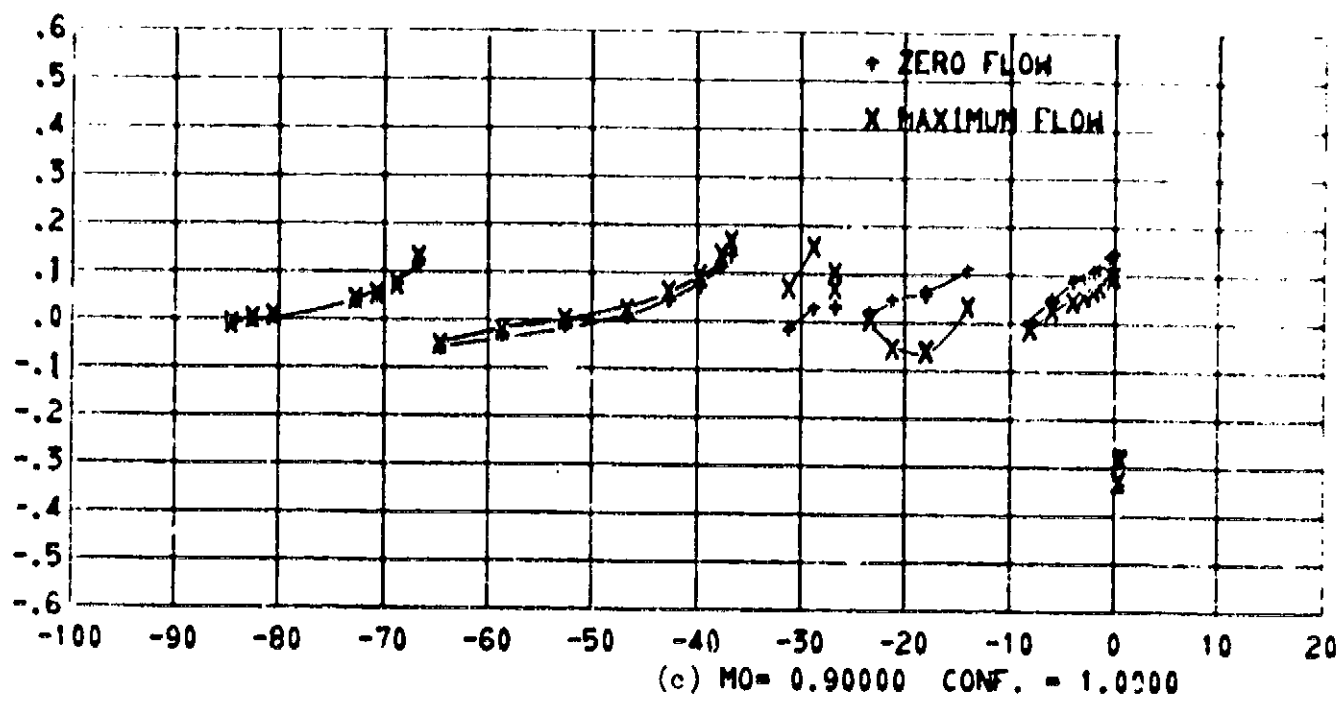


Figure 11. - Continued.

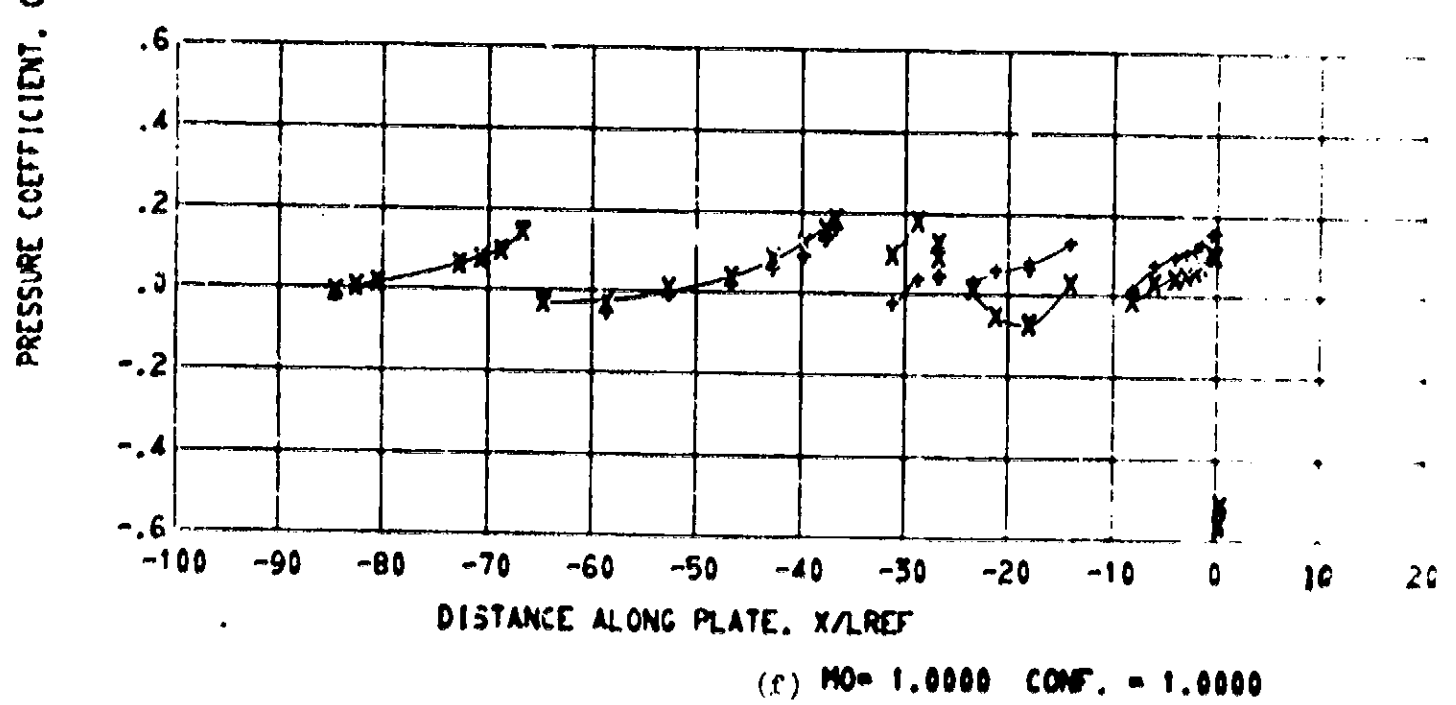
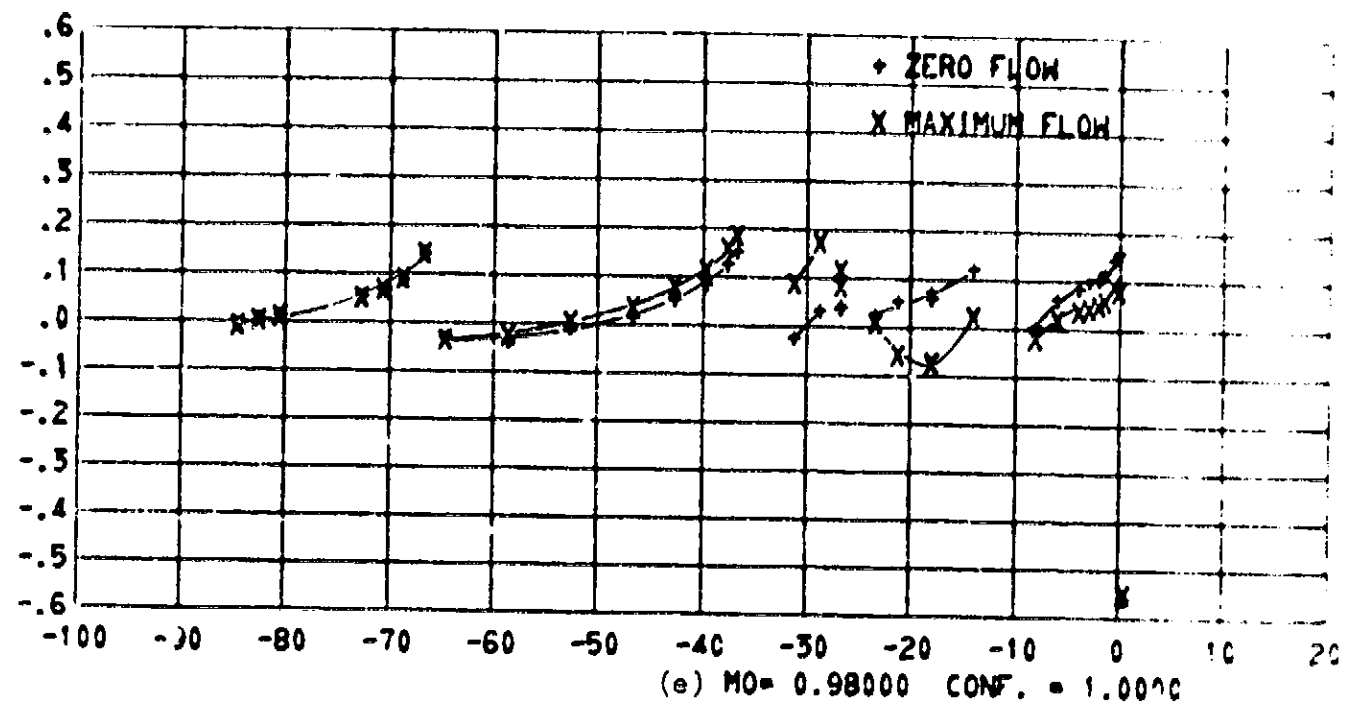
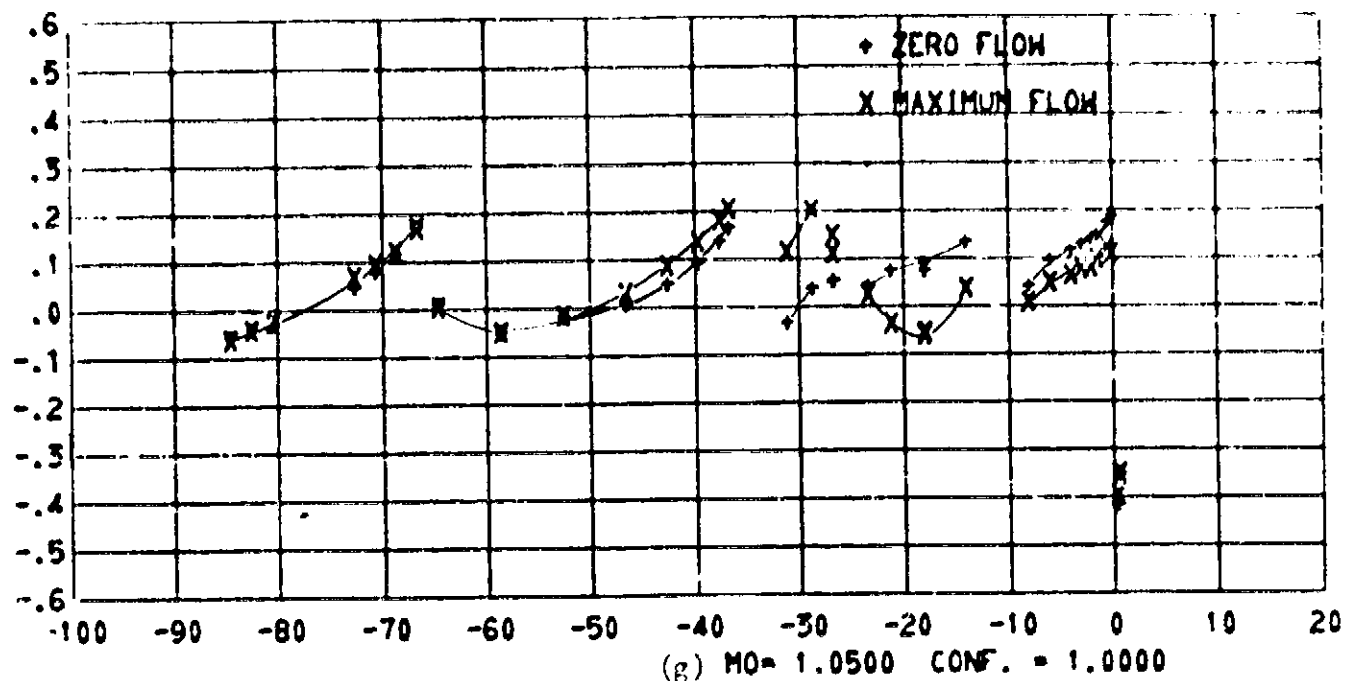


Figure 11. - Continued.

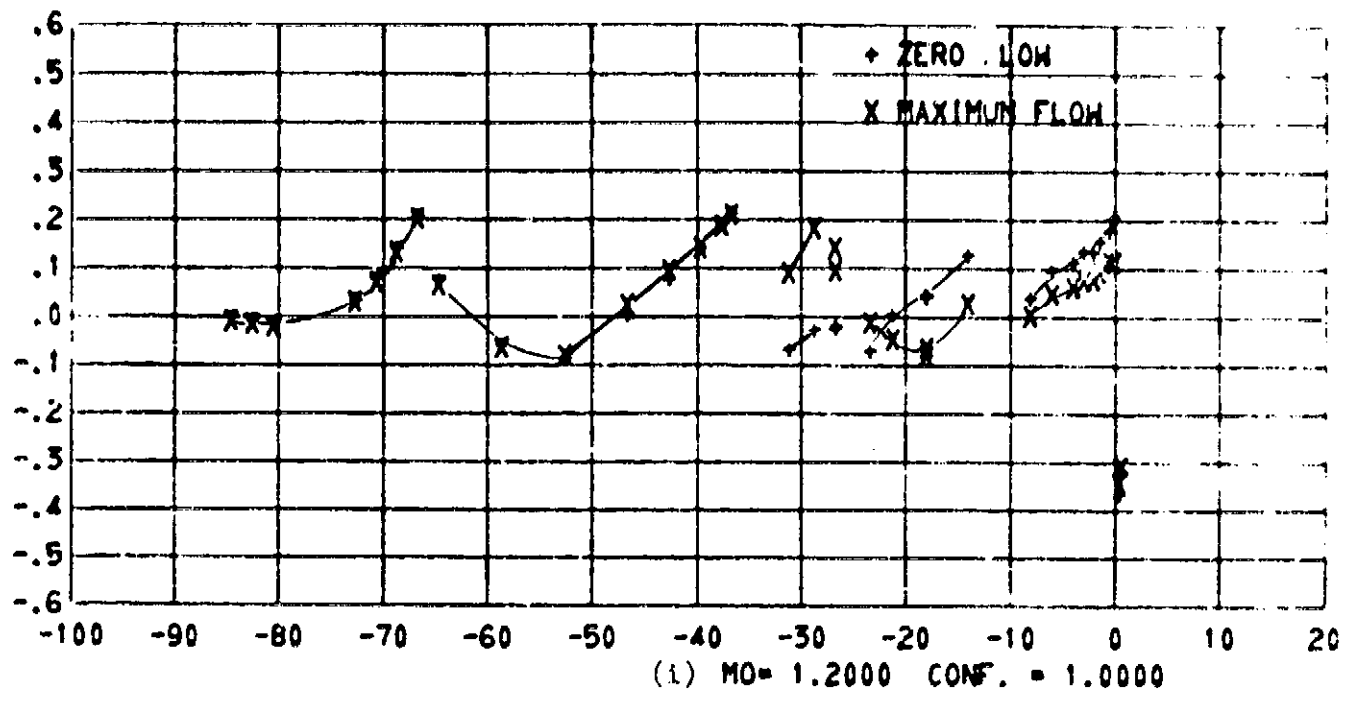
PRESSURE COEFFICIENT, CP



DISTANCE ALONG PLATE, X/L_{REF}

(h) $M_0 = 1.1000$ CONF. = 1.0000

Figure 11. - Continued.



PRESSURE COEFFICIENT, CP

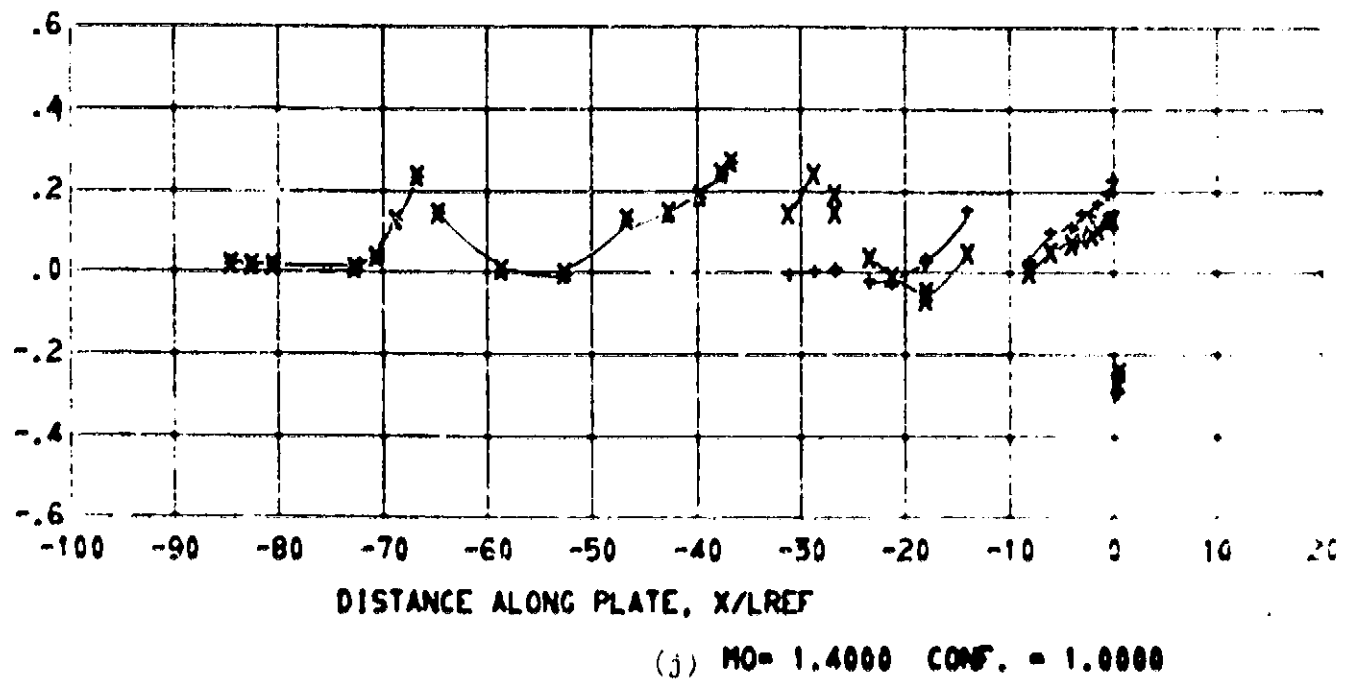


Figure 11. - Continued.

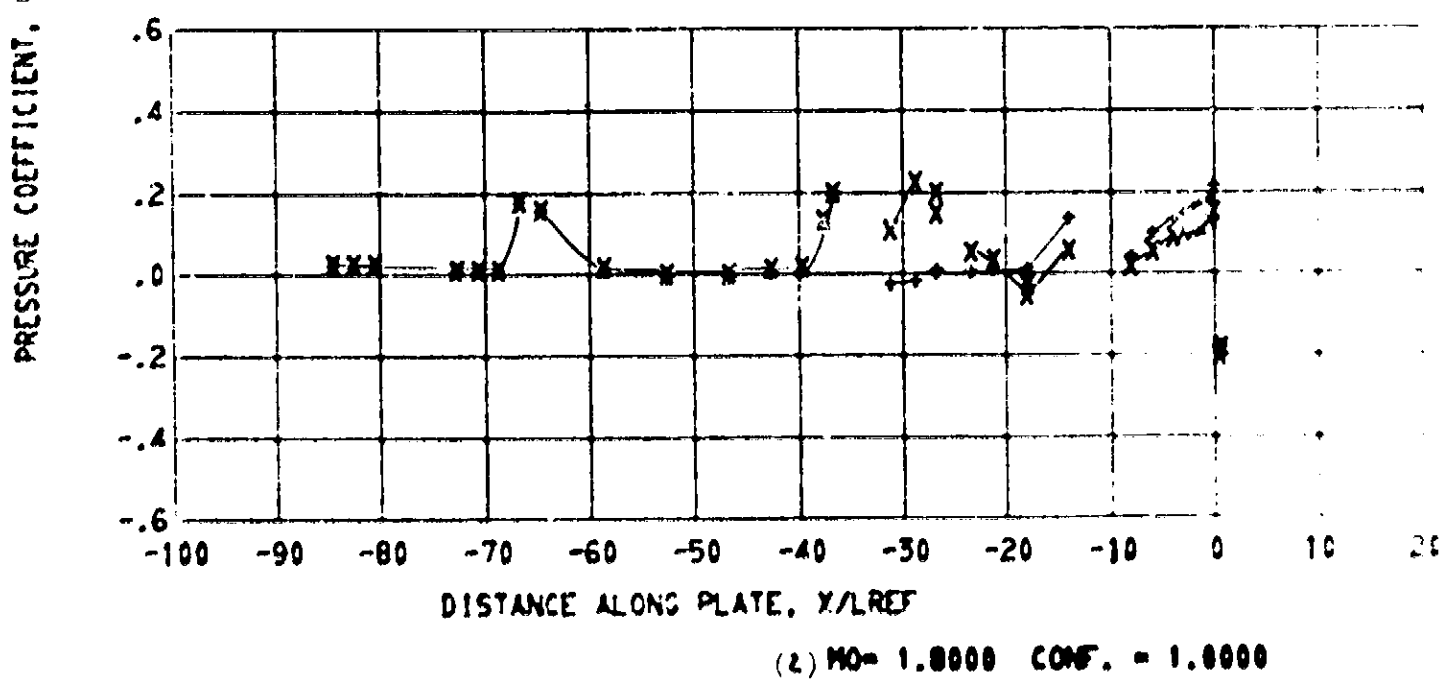
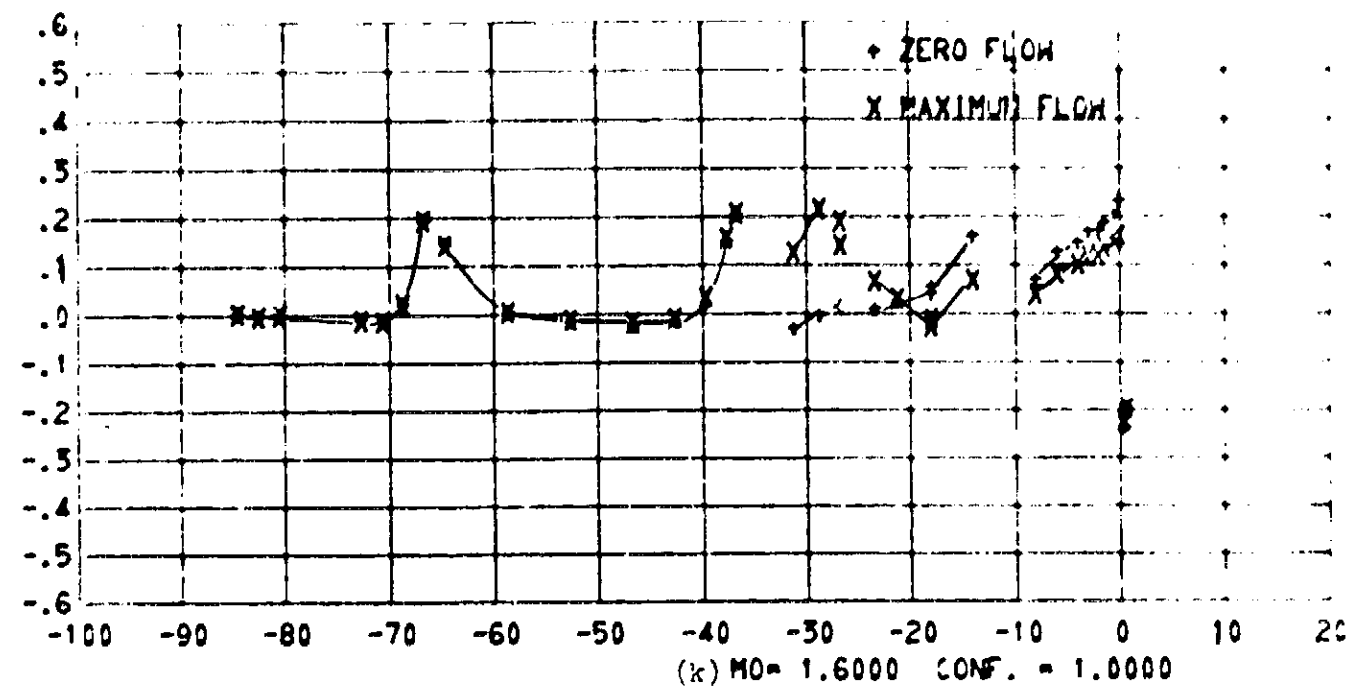


Figure 11. - Continued.

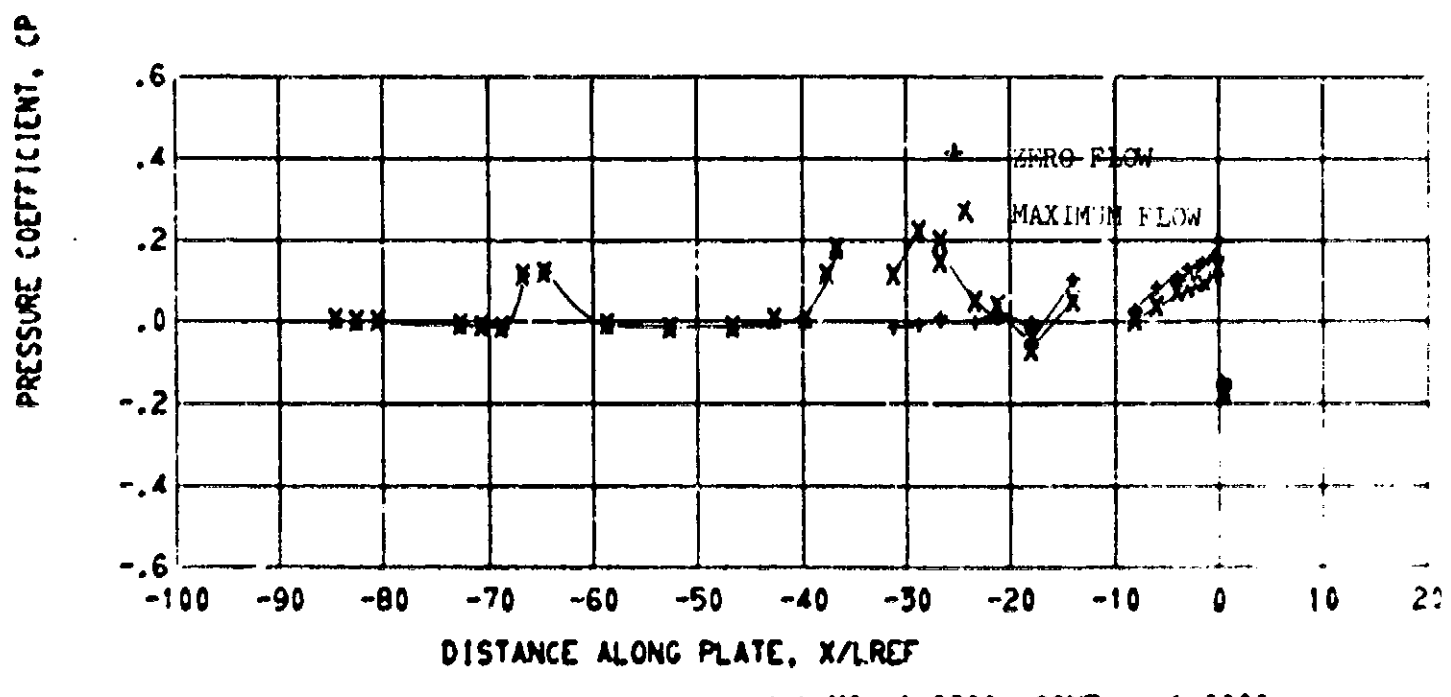


Figure 11. - Concluded.

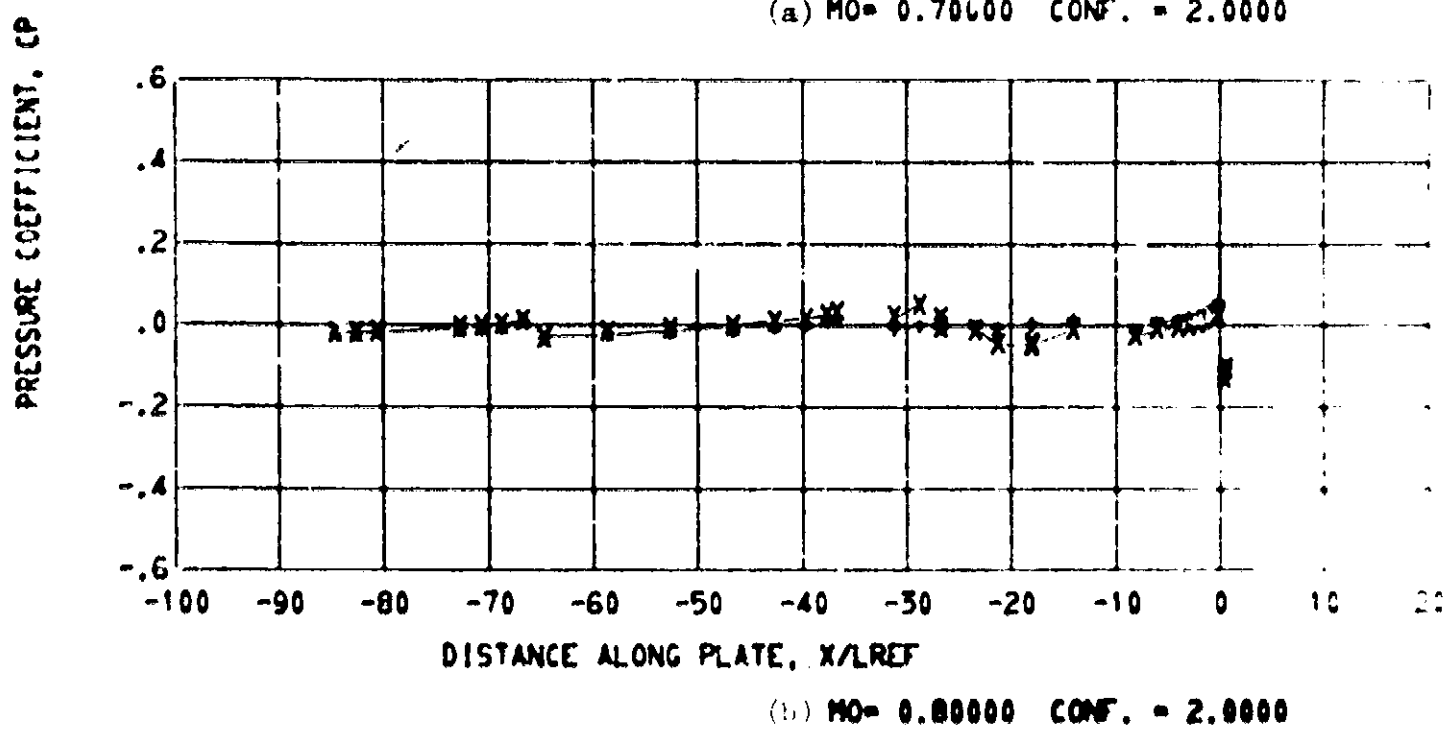
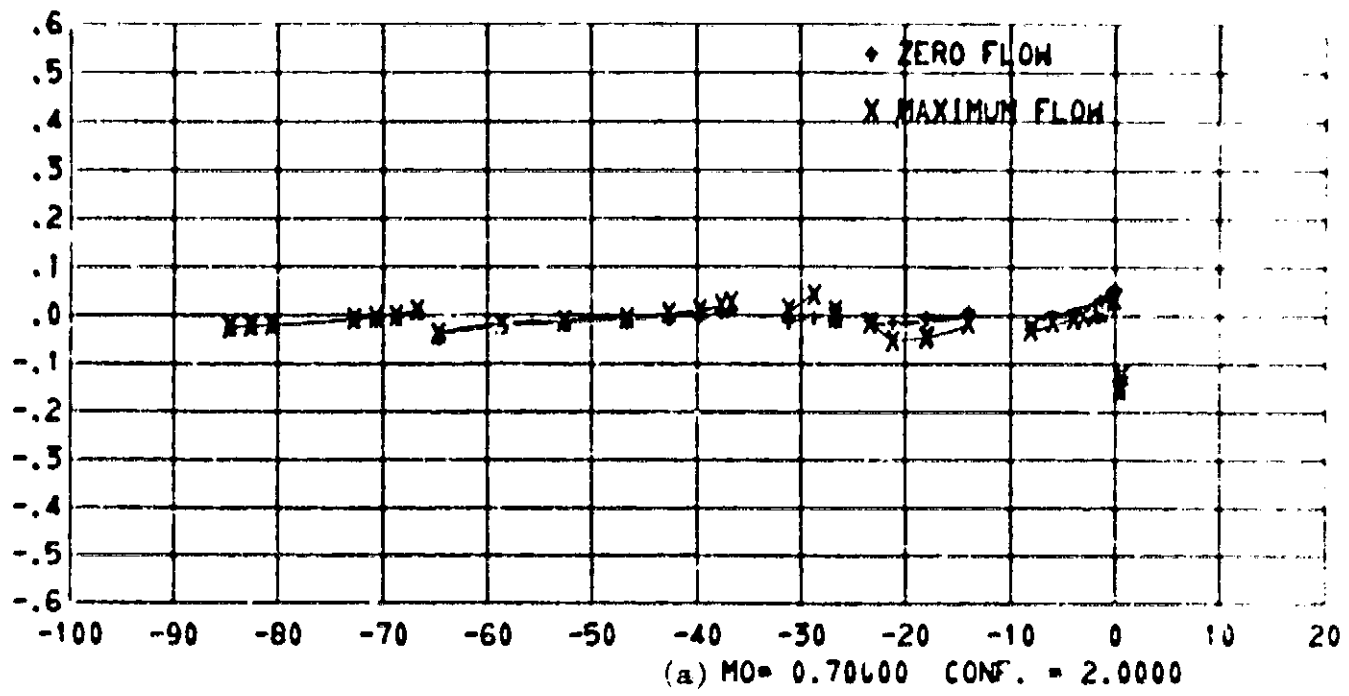


Figure 124 - Effect of vent flow on the pressure distribution. Configuration 2.

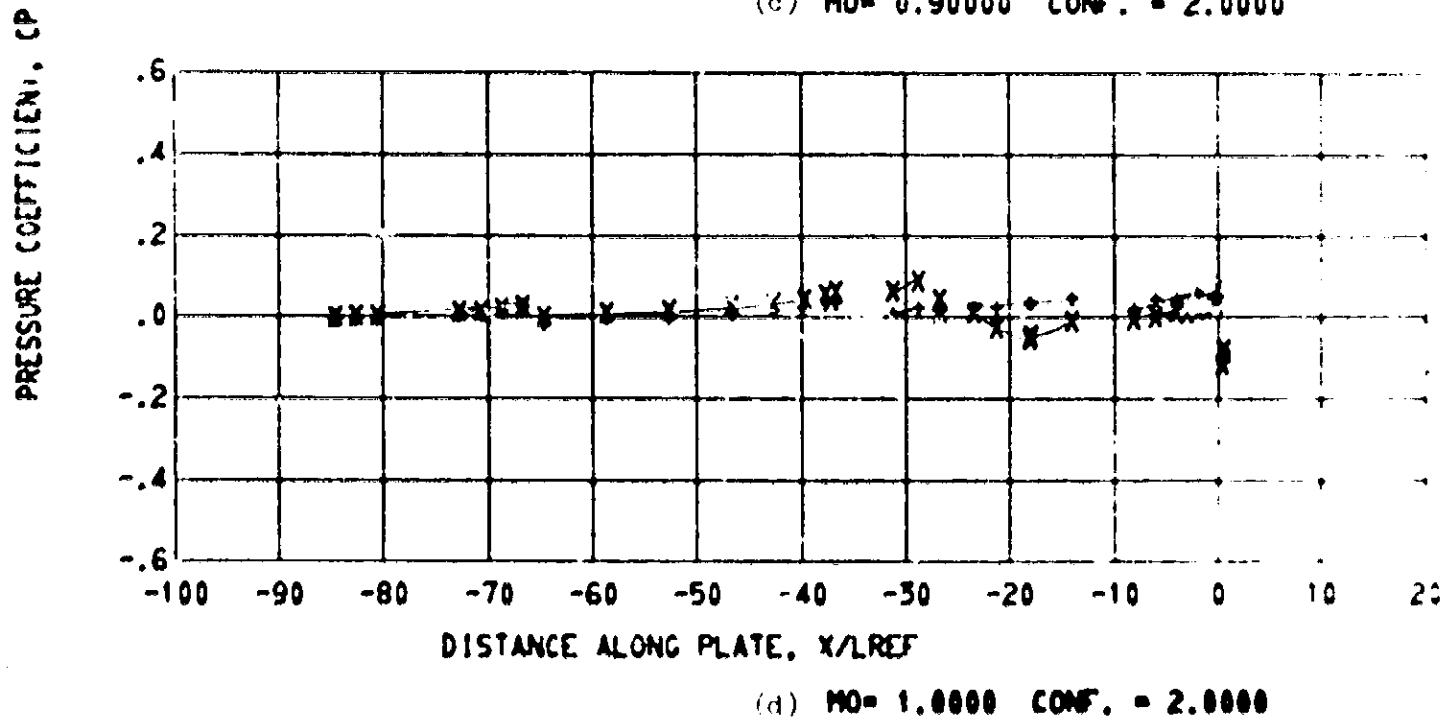
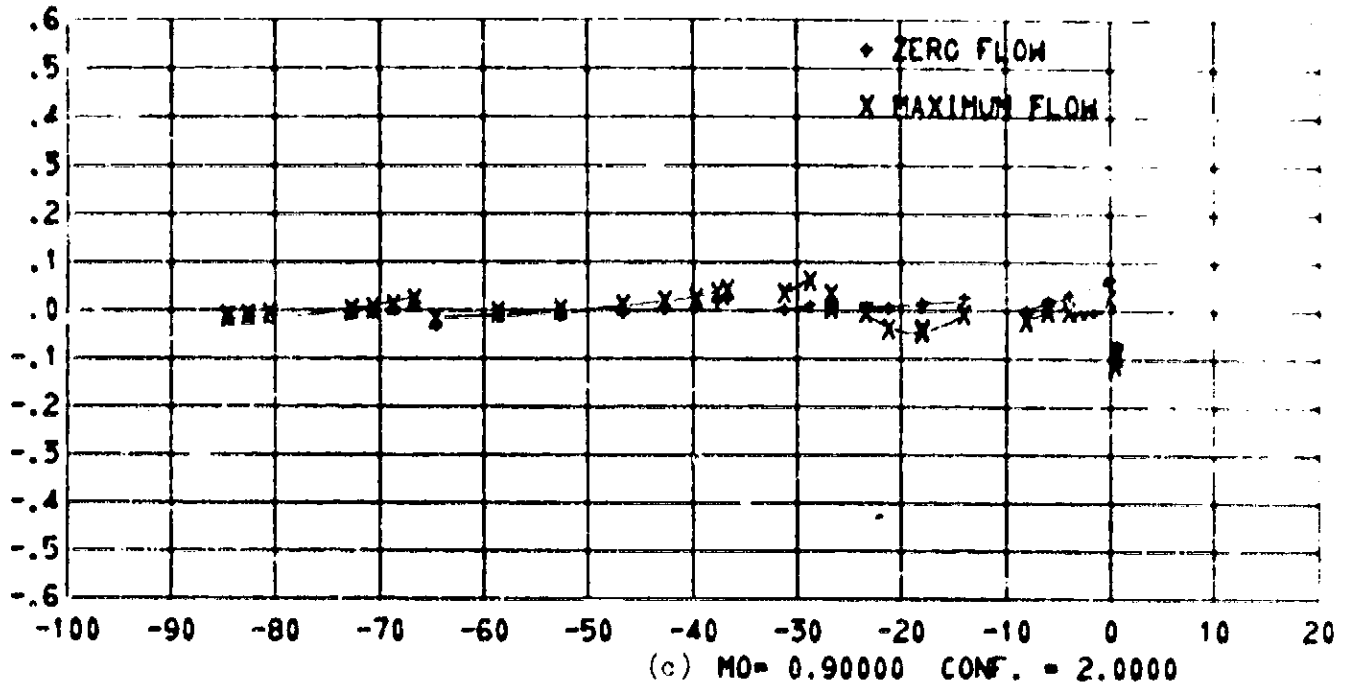


Figure 12. - continued.

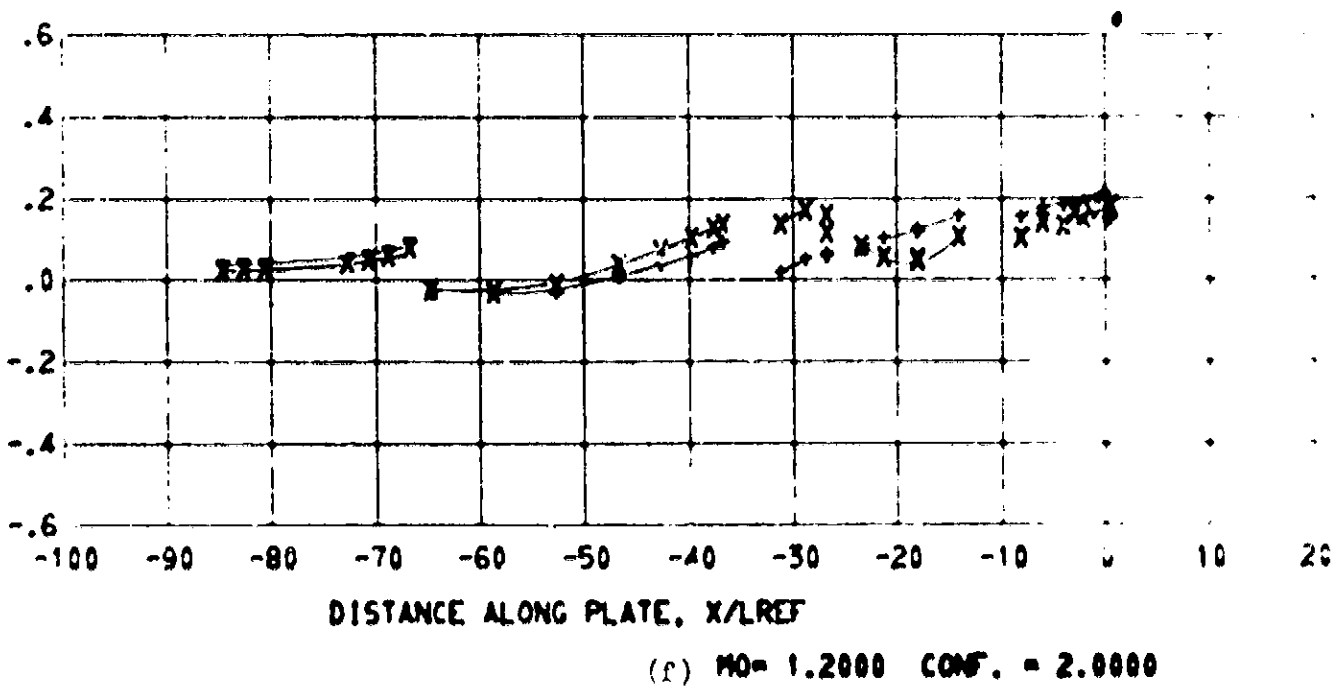
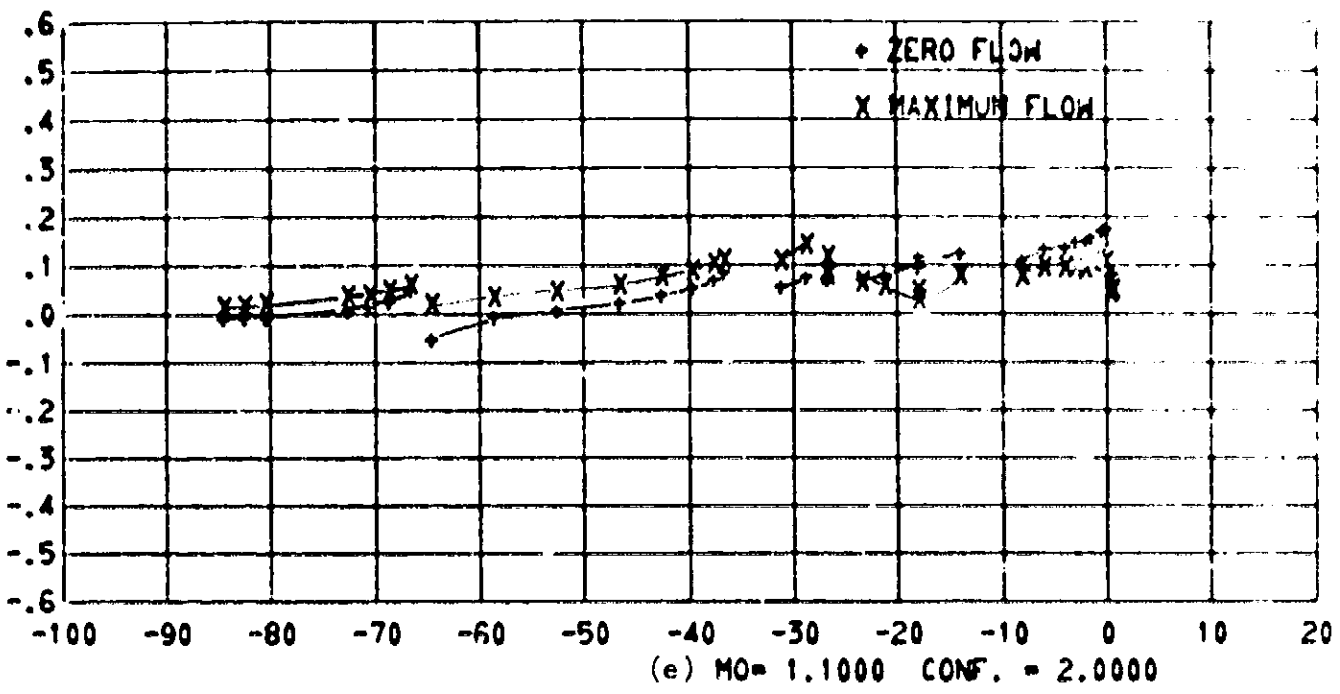


Figure 12. - Continued.

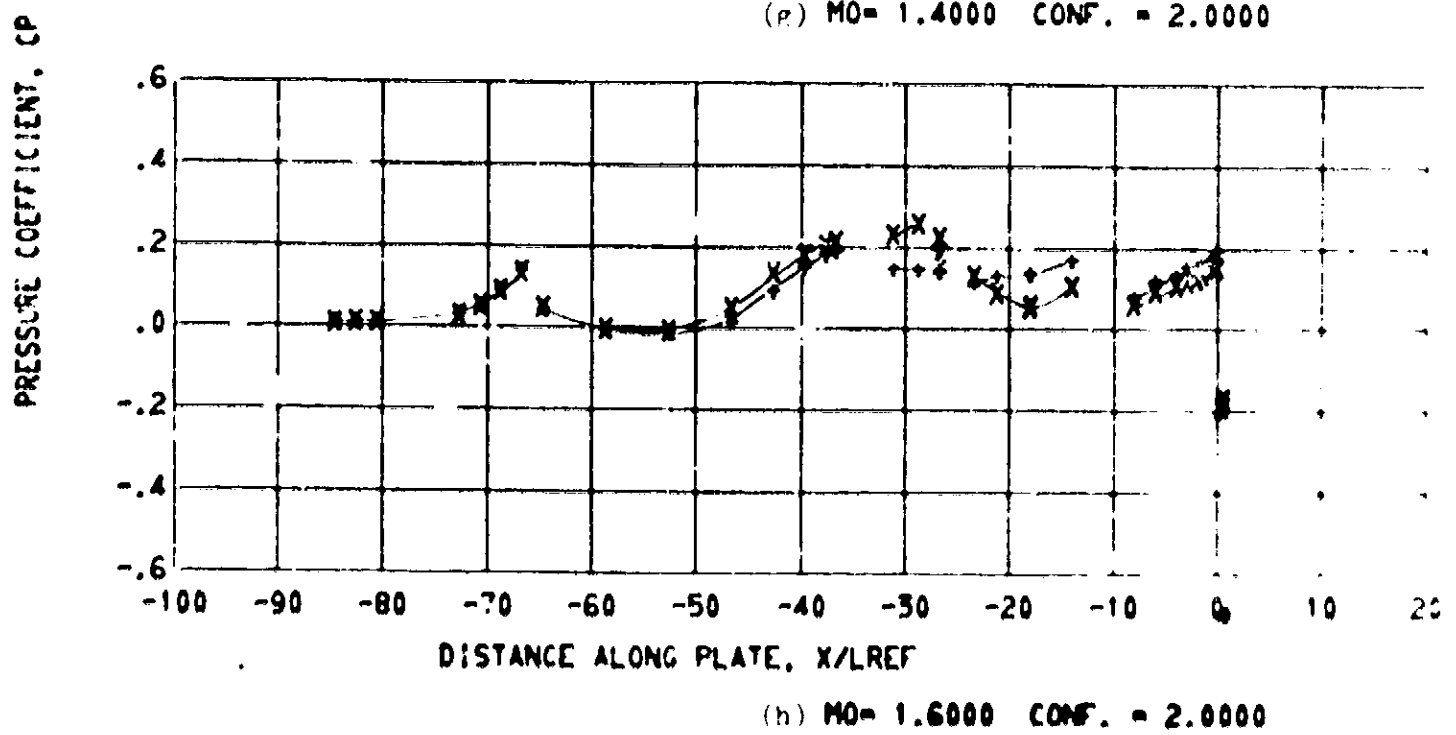
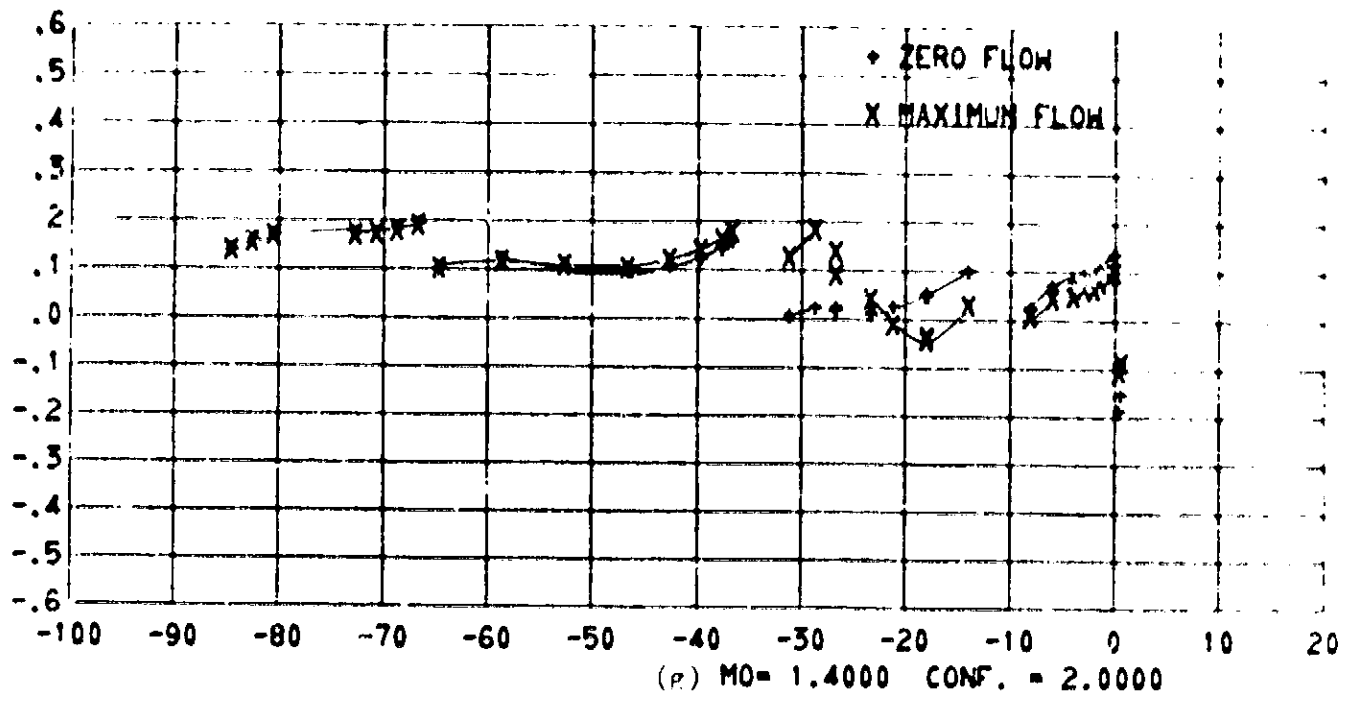


Figure 12. - Continued.

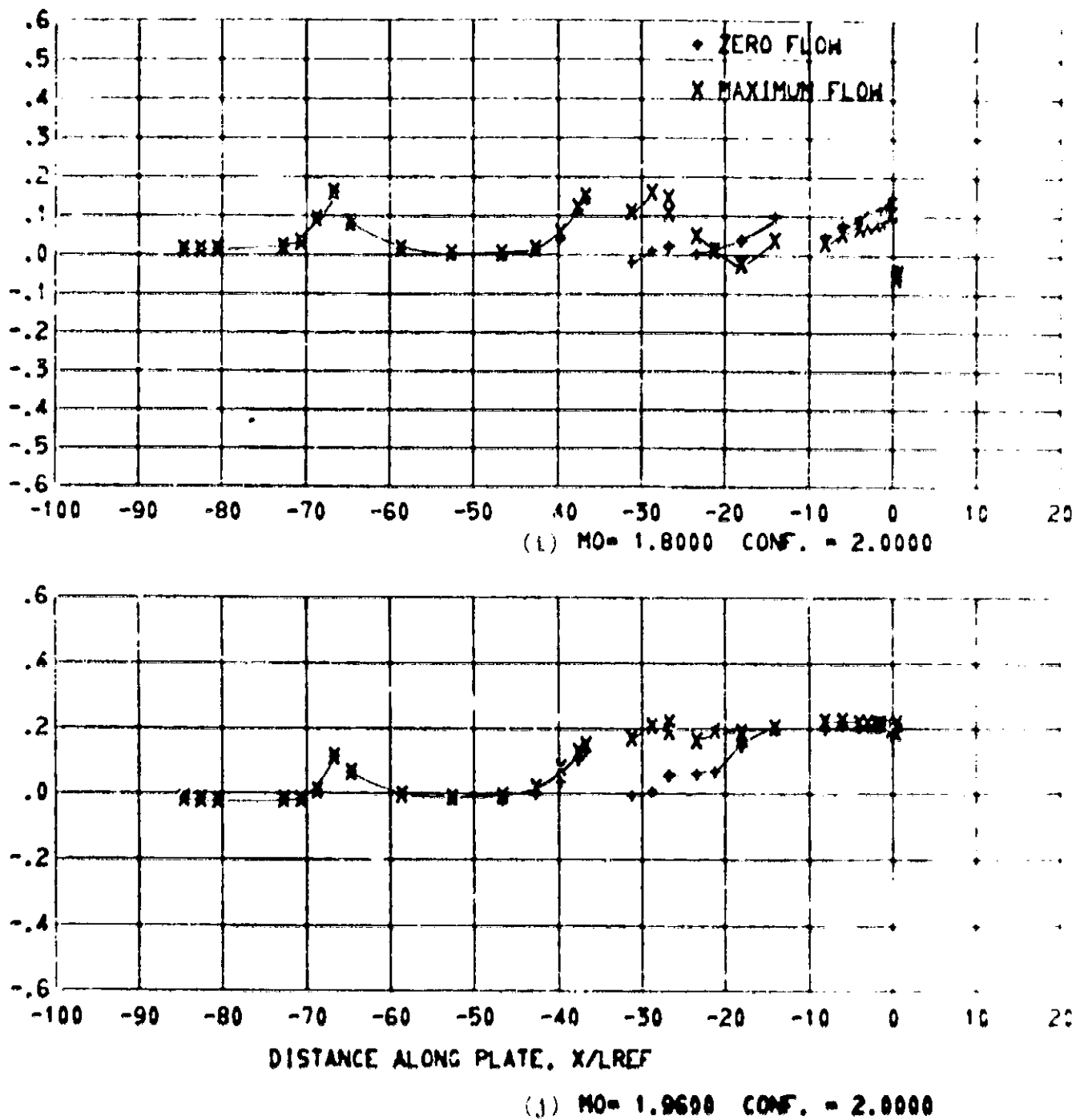


Figure 12. - (concluded.)

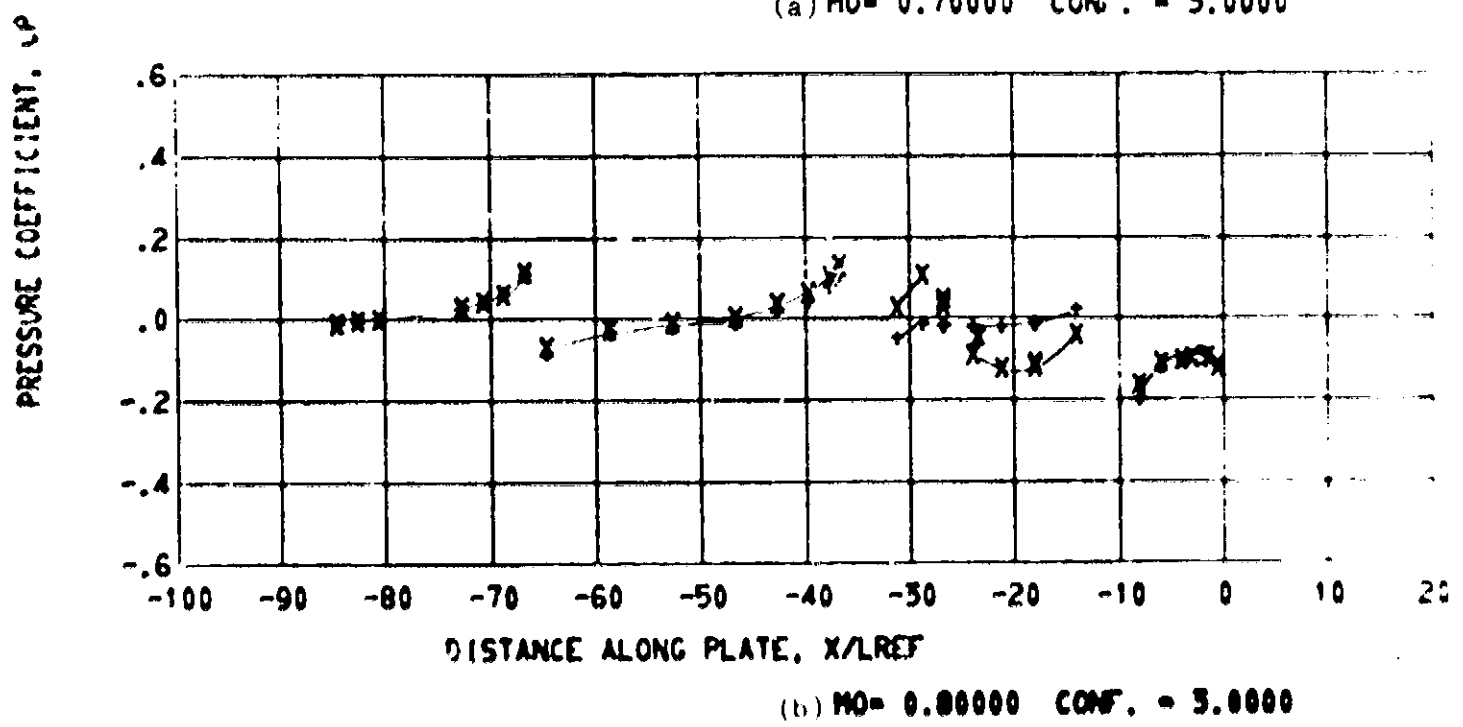
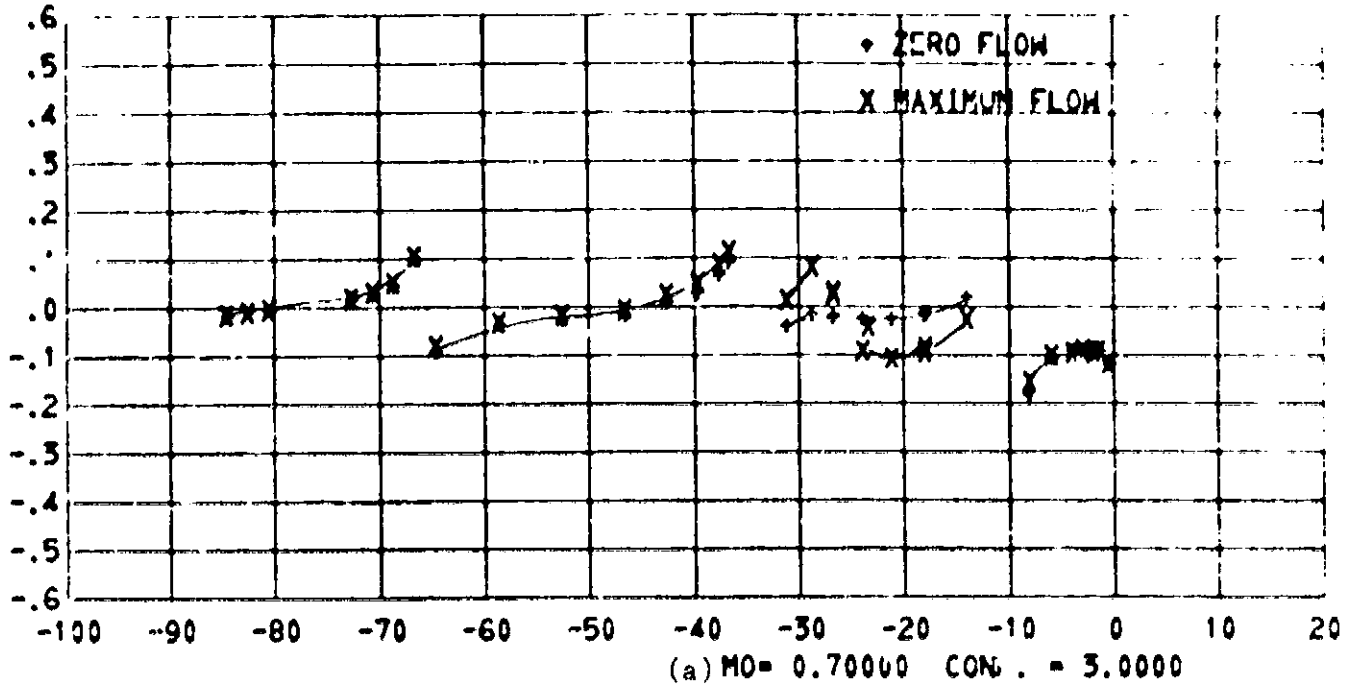


Figure 13. - Effect of vent flow on the pressure distribution. Configuration 3.

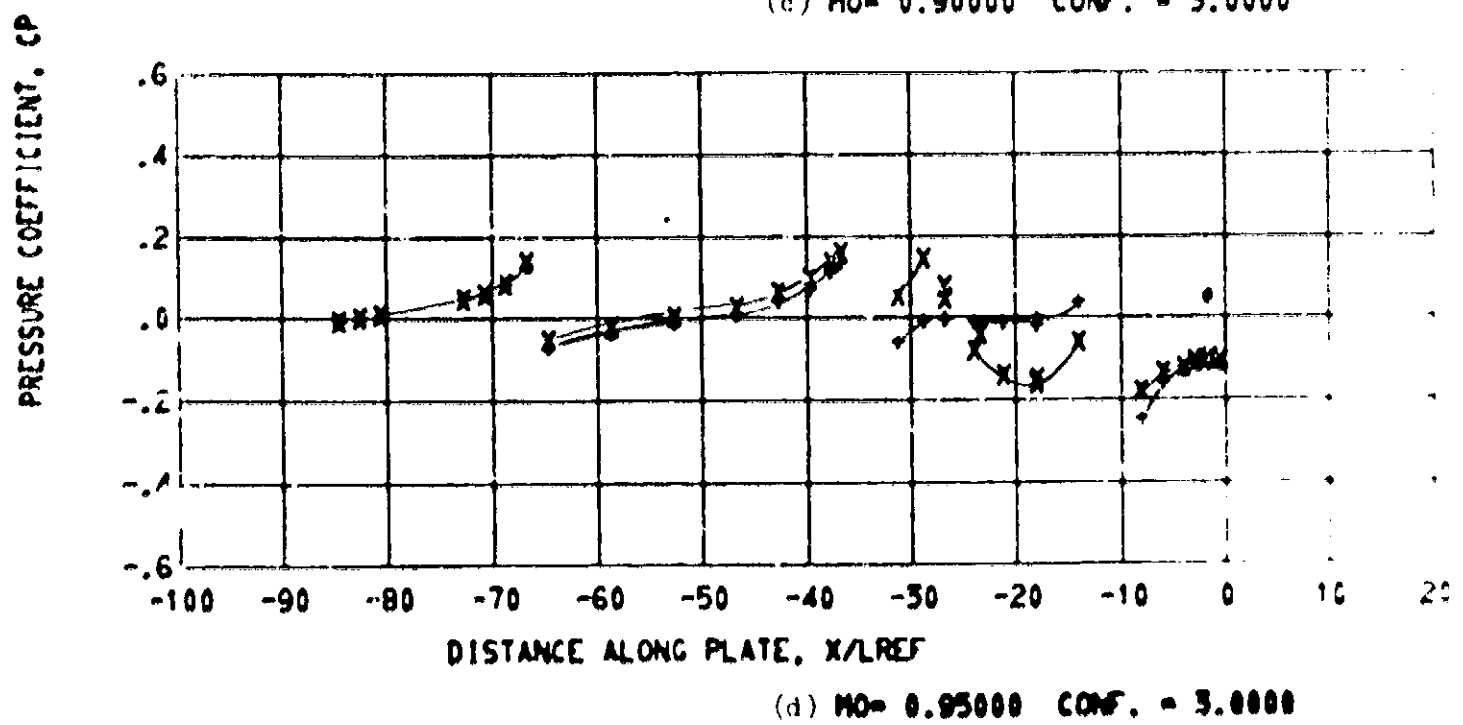
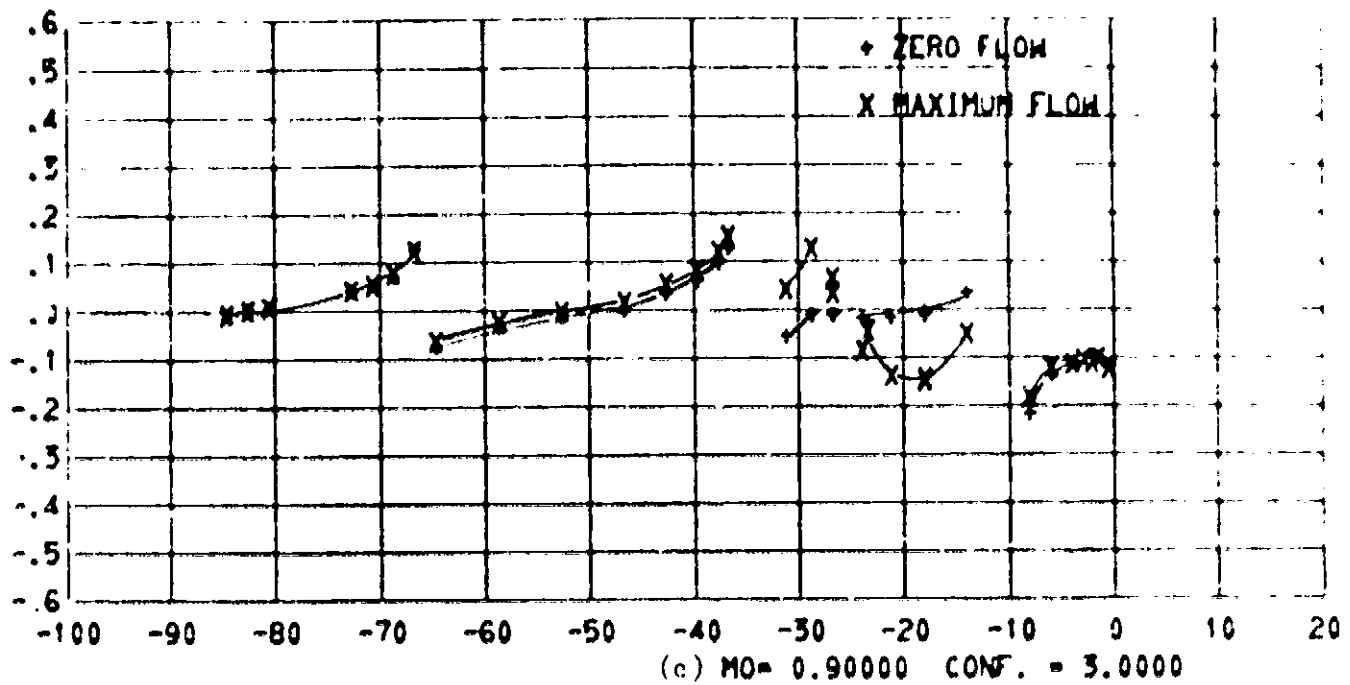


Figure 1c. - continued.

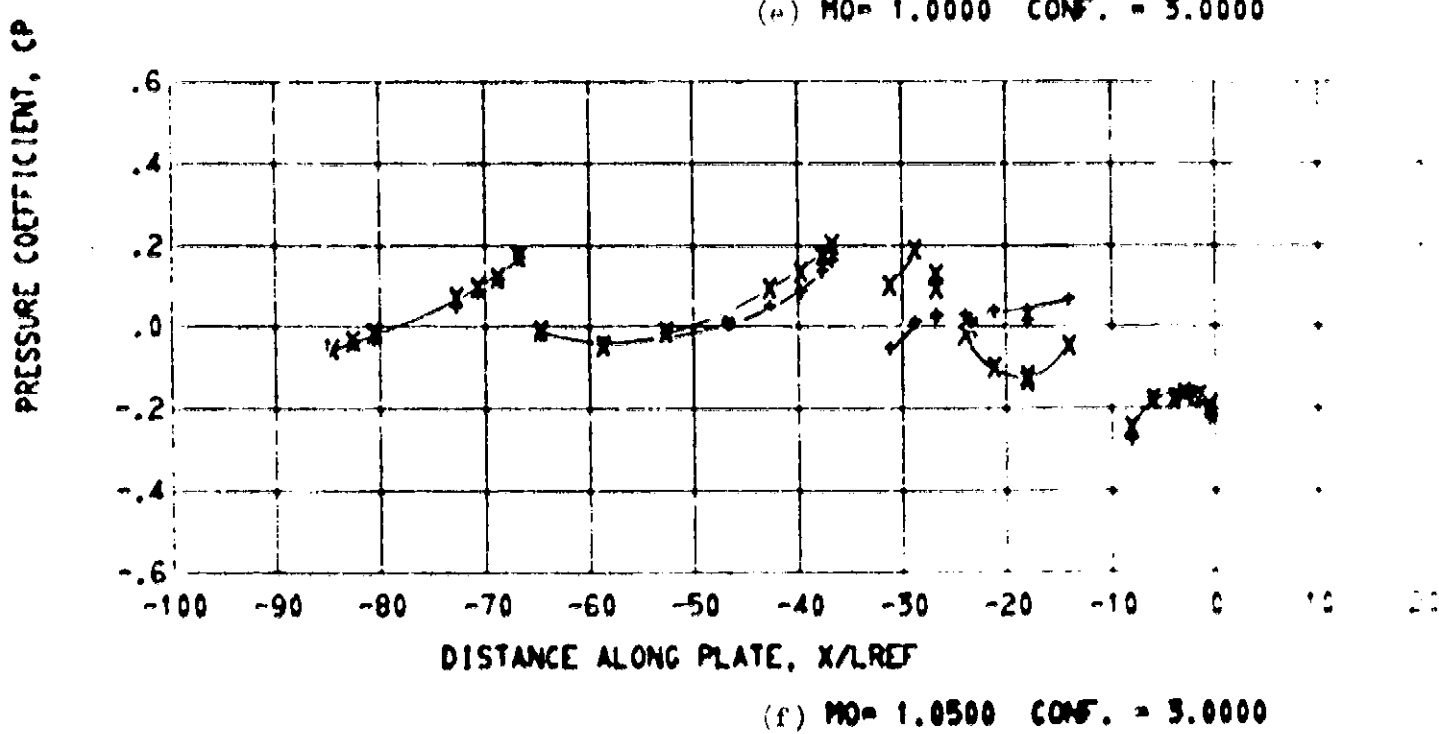
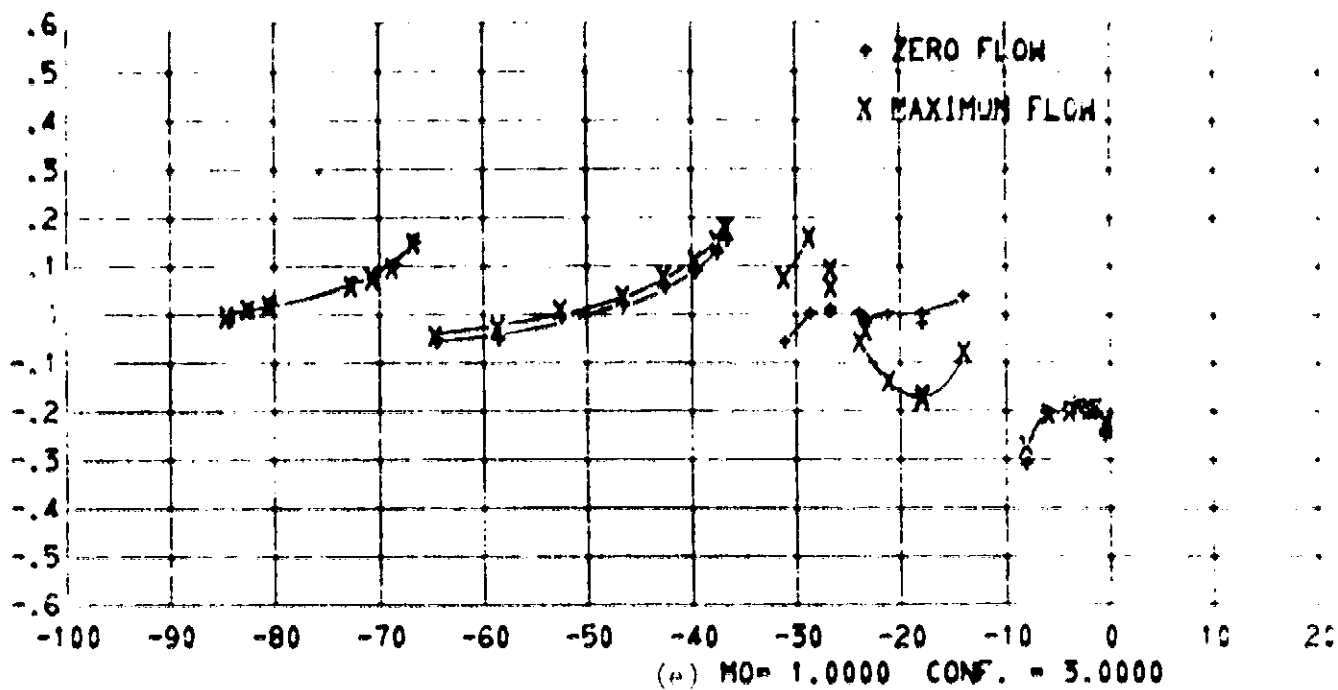


Figure 13. - Continued.

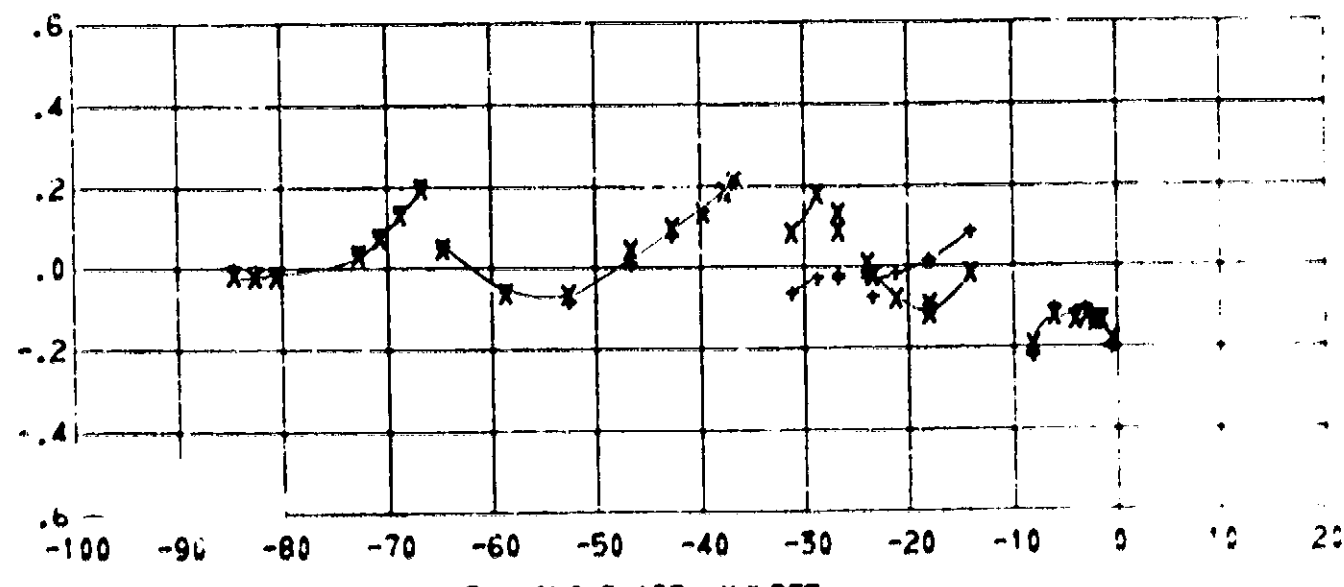
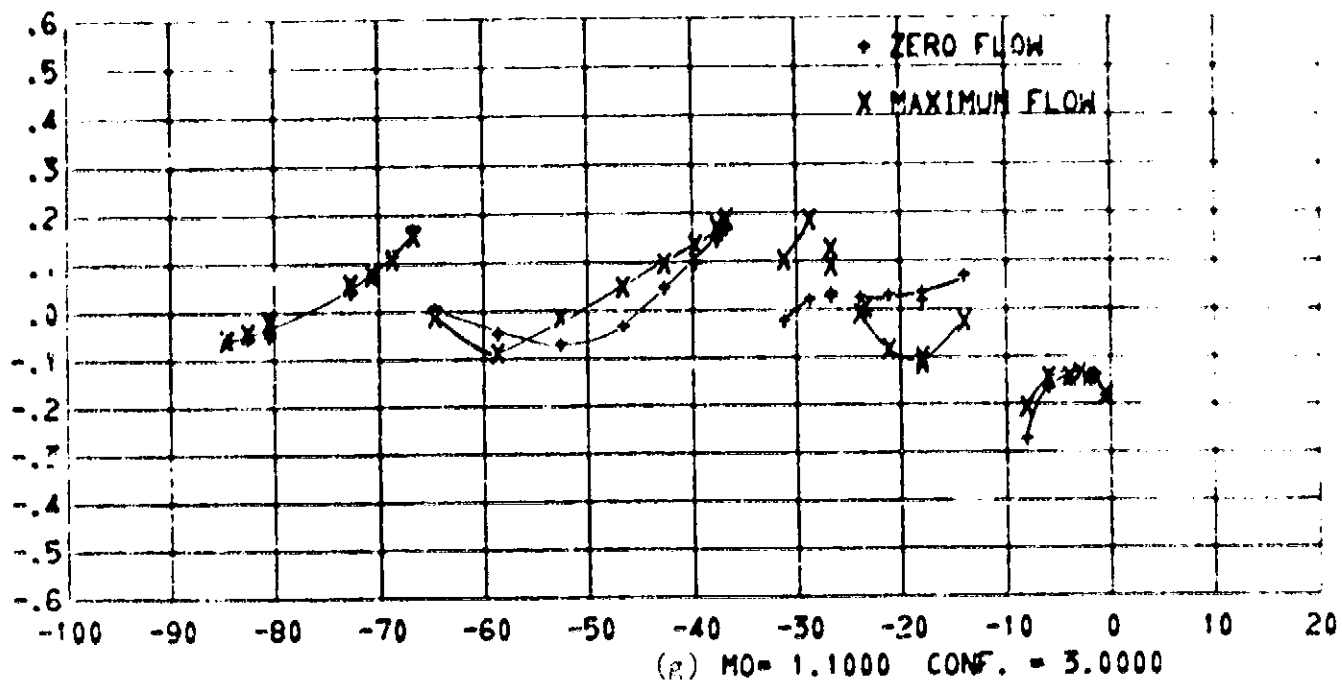


Figure 13. - Continued.

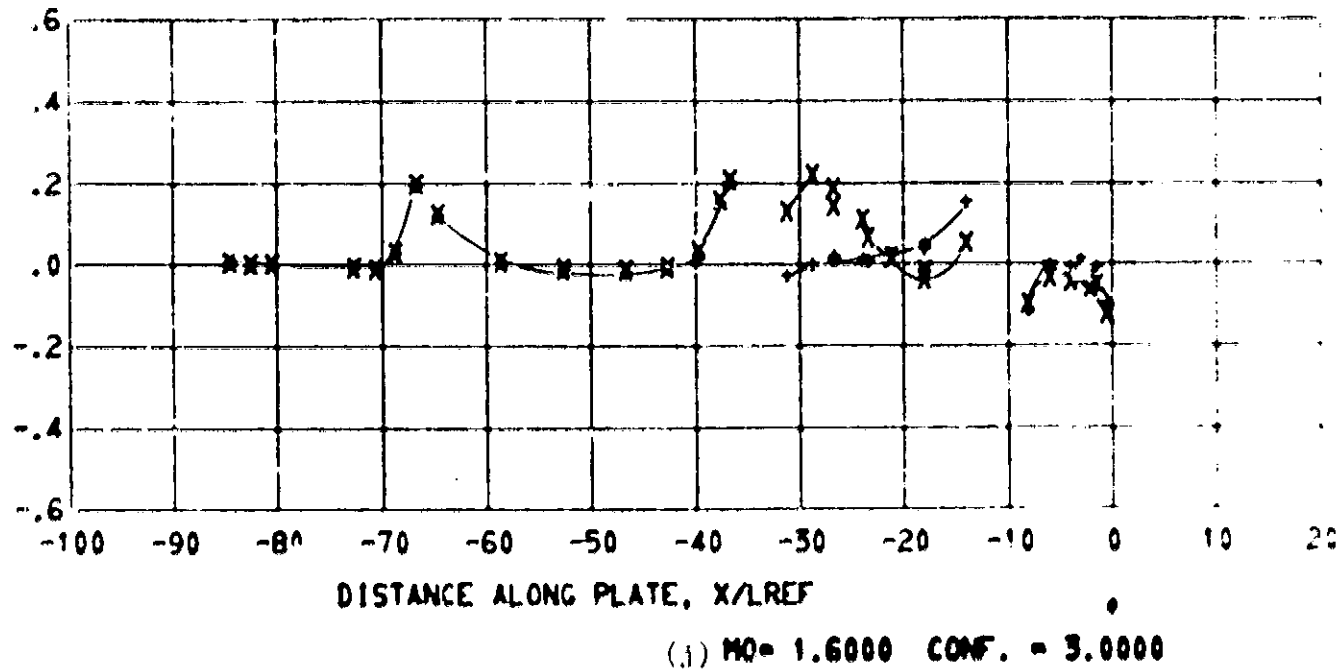
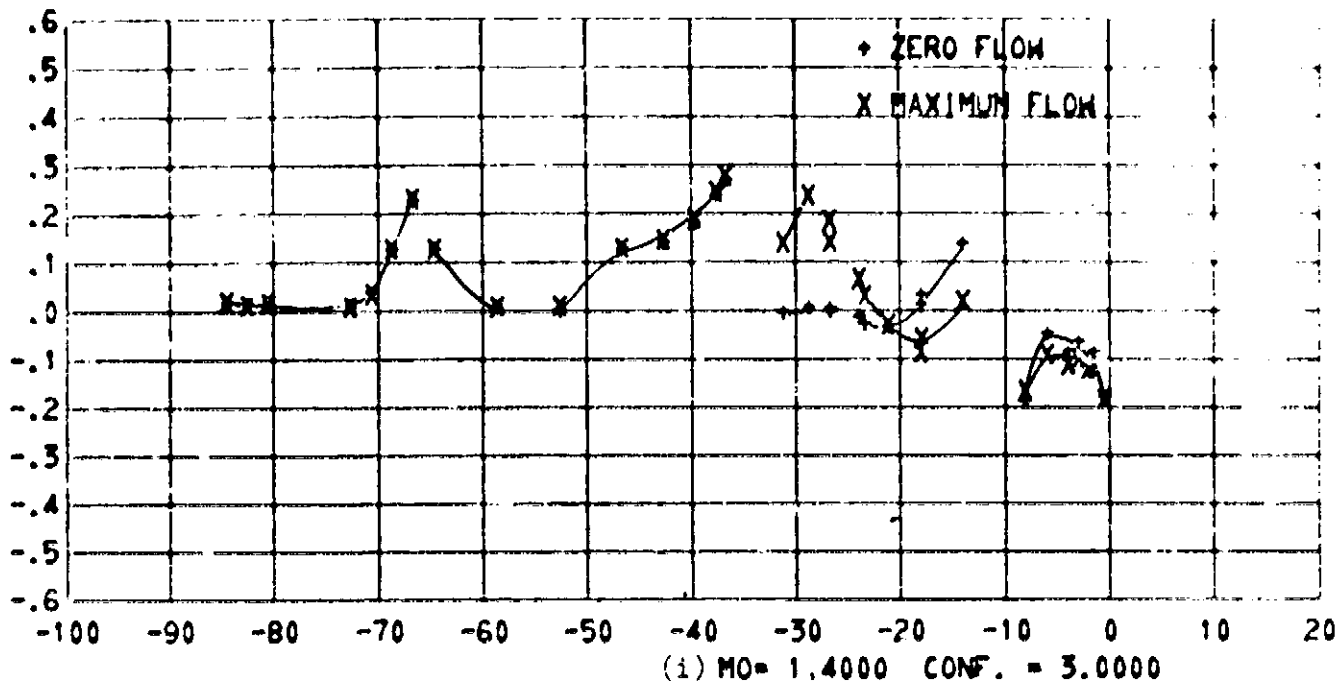


Figure 13. - Continued.

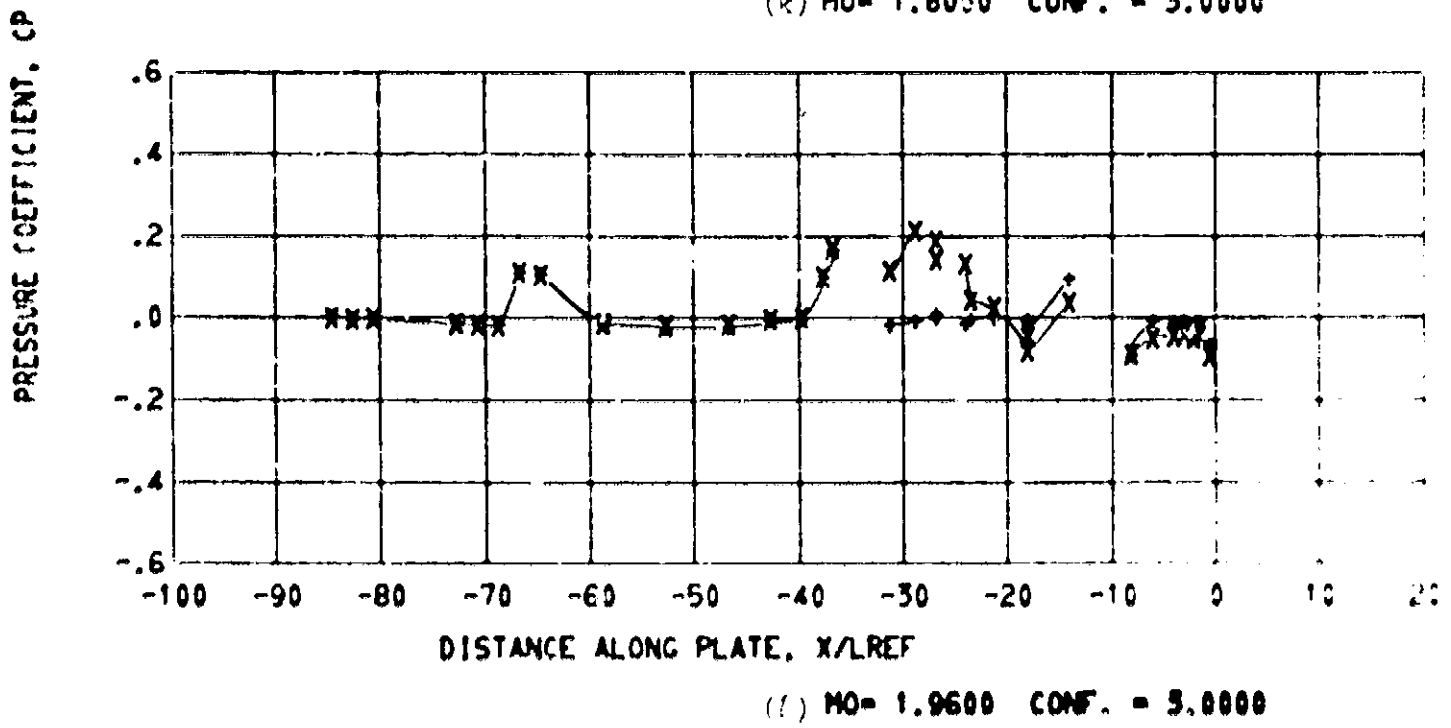
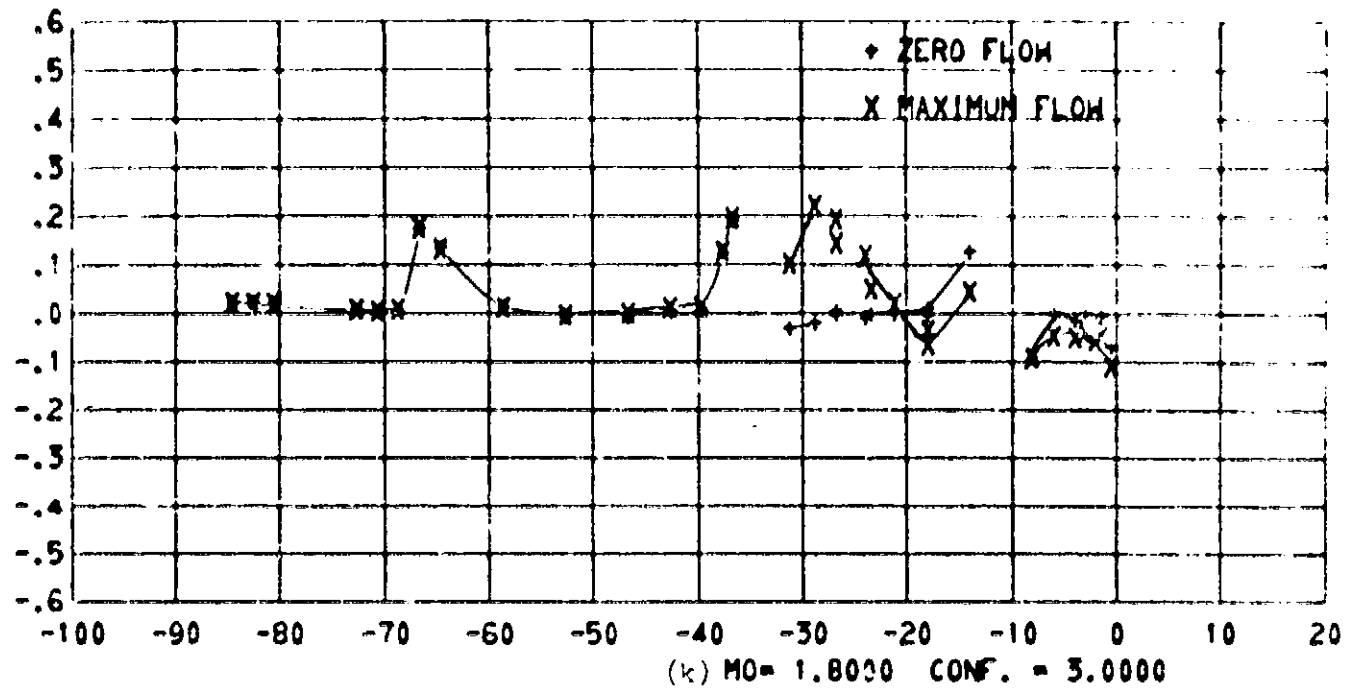
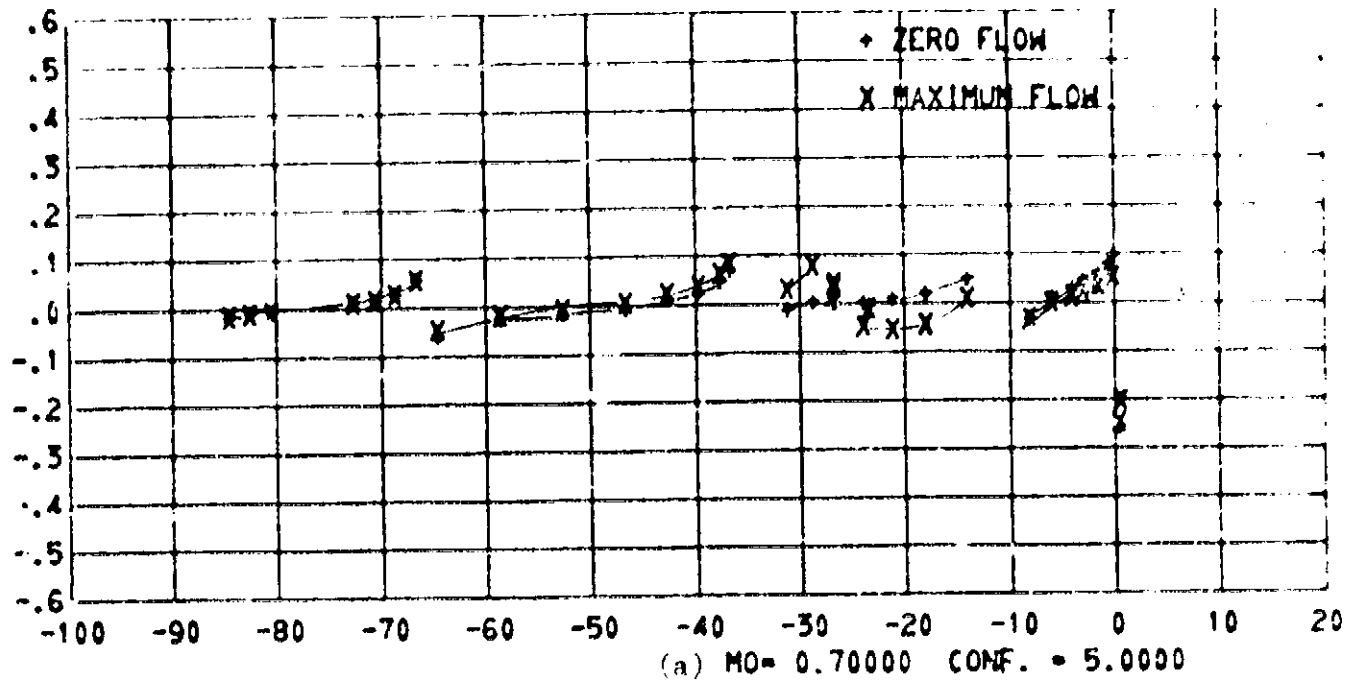


Figure 13. - Concluded.

PRESSURE COEFFICIENT, CP



DISTANCE ALONG PLATE, X/X_{REF}

(b) $M_0 = 0.00000$ CONF. = 5.0000

FIGURE 10. - Effect of vent flow on the pressure distribution. Configuration 2.

PRESSURE COEFFICIENT, CP

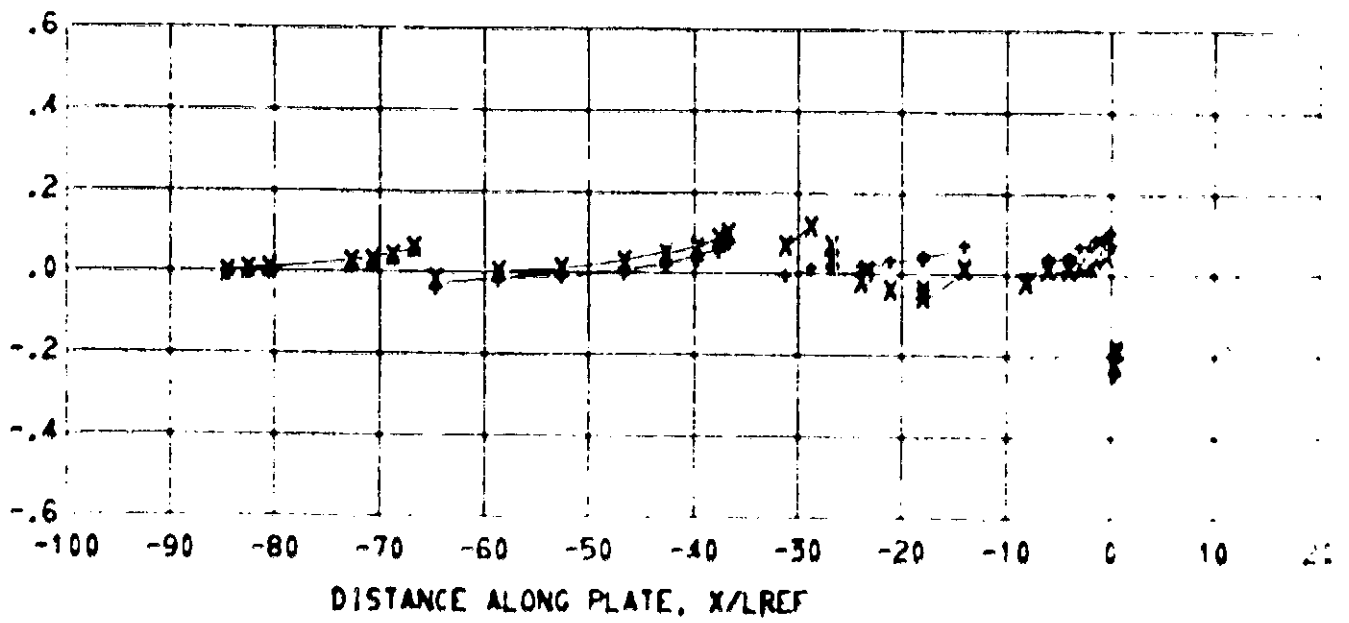
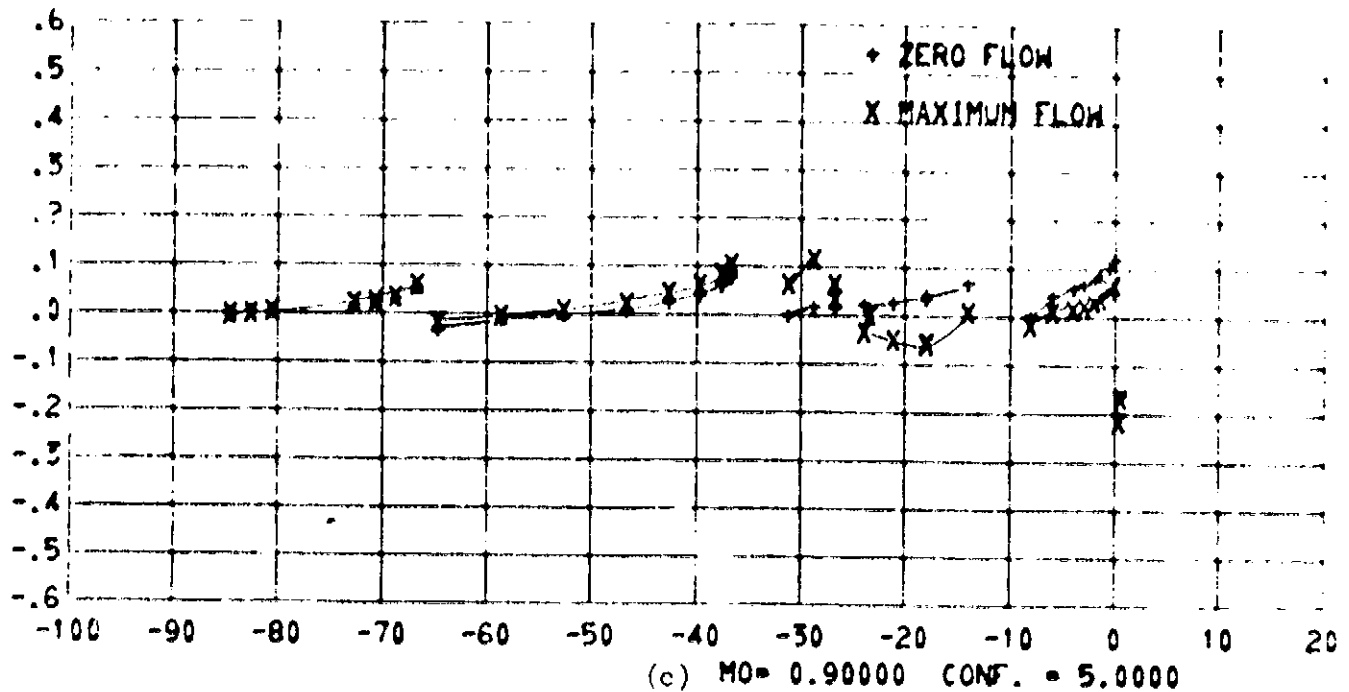
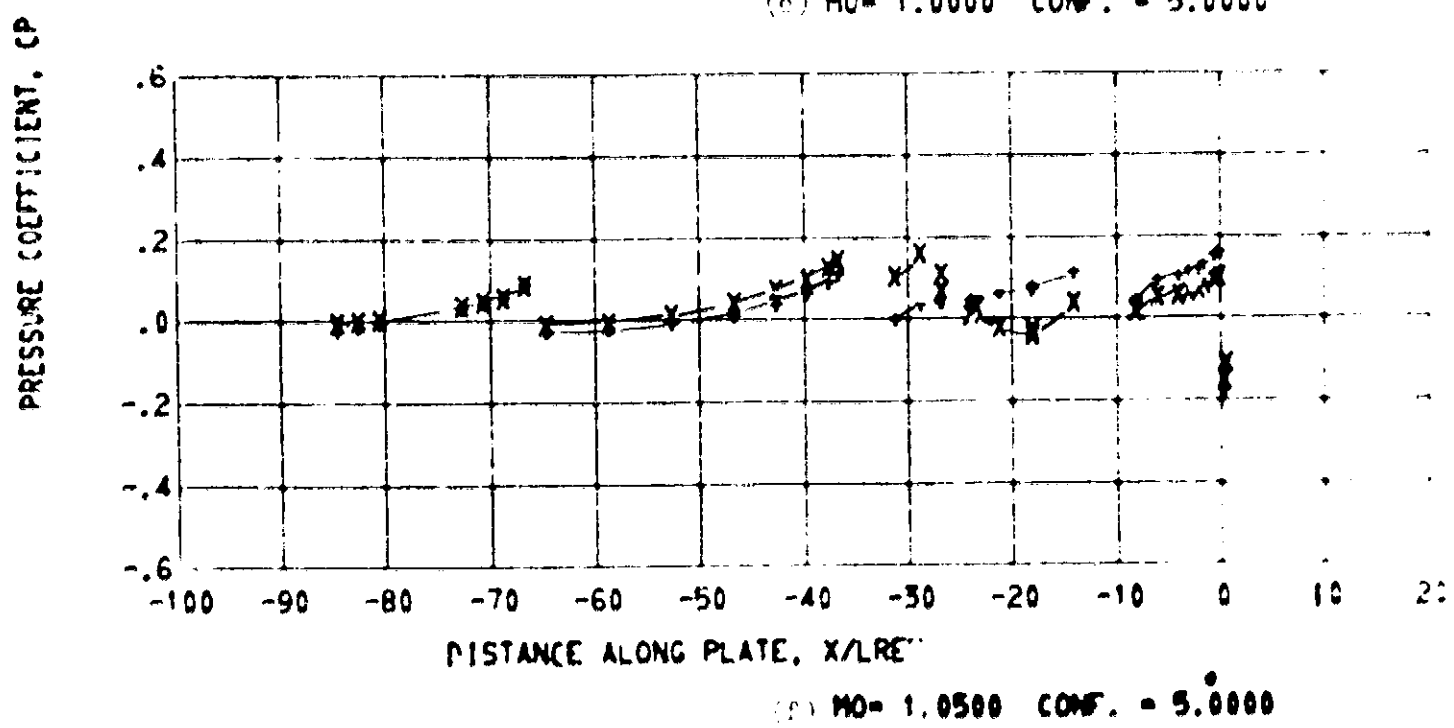
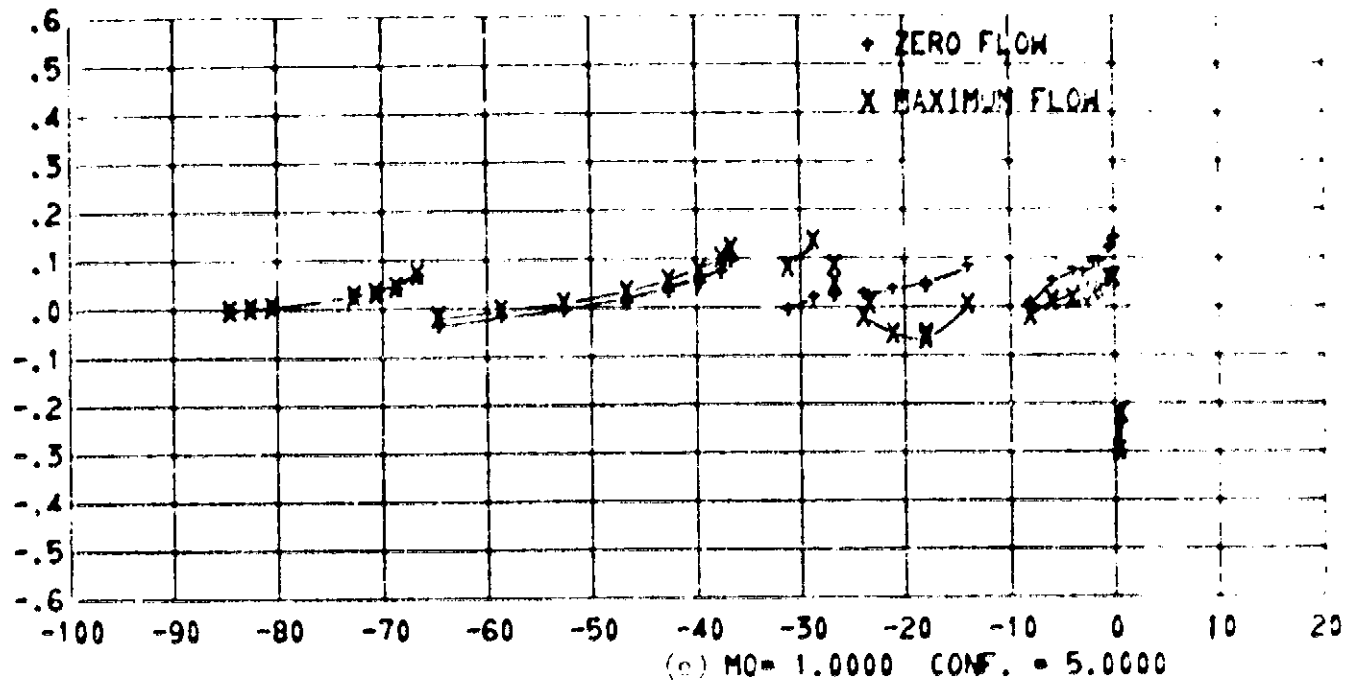


FIGURE 11. - (continued.)



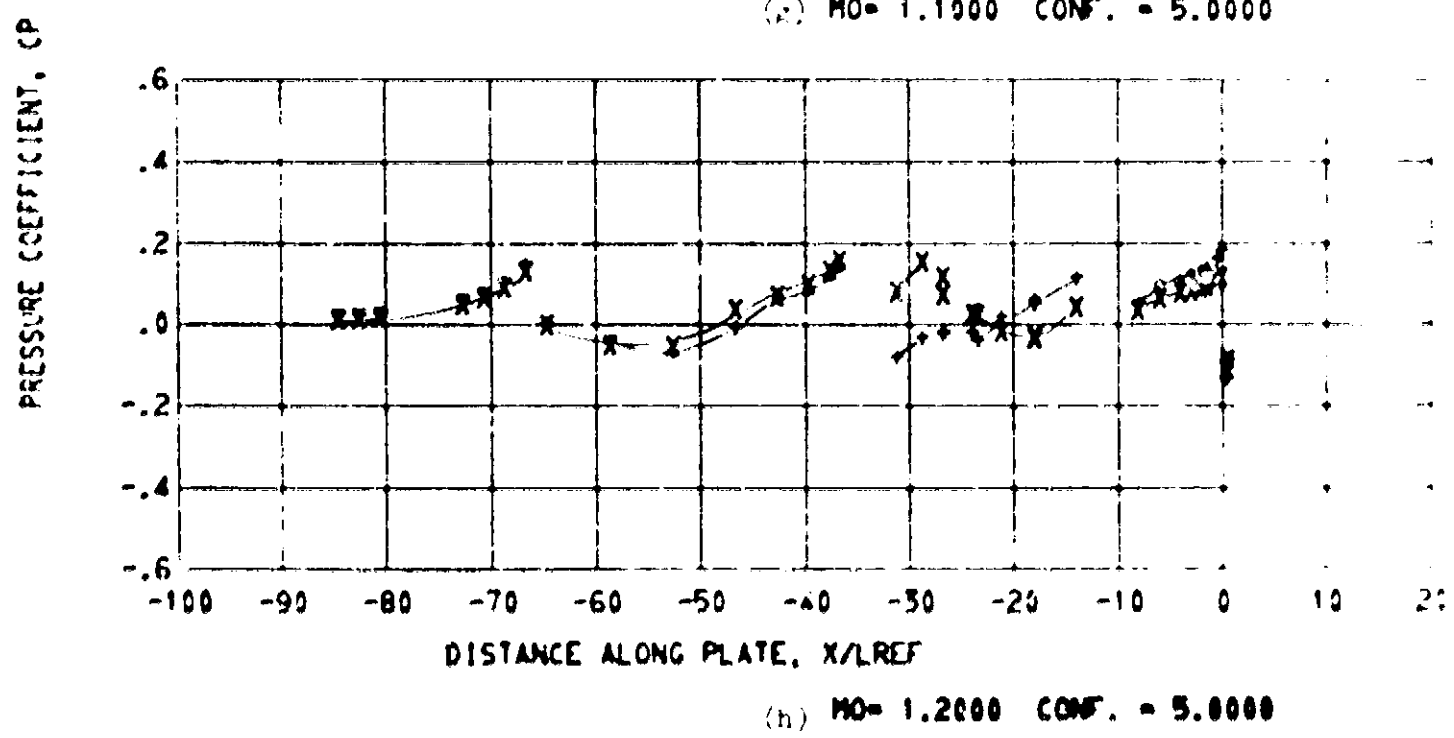
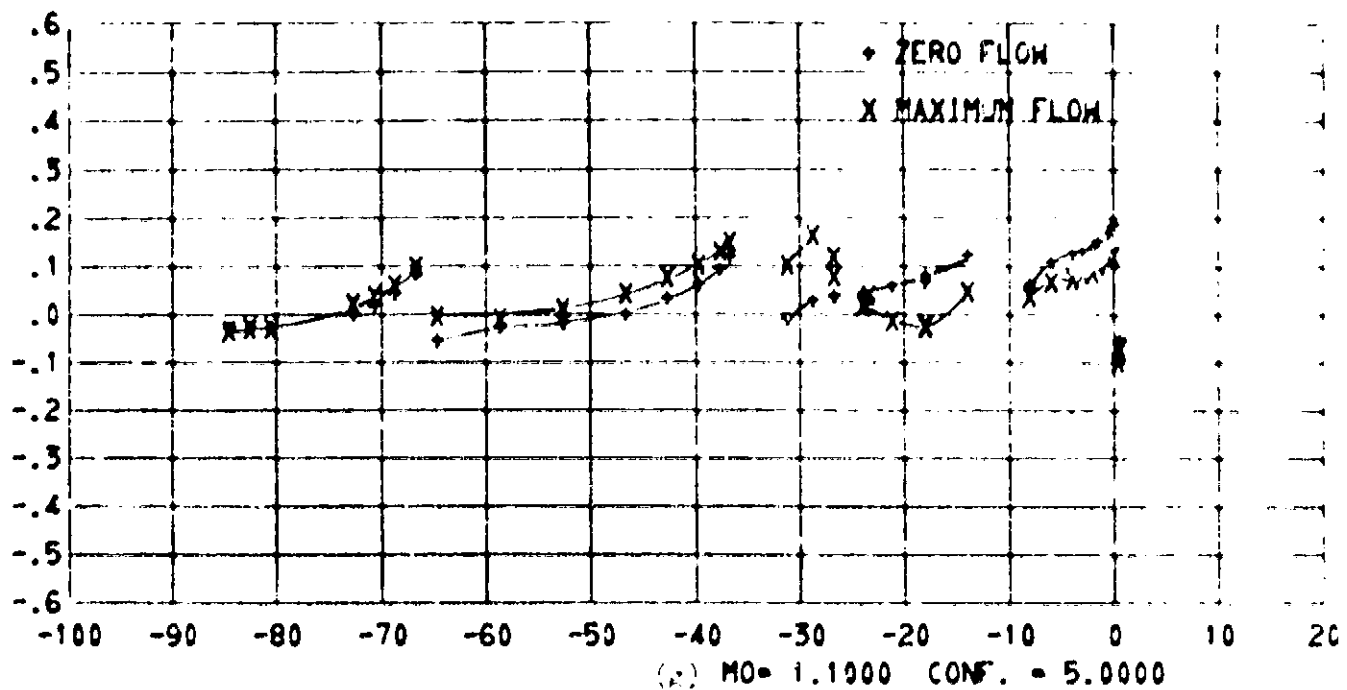


Figure 1h. - (continued).

PRESSURE COEFFICIENT, CP

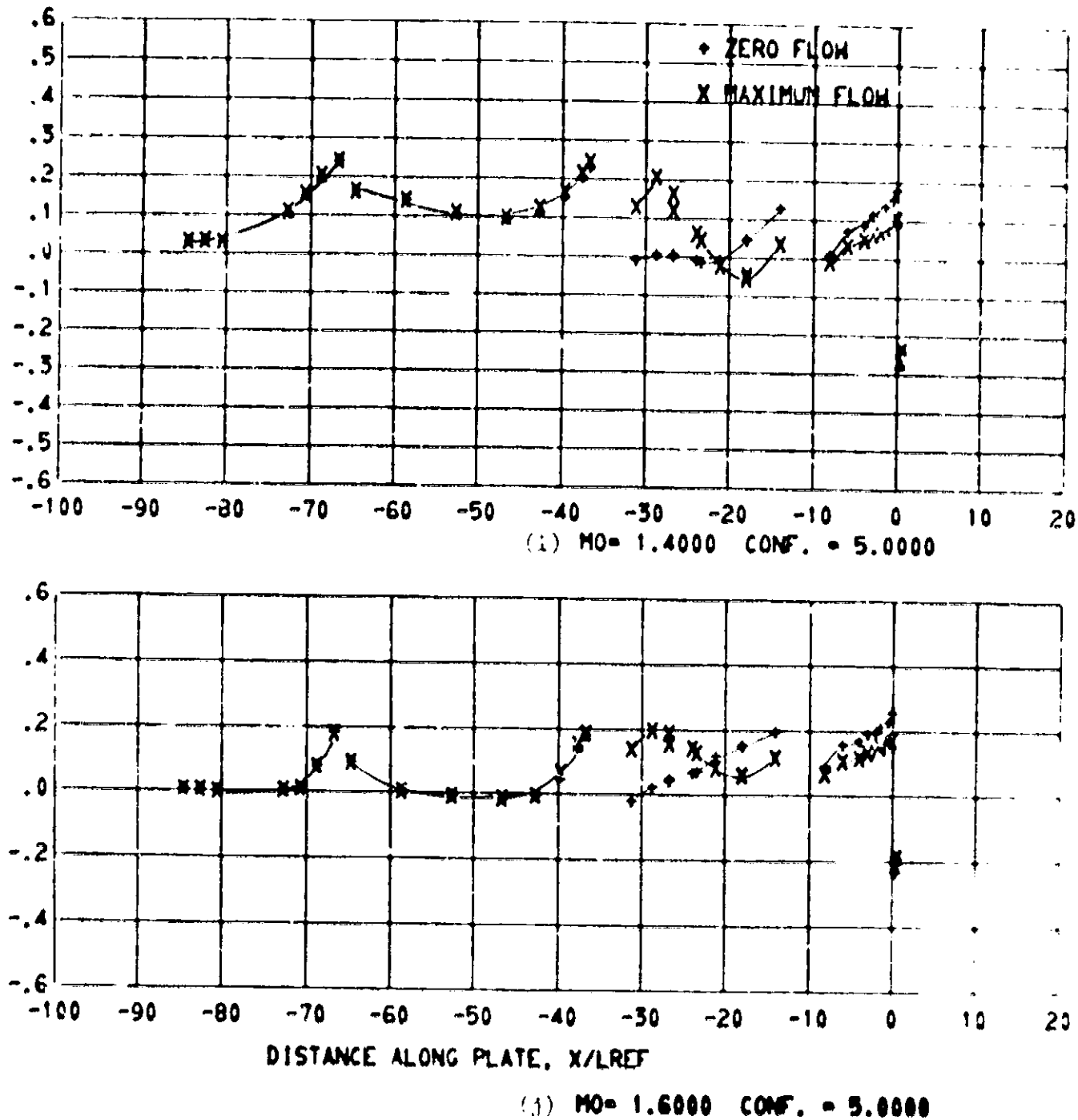


Figure 14. - (concluded).